Dissertation

submitted to the

Combined Faculties for the Natural Sciences and for Mathematics

of the Ruperto-Carola University of Heidelberg, Germany

for the degree of

Doctor of Natural Sciences

Presented by

M.Sc. Paris Roidos

born in Thessaloniki, Greece

Oral examination: 10.02.2020

Development of a high-throughput CRISPR/Cas9 based fluorescent reporter to study DNA double-strand break repair choices.

Referees: Prof. Dr. Benedikt Brors

Dr. Dr. Amir Abdollahi

Acknowledgments

This work was supported by the collaboration between Merck KGaA and BioMed X GmbH through the TiP Oncology platform.

First and foremost, I would like to thank my supervisor Dr. Balca R. Mardin, who allowed me to conduct my Ph.D. research in her laboratory and vitally influenced my development as a life scientist. She showed me how to pursuit projects and evaluate results with constant encouragement and excitement. Balca gave me the chance to familiarize myself with the growing field of functional genomics and its interplay with bioinformatics. Balca mentored, supported, and motivated me through each stage of my Ph.D, and I am very thankful.

I would also like to acknowledge my Thesis Advisory Committee (TAC) members, Prof. Brors, Dr. Abdollahi, and Dr. Korbel who provided me with valuable comments and suggestions in every TAC meeting. Those meetings were decision-making timepoints and played a crucial role in the outcome of my thesis. Also, I am very grateful to Dr. Papavasiliou, and Dr. Stegle who were able to become examiners for my defense. In addition, I would like to thank Dr. Zenke for providing valuable guidance and support during the frequent meetings with the DNA Damage in Cancer group.

Next, I would like to express my sincere gratitude to Dr. Özdemirhan Serçin, who supported me throughout my Ph.D. Özdemirhan enabled me to think out of the box and critically observe science. His passion for science inspired me to see biological phenomena from a different point of views and discuss their meaning in detail.

Many thanks to Dr. Salvatore Benfatto, who helped me during several projects, especially when involving bioinformatic analysis. He provided many creative ideas and advice essential for the development of my work. I would also like to acknowledge Dr. Francesca Dejure, who supported and advised me throughout my studies in diverse matters. Along with them, I would also like to thank the rest members of the Mardin laboratory for the inspiring scientific discussions, as well as the BioMed X colleagues that helped me throughout my Ph.D. in diverse matters. I much appreciated the help of the EMBL facilities, such as the FACS, the Gene Core, and the ALMF for their excellent assistance when needed.

Moreover, I would like to express my genuine appreciation to my family for their support and encouragement along all those years. My mother Konstantina and my father Eleftherios supported me throughout my studies and played an essential part in my growth as a scientist, and as a person. Their constant belief in biological sciences motivated me and drove me further to achieve the highest academic degree. Their conscious and wisdom will always follow me as a person.

Finally, I would like to show gratitude to my wife Xanthi who supported me throughout my Ph.D., encouraged me in the difficult times and endured my physical absence to accomplish my career goals. She always advised me when I needed it and gave me the courage to move on and achieve more. She supported my work but also my life by forging me to be a better man, and for that, I will always be thankful.

I would like to dedicate this Ph.D. thesis to my current and future family. I want my efforts and achievements to be a legacy of excellence and provide a better future for my family.

To my current & future family

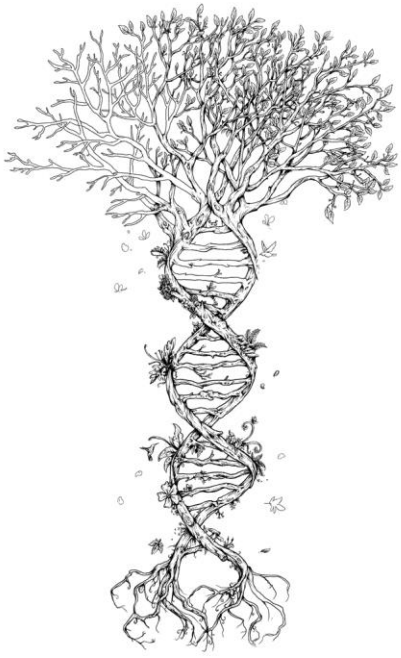

Abstract

One of the most toxic types of DNA lesions are the DNA double-stranded breaks (DSBs). The cells can repair such lesions through several distinct strategies that can be grouped into end-protection and end-resection based mechanisms.

Over the past decades, a number of reporter assays have been developed to examine the consequences of DNA damage and repair (DDR), mostly focusing on one DSB repair pathway at a time. However, a simple reporter that can visualize different DNA DSB repair outcomes with high resolution has been missing. Therefore, we developed a fluorescent reporter Color Assay Tracing Repair (CAT-R) to assess different DNA DSB repair outcomes by measuring the rates of end-protection vs. end-resection-based repair mechanisms.

I integrated the CAT-R reporter at a single locus in two cell lines and took advantage of the highly efficient CRISPR/Cas9 system to mediate a site-specific DSB. I studied the rate of small InDels vs. large deletions and found that large deletions occur as frequently as small InDels upon Cas9-mediated breaks, consistent with the recent findings. I generated several different knock-outs in major genes of the DNA DSB repair and showed that the rate of these repair outcomes can be dynamically altered.

Since I achieved a high resolution of the DSB events that allowed me to measure even minor changes in the DSB repair activity, I combined CAT-R with high-throughput flow cytometry to screen small pharmacological compounds. I compared 24 drug compounds that are currently in clinical trials or used in preclinical studies, targeting key DNA DSB repair enzymes such as ATM, DNA-PK, ATR, and PARP as well as a class of inhibitors targeting histone deacetylases.

I quantify the levels of enzyme inhibition based on their effects on the associated DNA repair pathway and present variances across their *in vitro* drug potencies of the inhibitor compounds.

Next, I combined CAT-R with a custom CRISPR/Cas9 arrayed genetic screen targeting 417 genes involved in DNA damage response (DDR) and evaluated their contribution in DNA DSB repair choice. I confirmed the roles of the established players of DSB repair but also revealed potentially novel components of DSB repair. In addition, I uncovered how Cas9-mediated DSB repair could be modulated to increase the rate of error-free repair, which may have important implications for the generation of knock-ins by CRISPR/Cas9.

Finally, to identify novel PARP1 interactions within the DDR, I applied CAT-R on the custom arrayed genetic screen and combined it with PARP inhibition. I uncovered a gene cluster that is significantly affected by PARP inhibition regulating a key step during end-resection, highlighting potentially new interactions of PARP1 with DDR. Besides, I propose PARP inhibition as an alternative approach to increase the chances of a successful knock-in, based on my experiments demonstrating that PARP inhibition increases the rates of error-free repair to a similar extent with other well-known strategies.

In summary, in this Ph.D. thesis, I show how CAT-R can be used to assess the functions of DNA DSB repair genes and how it can be adapted to genetic and/or chemical screens in a variety of cell lines.

Zusammenfassung

Eine der toxischsten Arten von DNA-Läsionen sind die DNA-Doppelstrangbrüche (DSBs). Zellen können solche Läsionen durch verschiedene unterschiedliche Strategien reparieren, die sich in Mechanismen auf der Basis von Endschutz und Endresektion unterteilen lassen.

In den letzten Jahrzehnten wurde eine Reihe von Reporter-Assays entwickelt, um die Konsequenzen von DNA-Schäden und -Reparaturen (DDR) zu untersuchen. Im Allgemeinen ermöglichen diese Reporter die Untersuchung eines einzigen DSB-Reparaturweg. Es fehlte jedoch ein einfacher Reporter, der parallel mehrere verschiedene DNA-DSB-Reparaturergebnisse mit hoher Auflösung visualisieren kann. Aus diesem Grund haben wir einen fluoreszierenden Reporter für die Reparatur von Farbassays (Color Assay Tracing Repair, CAT-R) entwickelt, um verschiedene DNA-DSB-Reparaturergebnisse durch Messung der Endschutzraten im Vergleich zu Reparaturmechanismen auf der Basis von Endresektionen zu bewerten.

Ich habe den CAT-R-Reporter lokusspezifisch in zwei Zelllinien integriert und dann das hocheffiziente CRISPR/Cas9-System zur Vermittlung eines positionell klar definierten DSB verwendet. Daraufhin habe ich die Rate kleiner InDels im Vergleich zu großen Deletionen untersucht und festgestellt, dass, nach Cas9-vermittelten Brüchen, große Deletionen, in Übereinstimmung mit der aktuellen Literatur, genauso häufig auftreten wie kleine InDels. Des Weiteren habe ich verschiedene Knock-outs in den wichtigsten Genen der DNA-DSB-Reparatur erzeugt und gezeigt, dass die Rate dieser Reparaturergebnisse dynamisch geändert werden kann.

Da ich eine hohe Auflösung der DSB-Ereignisse erreichte, die es mir ermöglichte, auch geringfügige Änderungen der DSB-Reparaturaktivität zu messen, habe ich CAT-R mit Hochdurchsatzdurchflusszytometrie kombiniert, um die Wirkung pharmakologischer Verbindungen auf die DNA-DSB-Reparatur zu untersuchen. Ich verglich 24 Wirkstoffe, die sich derzeit in klinischen Studien befinden oder in präklinischen Studien verwendet werden, um wichtige DNA-DSB-Reparaturenzyme wie ATM, DNA-PK, ATR und PARP sowie eine Klasse von Inhibitoren gegen Histondeacetylasen zu untersuchen. Ich habe dann das Ausmaß der Enzymhemmung basierend auf ihrer Auswirkung auf den jeweils assoziierten DNA-Reparaturweg quantifiziert und Unterschiede in der in vitro Arzneimittelpotenz der Inhibitorverbindungen detektiert.

Als nächstes habe ich CAT-R mit einem benutzerdefinierten CRISPR / Cas9-Array-Gen-Screening kombiniert, das auf 417 Gene abzielte, die an der DNA-Schadensantwort (DDR) beteiligt sind, und ihren Beitrag zur Auswahl der DNA-DSB-Reparatur getestet. Ich konnte die Rollen der etablierten Akteure der DSB-Reparatur bestätigen, deckte aber auch potenziell neuartige Komponenten der DSB-Reparatur auf. Außerdem habe ich herausgefunden, wie die Cas9-vermittelte DSB-Reparatur moduliert werden kann, um die Rate fehlerfreier Reparaturen zu erhöhen, was wichtige Auswirkungen auf die Erzeugung von Knock-Ins durch CRISPR / Cas9 haben kann.

Um neuartige PARP1-Wechselwirkungen innerhalb der DDR zu identifizieren, habe ich CAT-R schließlich auf dem benutzerdefinierten Array-Gen-Screen angewendet und mit der PARP-Hemmung kombiniert. Ich habe einen Gencluster entdeckt, der signifikant von der PARP-Hemmung beeinflusst wird, die einen Schlüsselschritt während der Endresektion reguliert, und dabei potenziell neue Wechselwirkungen von PARP1 mit DDR hervorgehoben. Außerdem

schlage ich die PARP-Hemmung als alternativen Ansatz vor, um die Chancen für ein erfolgreiches Knock-In zu erhöhen. Dies basiert auf meinen Experimenten, die zeigen, dass die PARP-Hemmung die Fehlerfreiheit in ähnlichem Maße erhöht wie andere bekannte Strategien.

Zusammenfassend zeige ich in meiner Dissertation wie CAT-R verwendet werden kann, um die Funktionen von DNA-DSB-Reparaturgenen zu bewerten und wie dieses DDR-Reportersystem an genetische und/oder chemische Screenings in einer Vielzahl von Zelllinien angepasst werden kann.

Table of Contents

Abbreviations

Alt-EJ	Alternative End Joining
ATM	Ataxia Telangiectasia Mutated
ATR	Ataxia Telangiectasia and Rad3 related
BER	Base Excision Repair
BFP	Blue Fluorescent Protein
bp	Base pair
Cas	CRISPR-associated genes
Cas9	CRISPR associated endonuclease 9
cDNA	Complementary Deoxyribonucleic Acid
Chr	Chromosome
c-NHEJ	Canonical Non-Homologous End-Joining
CRISPR	Clustered Regularly Interspaced Short Palindromic Repeats
crRNA	CRISPR RNA
DNA-PK_{cs}	DNA-dependent Protein Kinase, catalytic subunit
DSB	Double-Strand Break
FA	Fanconi Anemia
FACS	Fluorescent Activated Cell Sorting
GFP	Green Fluorescent Protein
gRNA	guide RNA
HDAC	Histone Deacetylases
HR	Homologous Recombination
IF	Immunofluorescence
InDel	Insertions/Deletions
IVT	In-vitro transcribed
LTGC	Long Tract Gene Conversion
MMEJ	Microhomology-Mediated End-Joining

MMR	Microhomology Mediated Repair
MOI	Multiplicity of Infection
NER	Nucleotide Excision Repair
NGS	Next-Generation Sequencing
NHEJ	Non-Homologous End Joining
nt	Nucleotides
PAM	Protospacer-Adjacent Motif
PARP	Poly ADP Ribose Polymerase
PCR	Polymerase Chain Reaction
pDNA	Plasmid DNA
PM	Point Mutation
RGN	RNA-guided Cas9 nuclease
RNP	Ribonucleoprotein
SSA	Single Strand Annealing
ssODN	Single Strand Oligodeoxynucleotide
SSTR	Single Strand Template Repair
STGC	Short Tract Gene Conversion
TALEN	Transcription-Activator Like Effector Nuclease
tracrRNA	Trans-activating crRNA
ZFN	Zinc-Finger Nuclease

List of scientific publications

Published Papers

Publications with the peer-review process:

1. **A solid-phase transfection platform for arrayed CRISPR screens**.

   Özdemirhan Serçin, Sabine Reither, Paris Roidos, Nadja Ballin, Spyridon Palikyras, Anna Baginska, Katrin Rein, Maria Llamazares, Thomas Muley, Renata Jurkowska, Amir Abdollahi, Frank T. Zenke, Beate Neumann, Balca R. Mardin, (2019): Accepted for printing in Molecular Systems Biology.

Submitted publications with the peer-review process:

2. **A scalable CRISPR/Cas9-based fluorescent reporter assay to study DNA double-strand break repair choice**.

   Paris Roidos, Stephanie Sungalee, Salvatore Benfatto, Özdemirhan Sercin, Amir Abdollahi, Jan Mauer, Frank T. Zenke, Jan O. Korbel, Balca R. Mardin, (2019): [In Revesion].

Presentations at International Conferences

1. The DNA-damage response in cell physiology and disease, EMBO Athens (2019).
2. AEK International Cancer Congress, EMBL Heidelberg (2019).

Introduction

Chapter 1

DNA repair & Cancer

The study of DNA repair is experiencing a remarkable time of interest with genome integrity to be a crucial aspect of cell survival. Some types of cells (cancer cells) can tip the balance of the cell cycle by creating a nonstop drive for proliferation. Throughout this process, cancer cells ignore or even override cell signals that instruct a naturally occurring DNA damage to repair successfully (Jackson and Bartek 2009; Khanna and Jackson 2001; Rich, Allen, and Wyllie 2000; Zhou and Elledge 2000). This behavior promotes cancer cell's mutagenesis, aggressiveness, and can even lead to treatment resistance (Curtin 2012; Tubbs and Nussenzweig 2017).

Fortunately, cells have developed specialized DNA repair pathways that can classify into the type of DNA damage they repair and collectively are known as the DNA Damage Response (DDR) (Lord and Ashworth 2012), and DDR plays a vital role in maintaining genome integrity. The investigation of DDR pathways has led to the identification of a complex system composing of sensors, transducers, and effectors that ensure the transduction of damage signaling, and activation of the appropriate responses such as DNA repair machinery, cell cycle arrest and apoptosis (Mondesert et al. 2015). The major DNA repair pathways are base excision

repair (BER), mismatch repair (MMR), nucleotide excision repair (NER), and double-strand break (DSB) repair (Sugawara and Nikaido 2014).

In this Ph.D. study, I developed a novel system to assess the DNA double-strand repair pathway choice and evaluate the importance of several DNA repair components after a DSB.

1.1. Hallmarks of Cancer

Cancer is a genetic disease that can be caused by the accumulation of mutations in the genome that arise through exogenous or endogenous sources like ionizing radiation (IR), genotoxic drugs, or such as reactive oxygen species (ROS), and problems encountered during DNA replication that trigger replication fork to collapse (Stracker, Usui, and Petrini 2009), (Rich et al. 2000). Elevated levels of DNA damage contribute to genomic instability, which is referred to as a "Hallmark of Cancer" (Hanahan and Weinberg 2000), (Hanahan and Weinberg 2011).

1.1.1. Genome instability and double-strand breaks

One crucial factor contributing to genomic instability is the formation of DNA double-strand breaks (DSBs) (Ceccaldi, Rondinelli, and D'Andrea 2016). These lesions are the most serious, toxic, and difficult to repair forms of DNA damage since they disrupt the continuity of the chromosome (Torgovnick and Schumacher 2015). If these lesions are not repaired correctly, they can lead to mutations, deletions, translocations, or genome amplification that scramble the encoded information (Costanzo et al. 2009). Therefore the repair of DSBs is fundamental to cell survival and uphold of genome integrity (van Gent, Hoeijmakers, and Kanaar 2001), (Khanna and Jackson 2001).

1.2. DNA double-strand breaks

The most common kinds of double-strand breaks are caused either due to breaks in replication forks when polymerase stall at the site of unrepaired base lesion or due to breaks in both DNA strands of the DNA double helix (Shibata et al. 2014a). Cells employ two distinct strategies for DNA double-strand break repair: end-resection and end-protection based mechanisms (Chiruvella, Liang, and Wilson 2013). The primary representative pathways of the two strategies are non-homologous end-joining (NHEJ), and homologous recombination (HR) (Bartek 2011; Huertas 2010; Knobel and Marti 2011).

The pathway choice depends on the cell cycle phase, the complexity of repair, and whether the damaged DNA ends are “blunt” (easy to re-join) or “dirty” (not-ligatable). Among others, the two pathways differ in their requirement for a homologous template DNA and the fidelity of DSB repair (Sugawara and Nikaido 2014). On the one hand, NHEJ is more error-prone (Lieber 2011), (Sugawara and Nikaido 2014) since it directly ligates the DNA broken ends after a DSB by forming small insertions or deletions (InDels). On the other hand, HR remains, in most cases, an error-free mechanism (Li and Heyer 2008) with its meticulous template-based activity to ensure the highest fidelity of repair. NHEJ is faster and is used more frequent on DSBs since it is more available than HR. Consequently, NHEJ is considered to be a source of genomic instability (Bunting and Nussenzweig 2013). Besides, NHEJ can operate during any cell cycle phase but is most active in G0 and G1 cell cycle phase, just before DNA replication, whereas HR activity occurs during S and G2 phases, right after replication (Lord and Ashworth 2012; Marnef and Legube 2017; Torgovnick and Schumacher 2015; Zhou and Elledge 2000).

Collectively, all DNA repair pathways follow five steps of repair: (i) recognition, (ii) recruitment, (iii) removal, (iv) reconstruction, and (v) reinstatement with some repair pathways to be more active in certain parts of the cell cycle than others (Sugawara and Nikaido 2014), (Mondesert et al. 2015).

1.2.1. Nonhomologous End-Joining

Nonhomologous end-joining (NHEJ) is one of the DNA repair pathways that the cells are using to repair DSBs. The term "non-homologous" refers to the lack of requirement for a DNA template, whereas the term classical is often used to highlight the preferred choice among other NHEJ pathways (Haber and Moore 1996). In comparison to HR that is restricted to post-DNA replication phases of the cell cycle, classical-NHEJ is active throughout the cell cycle and re-joins DSB ends with minimal processing (Lieber 2011). It does not search for or use a large segment of DNA, and the repair proceeds quickly with the potential for loss of nucleotides from either side of the DSB junctions or base-pair changes at the breakpoint sequence.

In simple terms, c-NHEJ initially align and protects the DSB ends, minimally processes the damage by removing un-ligatable DNA ends, and fills the break in a fast and potentially erroneous way (Lieber 2011; Liu and Huang 2016; Shibata et al. 2014b).

Data from several studies suggest that classical NHEJ often does a more accurate job than initially thought (Davis and Chen 2013; Lieber 2011). Repair of clean breaks usually does not result in any information loss of chromosomal rearrangements, but repair of "dirty" breaks can result in loss of genetic information (Bétermier, Bertrand, and Lopez 2014). Typically, DSB junctions that are repaired by c-NHEJ display evidence of small deletions of 1 - 4 bp at the breakpoints.

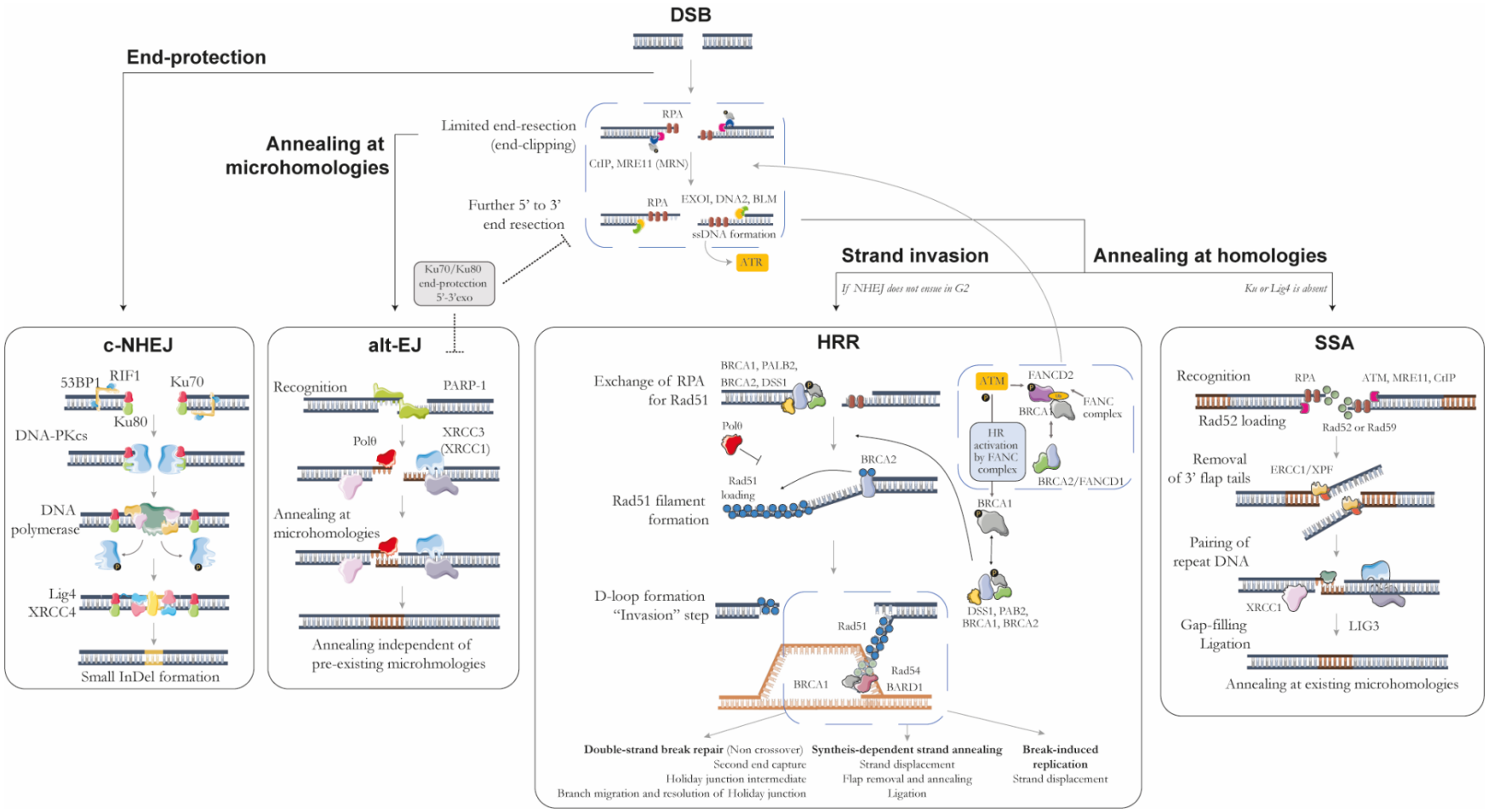

Figure 1: Schematic overview of the pathway choice after a double-strand break. Two distinct repair mechanisms dictate the DSB repair. End-protection mechanisms (NHEJ) favor a quick repair with the creation of small InDels, whereas end-resection mechanisms act in multiple ways. After the limited end-resection, alt-EJ can process the repair by annealing the broken DNA at microhomologies, creating small InDels. If further resection occurs, then it is possible to anneal the broken DNA at homologies that can extend up to 400 bp. This type of repair leads to large fragments of DNA to be lost. Strand invasion will take place if NHEJ does not fix the damage in G2. This type of repair requires a template from which an original copy will be used to fix the repair.

The eukaryotic Ku70/Ku80 heterodimer (*XRCC6, XRCC5*) is a damage sensor that initiates protection of the double-stranded break (Ferguson et al. 2000), (Difilippantonio et al. 2000), (Bunting and Nussenzweig 2013) by forming a ring around the DNA ends recruiting several proteins for end-processing (**Figure 1**). One of them is the DNA-dependent protein kinase catalytic subunit (DNA-PK_{cs}) that plays a central role in c-NHEJ repair (Chirgadze et al. 2017). The actions of DNA-PK_{cs} are setting up the stage for the assembly of the actors in c-NHEJ, which include Artemis, XRCC4/DNA ligase IV complex, and XLF (Lieber 2011; O'Driscoll and Jeggo 2006; Ochi et al. 2010). Given the importance of DNA-PK_{cs} in c-NHEJ repair, it is safe to assume that it also dictates the rate of c-NHEJ acting as a rate-limiting step of the repair process.

The end-processing step of the c-NHEJ repair includes nucleases such as Artemis, a 5' to 3' endonuclease, which is activated by DNA-PK_{cs} phosphorylation (Moshous et al. 2001). The complex that creates a filament to bridge the broken ends is the XRCC4/DNA ligase IV, and XLF complex (**Figure 1**). After the initial end-processing step, the XRCC4/DNA ligase IV complex promotes efficient ligation since DNA ligase IV (LIG4) has the necessary plasticity to ligate across DNA gaps and re-join incompatible DNA ends (Grawunder et al. 1997). The DNA repair protein NHEJ1 (also known as XLF) also interacts with XRCC4 and increases the efficiency of LIG4 DNA ligations (Buck et al. 2006).

It has been noted that in mammalian cells, the active component of c-NHEJ is highly efficient (typical half times of 15 - 30 min) and is responsible for repairing ~ 70% of DSBs (Daley et al. 2014; Deriano and Roth 2013).

Alternative End-Joining

Based on the current literature, there are two types of potential end-joining outcomes. One that is formed by a direct ligation of DNA ends (c-NHEJ), and another occurs in the absence of Ku70/Ku80 dimer, bears small sections of microhomology at the sites close to DSB (Roth, Porter, and Wilson 1985), (Roth and Wilson 1986), (Boulton and Jackson 1996a), (Boulton and Jackson 1996b). In the literature, the emergence of three different names assigned to alternative EJ repair has been used interchangeably: backup NHEJ, microhomology-mediated end-joining (MMEJ), and noncanonical NHEJ. Throughout this Ph.D. thesis, the name alternative end-joining (alt-EJ) is used, which reflects its independence for c-NHEJ (Dueva and Iliakis 2013; Frit et al. 2014).

Previous studies have reported that alt-EJ may actively compete with both c-NHEJ and HR repair. Biochemical data (Wang et al. 2003), (Daley and Wilson 2005) show that DSBs can be repaired independently of the Ku-mediated c-NHEJ repair mechanism and instead require an alternative end-joining (alt-EJ) pathway that uses 6 to 8 bp of microhomology as an intermediate step (Bunting and Nussenzweig 2013), (Gomez-Cabello et al. 2013). Studies show that DNA resection, which is a prerequisite for the microhomology intermediate step, only happens in the S and G2 phase and it is inhibited by Ku70/Ku80 heterodimers (Liu and Huang 2016).

The first responders to alt-EJ repair are poly [ADP-ribose] polymerase 1 (PARP1) and p53-binding protein 1 (53BP1) (**Figure 1**). However, the DSB repair protein MRE11 and the DNA endonuclease RBBP8 (CtIP) are also implicated in the initial end-resection step (Mojumdar et al. 2019; Stracker and Petrini 2011). Recent studies identified DNA polymerase Q (POLQ) as a possible player in alt-EJ (Malaby et al. 2017) with DNA ligase I (LIG1) or DNA ligase III

(LIG3) to perform the final DNA ligation step (Pace et al. 2010). The LIG3 cofactor, XRCC1, is also implicated in alt-EJ (Bunting et al. 2012). However, the exact mechanism of repair is still unknown, with several players of alt-EJ to be missing (**Figure 1**).

Evidence suggests that c-NHEJ causes a low rate of translocations, but when absent, alt-EJ becomes active and produces an increased number of chromosome rearrangements (Howard H.Y. Chang et al. 2017). Therefore alt-EJ is of particular interest in research since its microhomology signatures are reported at the breakpoints of chromosomal rearrangements in human cancer cells (McVey and Lee 2008), (Tsai et al. 2008), (Bunting and Nussenzweig 2013). There are some features that characterize the alt-EJ pathway. Initially, the DNA repair results in higher rates of deletions, with or without signs of neighboring microhomology sequence. Consequently, lower rates of fidelity are anticipated.

1.2.2. Homologous Recombination

Upon DNA double-strand breaks, homologous recombination repair (HR) mediates accurate repair, protects the genome from chromosomal rearrangements or gross chromosomal loss, and cell death in a complicated template-directed repair (**Figure 1**). HR factors contribute to the protection and duplication of the genome fundamentally with mutations in HR gene, to have been linked to carcinogenesis (Bunting and Nussenzweig 2013; Li and Heyer 2008; Shibata et al. 2014a).

HR matches the break ends to an intact DNA molecule of identical or near-identical DNA sequences. The pathway can be broken down into four stages: (1) DNA end resection, (2) RAD51 filament formation on the newly created single-stranded DNA overhang, (3) RAD51

dependent strand exchange between the broken DNA and the intact sequence donor, (4) DNA repair synthesis and resolution of the joint molecule repair intermediate.

The first step of HR is the activation of checkpoint kinases by the MRE11-RAD50-NBS1 (MRN) complex. This action arrests the cell cycle and simultaneously recruits additional DNA repair proteins at the DSB end. During the initial end-resection, MRN generates a single-stranded DNA (ssDNA) that is important for initiating homologous recombination (**Figure 1**). This step commits the DNA repair to HR and simultaneously prevents NHEJ from interfering. Together, those steps of creating small overhangs are called "presynapsis" (Ceccaldi et al. 2016; Gudmundsdottir and Ashworth 2006; Shibata et al. 2014a). The occurring ssDNA extends way past the original DSB point with replication protein A (RPA1) molecules to coat and protect the exposed stretch of DNA.

The above step is a crucial feature for enabling Rad51 filament to attach to the ssDNA's 3' end and to search for an area of homology on the sister chromatid (**Figure 1**). Once Rad51 identifies an area of homology, it attacks the homologous sequence and transfers part of its DNA strand. Rad51 pulls part of the DNA strand and creates a DNA heteroduplex (D-loop). During this process, Rad51 superintendents the exchange and pairing of the homologous DNA sequence with the sister chromatid. Several proteins are involved in protecting the broken DNA ends from nuclease activity, enabling the strand invasion and filament migration, and guarantee the synthesis of more than 50 newly synthesized nucleotides (**Figure 1**).

1.2.3. Single-Strand Annealing

Single-strand annealing (SSA) is a DNA repair process that initiates when a double-strand break occurs among two repeated sequences (Bhargava, Onyango, and Stark 2016; Raphael, Beatrice, and D'Andrea 2016). Single-stranded regions are created adjacent to the DNA break (**Figure 1**). If they extend until the repeated sequences, then the complementary strands can anneal to each other. This annealed intermediate can be processed by digesting the single-stranded tails and filling in the gaps. The smallest homology reported is at 29 bp, but it can reach much more than hundreds of bps (Bennardo et al. 2008; Ceccaldi et al. 2016; Howard H. Y. Chang et al. 2017).

The DNA repair protein Rad52 is required for recombination processes, including SSA (**Figure 1**). It possesses the ability to bind to the 3' ends of DNA (Sugawara et al. 2002). Rad59 is a homolog of Rad52, and it is also required for SSA since it possesses the same DNA binding properties and strand annealing activity as Rad52 (Chakraborty et al. 2016; George and Alani 2012). RPA is another DNA binding factor implicated at SSA. The RPA complex is required to coat the single-stranded DNA ends. Interestingly, Rad51 is not required for SSA since it is involved in strand invasion and hence is not expected to play a role in SSA, where two strands interact by intertwining around each other (Howard H. Y. Chang et al. 2017; Mansour et al. 2008).

The mismatch repair proteins MSH2 and MSH3 are also required for efficient SSA. They remove the non-homologous 3' tails from the annealed intermediate during the repair process (Eichmiller et al. 2018). MSH2 and MSH3 complex has a strong preference for recognizing "loop-out" structures such as those formed by frameshift replication errors. Possibly MSH2

and MSH3 bind to the branched junction between the single and double-stranded DNA (Sugawara et al. 2002, 2004). The complex stabilizes the annealed intermediate and signals the endonuclease to cleave the single-stranded tail. MSH2 and MSH3 may act to stabilize junction where the repeat sequences are small, e.g., 0.2 kb (Bennardo et al. 2009; George and Alani 2012).

1.2.4. The battle between end-protection and end-resection

Previous studies have reported that the first responder to a DSB is the damage sensor complex MRN familiar to both HR and NHEJ (Shibata et al. 2014a). Its configuration appears to influence the pathway choice. Resection of the 5' DNA strand is a requirement and a definitive commitment to DNA double-strand break repair by HR (Dimitrova and de Lange 2009; Gu, Lin, and Hong 2017; Liu and Huang 2016; Shibata et al. 2014b). On the other hand, NHEJ factor Ku70/Ku80 binds and protects DNA ends to favor for a quick DNA re-ligation (**Figure 2**). The balance between p53-binding protein 1 (53BP1) and breast cancer type 1 susceptibility protein (BRCA1) mediates the extent of end-resection since BRCA1 antagonizes 53BP1 to promote resection in the S and G2 cell cycle phase (Escribano-Díaz et al. 2013; Grabarz et al. 2013; Liu and Huang 2016; Zhang and Jasin 2011). MRE11 and retinoblastoma-binding protein 8 (RBBP8, also known as CtIP) mediate the initial limited end-resection step (end clipping) and typically results in resection of 20 bp or less. This short resection tips the balance of DNA double-strand break repair pathway choice from NHEJ in G1 towards HR in S and G2 phase of the cell cycle. At a time when the newly synthesized sister chromatid can act as a homologous repair template. The second, more extensive phase of end-resection (**Figure 2**), is mediated by exonuclease 1 (EXO1), BLM RecQ like helicase (BLM), DNA replication

Helicase/Nuclease 2 (DNA2), and WRN RecQ like helicase (WRN) that definitely commits the choice to HR or SSA, but not to alternative end-joining repair (Liu and Huang 2016; Shibata et al. 2014b; Wang et al. 2015). What is not yet clear is the connection between other components or even pathways of the DDR that can modify the DSB repair choice.

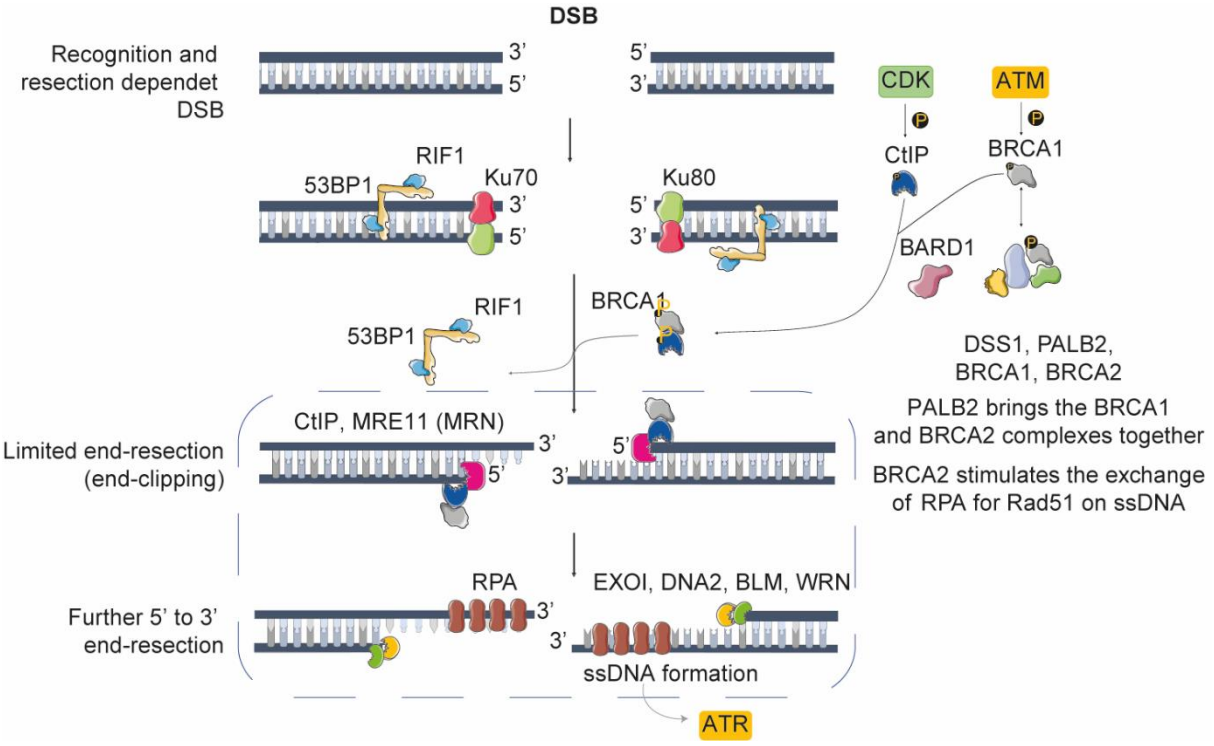

Figure 2: The battle between End-protection and End-resection. Schematic illustration of the immediate steps after the induction of a double-strand break (DSB). 53BP1 and RIF1 stabilize the broken ends to favor a fast ligation initiated by Ku70/Ku80 dimer. BRCA1 and CtIP are antagonizing 53BP1 and RIF1 to enable end-resection.

Chapter 2

Clinical inhibitors: Targeting DNA repair

2.1. Small pharmacological compounds

The use of specific DNA repair inhibitors targeting prominent DNA repair kinases in cancer treatment is rapidly expanding as a therapeutic strategy. Therefore, the development of additional small pharmacological compounds is rapidly moving through the preclinical developmental pipeline. Several studies describe the selectivity, efficacy, and cytotoxicity of various inhibitors *in vitro* or *in vivo*. There are a handful of DDR inhibitors and they typically require a different type of *in vitro* test to evaluate their level of engagement in the choice of DNA repair.

In this Ph.D. study, I performed experiments to compare several different compounds with the same *in vitro* DNA repair assay. I present interesting differences within compounds of the same class and address specific aspects of pharmacodynamics that can explain how the inhibitors can tip the balance of DNA repair choice.

2.1.1. Targeting end-protection with DNA-PK$_{cs}$ inhibitors

DNA-dependent protein kinase, catalytic subunit (DNA-PK$_{cs}$) has a pivotal role in c-NHEJ and the regulation of DNA damage response. In humans, it is encoded by the gene designated as *PRKDC*. It is a DNA-activated serine/threonine-protein kinase, abundantly expressed in almost all mammalian cells, and it functions as the catalytic subunit of the DNA-PK holoenzyme (Dungl, Maginn, and Stronach 2015). DNA-PK$_{cs}$ belongs to the phosphatidylinositol-3-OH kinase (PI(3)K)-related protein (PIKK) superfamily (Jiang et al. 2015). It is a colossal single-chain protein of 4128 amino acids (Moshous et al. 2001).

During the NHEJ process, DNA-PK$_{cs}$ interacts with Ku70/Ku80 heterodimers regulating a series of complex events: (1) the synapsis, (2) end-processing and (3) ligation (Lieber 2011). The Ku70/Ku80 dimer has a ring-like structure that binds first to the DNA break encircling the DNA end and allows the dimer to translocate along the duplex (Walker, Corpina, and Goldberg 2001). DNA-PK$_{cs}$ is recruited through interaction with the Ku80 C-terminus (Alt et al. 1992; Gell and Jackson 1999) and two DNA-PK$_{cs}$ complexes are required to hold the DNA ends close together (Chirgadze et al. 2017). The DNA-PK$_{cs}$ kinase is activated once associated with the Ku70/Ku80 dimer and the DNA terminus. Besides, DNA-PK$_{cs}$ can auto-phosphorylate, enabling a conformational change that releases the DNA ends and makes them available to other factors, including NHEJ components involved in DNA end-processing and ligation steps. DNA-PK$_{cs}$ kinases allow the DNA DSB to be repaired promptly when a sister chromatid is unavailable, a process that is also used in V(D)J recombination (Alt et al. 1992). As such, DNA-PK$_{cs}$ act as a “doorkeeper” that protects DNA ends from initial processing and ligation, until the two broken ends are correctly positioned (Costantini et al. 2007; Dip and Naegeli

2005; Jette and Lees-Miller 2015; Um et al. 2003). End-processing of complex DSBs requires trans-phosphorylation of DNA-PK_{cs} by ATM serine/threonine kinase. This activation serves to recruit Artemis endonuclease to the site of DNA damage. DNA-PK_{cs} phosphorylation may also affect DSB repair pathway choice since it has been shown that cells deficient in DNA-PK_{cs} demonstrate increased levels of HR-mediated repair of DSBs (van Oorschot et al. 2016). The activity of DNA-PK_{cs} kinase can also be stimulated by poly (ADP-ribose) polymerase (PARP), independently of the Ku70/Ku80 complex suggesting that PARP, in addition to its crucial role in BER, may additionally facilitate DNA DSB repair via inhibitory regulation of DNA-PK_{cs} (Ruscetti et al. 1998).

DNA-PK_{cs} is an attractive therapeutic target for cancer. In 1994, Lilly Pharmaceuticals reported the compound LY294002 as an inhibitor of PI3K (Velic et al. 2015). Despite LY294002 side-effects (*in vivo* cytotoxicity), its structure paved the way for the development of more potent and selective DNA-PK_{cs} ligands with improved physicochemical properties like the KU-0060648 and M3814 compounds (Harnor, Brennan, and Cano 2017). DNA-PK_{cs} inhibitors are tested clinically in solid tumors and hematological malignancies both as a monotherapy and combination with chemotherapy or radiotherapy (Klein et al. 2017). For instance, radiation therapy becomes one of the significant ancillary methods of liver cancer therapy (Pascale et al. 2016). Liver cancer cells repair their damaged DNA predominantly by non-homologous end-joining (Yang et al. 2016). Upon DNA-PK_{cs} inhibition, those cells with simultaneous administration of ionizing irradiation result in unresolved double-strand breaks in the genomic DNA of the target cells that lead to tumor cell death (Dolman et al. 2015).

2.1.2. Targeting ATM-CHK2 axis as a therapeutic target in cancer

As discussed earlier, the protection of the genome by DNA repair factors is rooted in a broader cellular response known as the DNA damage response. The ataxia-telangiectasia mutated serine-threonine kinase (ATM) signaling pathway is well conserved and is central to the maintenance of genome integrity (Awasthi, Foiani, and Kumar 2016). ATM kinase belongs to the phosphoinositide 3-kinase (PI3K)-related kinase (PIKK) family along with DNA-PK_{cs} and it phosphorylates proteins containing Ser or Thr residues that are followed by Gln (Bakkenist and Kastan 2004). ATM triggers a phosphorylation cascade that sets in motion a series of post-translational protein modifications that in the majority of the cases upregulate the cell cycle checkpoint pathways (Bakr et al. 2015; Batenburg et al. 2017; Geuting, Reul, and Löbrich 2013; Muraki et al. 2013). Once the DNA damage is induced, the ATM-CHK2 (checkpoint kinase 2) axis controls the G2/M checkpoint by delaying mitosis and allows cells to avoid the toxic levels of genome instability. In addition, ATM plays a part in the local response to DNA DSB (**Figure 3 A**). Even though ATM is the master kinase of the DNA damage response, it is not the first protein to arrive at a DNA double-strand break. As previously described, the MRN complex rapidly binds to the chromosomal breaks and acts as the primary sensor. Among other targets, ATM phosphorylates the histone variant H2AX which is also phosphorylated by DNA-PK_{cs} (Dimitrova and de Lange 2009; Geuting et al. 2013; Mansour et al. 2008; Rybanska-Spaeder et al. 2013).

ATM has long been considered as a potential drug target for cancer therapy since it is a facilitator of DNA damage response and is considered as a tumor suppressor (Kandoth et al. 2013). However, the generation of specific inhibitors for ATM is a difficult mission. The initial

compounds that have been used to inhibit ATM were pan-PI3K inhibitors like LY294002, caffeine, and wortmannin (Sarkaria et al. 1998, 1999). More specific ATM inhibitors have been developed over the years such as KU-55933, KU-60019, and KU-559403 (Batey et al. 2013; Fokas et al. 2012; Guo et al. 2014; Toledo et al. 2011). Recent evidence shows promising results that inhibition of ATM can sensitize cells to ionizing radiation (Klein et al. 2017; Ronco et al. 2017), therefore efforts to develop potent and selective compounds are still ongoing.

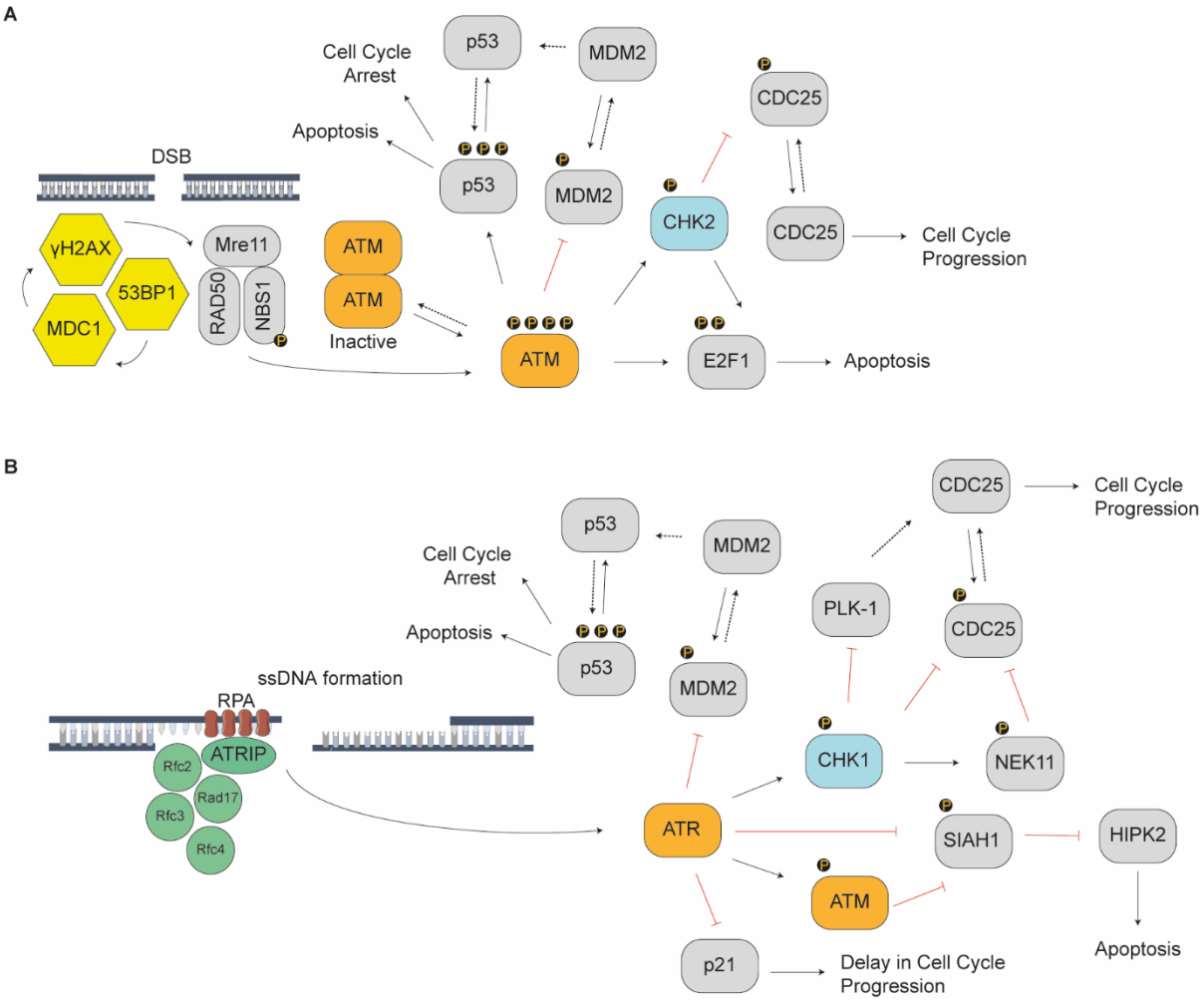

Figure 3: The ATM and ATR cell signaling axis. Schematic overview of the (**A**) ATM-CHK2, and (**B**) ATR-CHK1 axis. Illustration adapted from (Feehan and Shantz 2016), (Zhao et al. 2018).

2.1.3. Targeting ATR-CHK1 axis as a therapeutic target in cancer

Further vital components of the DDR are the ATM and Rad3-related serine-threonine kinase (ATR) and checkpoint kinase 1 (CHK1) (Rundle et al. 2017) that link DNA lesions to cell cycle checkpoint and repair. These protein kinases play a critical role since knock-out of ATR or CHK1 is lethal in early embryonic life (Brown and Baltimore 2000; Takai et al. 2000). The presence of single-stranded DNA (ssDNA) activates ATR and typically, ssDNA arises from stalled replication forks, nucleotide excision repair (NER) intermediates or resected DSBs that have been subject to exonuclease digestion. Therefore, ATR is suggested to play a role in both DNA damage repair and cell cycle checkpoint regulation. Besides, ATR kinase is as well a member of the PIKK family, exhibiting a similar structure to ATM and DNA-PK_{cs}. The primary phosphorylation target of ATR is CHK1 (**Figure 3 B**). Both ATR and CHK1 are responsible for transducing the signal to reduce replication stress and indicate single-strand DNA. Both are closely linked to DNA repair by regulating end-resection pathways. Early studies have shown that ATR-CHK1 signaling pathway phosphorylates and activates the critical homologous recombination repair (HR) regulatory protein BRCA1 (Tibbetts et al. 2000) and protects cells from 5-fluorouracil cytotoxicity (Fujinaka et al. 2012). Furthermore, it is reported that the depletion of ATR reduces the efficiency of HR in a DNA DSB repair reporter assay (Bakr et al. 2015; Fujinaka et al. 2012).

The functions of the S phase checkpoint proteins ATR, CHK1, and WEE1 become critically important in cancer with loss of G1 cell cycle checkpoint control. Those proteins ensure that significant time is provided to deal with replication problems and that the appropriate pathways of replication fork recovery are activated, avoiding premature mitosis. This results in the S and

G2 checkpoints dependency by the cells, a strategy that may be exploited by inhibiting the ATR, CHK1 and WEE1 kinases in cancer cells. Even if the early ATR and CHK1 inhibitors, such as UCN-01, were not specific enough (Senderowicz 2000), the most recently developed inhibitors exhibit greater potency and higher selectivity against its prospective targets, with new ATR inhibitors (AZD6738, M6620) to enhance tumor cell killing (Jin et al. 2018; Sarkaria et al. 1999).

Wee1 is an essential target of CHK1 acting as an inhibitor of CDK1 and takes part in the ATR-CHK1 pathway in multiple ways. A selective small-molecule inhibitor of WEE1 (MK-1775, now known as the AZD1775; IC_{50}= 5 nM) has been identified from a high-throughput screen based on an *in vitro* kinase assay (Garcia et al. 2017; Jin et al. 2018). The AZD1775 inhibitor causes G2/M checkpoint release after DNA damage, and it has demonstrated increased cytotoxicity in combination with specific chemotherapeutic drugs such as gemcitabine, platinum compounds, and topotecan in p53-deficient cells. Besides, it has shown antitumor efficacy in xenograft models and patient-derived tumor explants *ex vivo* (Hirai et al. 2009), (H. Kim et al. 2016). It has been reported that the AZD1775 compound inhibits WEE1, proto-oncogene tyrosine-protein kinase (YES1), protein kinase membrane-associated Tyrosine/Threonine 1 (PKMYT1) kinases as well as polo-like kinase1 (PLK1) with similar potency as the intended target WEE1 itself (Hirai et al. 2009; Wright et al. 2017). WEE1 kinase has been used for targeted molecular therapy of gastric cancer (H. Kim et al. 2016). The small-molecule inhibitor of WEE1, AZD1775 synergizes with a PARP inhibitor (Olaparib) by impairing HR and enhancing DNA damage and apoptosis in acute myeloid leukemia (AML) (Garcia et al. 2017).

2.1.4. HDAC inhibitors in cancer development and therapy

Epigenetic abnormalities have been linked with some classical "Hallmarks of Cancer" underlying a close connection between genetic and epigenetic mechanisms during the development of cancer (Li and Seto 2016), (Flavahan, Gaskell, and Bernstein 2017). Epigenetic mechanisms are implicated in critical steps of cancer such as tumor suppressor silencing or oncogene activation by repurposed enhancers or even cell fate transitions.

Histone acetylation is a process that is controlled by histone acetyltransferases (HATs) and histone deacetylases (HDACs). HDACs remove acetyl group and can alter transcription of oncogenes and tumor suppressor genes. In addition, HDACs deacetylate numerous nonhistone cellular substrates that govern a wide array of biological processes (Li and Seto 2016). Several studies implicate histone deacetylases (HDAC) during modulating the acetylation status of histone and nonhistone proteins (Barneda-Zahonero and Parra 2012; Chun 2015; Yang and Seto 2007). Post-translational modification of histones and non-histone proteins modulate gene transcription, chromatin remodeling, and nuclear architecture which are involved in the regulation of cell cycle, apoptosis, DDR, metastasis, angiogenesis, autophagy, and other cellular processes (Li and Zhu 2014), (Li and Seto 2016). There are 18 potential human HDACs grouped into four classes (class I, II, III, IV), with most of them to be involved in several different stages of cancer.

More specifically, HDAC1 and HDAC2 are recruited to DNA-damage sites to deacetylate histones H3K56 and H4K16, and to facilitate nonhomologous end-joining (c-NHEJ) (Miller et al. 2010). This behavior suggests a direct role for these two enzymes during DNA replication and double-strand break (DSB) repair. Moreover, HDAC3 is associated with DNA-damage

control, even if it is not localized to DSB DNA-damage sites. Besides, it is shown that class I HDACs can regulate other proteins that are involved in the DNA-damage response as well; including ATM, ATR, and BRCA1 (Thurn et al. 2013). Also, HDAC9 and HDAC10 are reported to be required for homologous recombination (HR) (Li and Seto 2016).

To date, numerous synthetic or natural molecules that target classes I, II, and IV enzymes have been developed and characterized, although interest in the class III family is increasing. Currently there are numerous HDACi under clinical development, which can be divided into three groups based on their specificity: (1) the nonselective HDACi, such as Vorinostat and Panobinostat; (2) the selective HDACi such as class I HDACi (Entinostat) and (3) the multi-pharmacological HDACi (Li and Seto 2016).

Vorinostat (SAHA) was the first HDACi to be approved by the FDA to treat cutaneous T-cell lymphoma (CTCL) in 2006. Since then, three more HDACi (Romidepsin, Belinostat, Panobinostat) have been approved for the treatment of different cancer types such as CTCL, peripheral T-cell lymphoma (PTCL) and multiple myeloma (MM) respectively (Li and Seto 2016).

Histone deacetylase (HDAC) inhibitors have shown to sensitize breast and ovarian cancer cell lines to PARP inhibition and cisplatin, in part via depletion of BRCA1 (Thurn et al. 2013). As the induction of BRCAness through BRCA1 downregulation mediated by HDAC, pan-HDAC inhibitors have been shown to cause transcriptional downregulation of RAD51 (House, Koch, and Freudenreich 2014). Current evidence suggests that HDAC inhibitors have a rather pleiotropic effect on HR genes and other cellular pathways (Chen et al. 2017). HDAC inhibitors decrease the protein levels of several HR factors, such as BRCA1 and BRCA2, RAD51 (Stengel and Hiebert 2015).

2.1.5. PARP inhibitors: Synthetic lethality in the clinic

The nuclear enzyme poly(ADP-ribose) polymerase (PARP-1) is an essential target in cancer therapy, and it is acknowledged that inhibiting PARP in patients could also have therapeutic potential in the treatment of many other diseases (Ray Chaudhuri and Nussenzweig 2017).

PARP is a superfamily of proteins localized in the nuclei. So far, three members of this family have been recognized to have a role in DNA repair, with PARP1 leading that activity. PARP1 is also known as a molecular nick-sensor, and it is part of the enzymatic machinery of the BER pathway (Wood and Doublié 2016). PARP1's role is to sense SSBs, assess the extent of their damage, decide whether the damage can or should be repaired, and approve the repair or trigger apoptosis (**Figure 4**). PARP1 "flags" the damaged DNA by binding to the damaged site. Then it undergoes a conformational change, which recruits proteins to relax the chromatin, scaffold the damage, and repair the site (Bourton et al. 2017; Brown et al. 2017; Forst et al. 2013; Gu et al. 2017). PARP is inactive until bound to a DNA strand break. This binding activates the enzyme creating a negatively charged target at the SSB which recruits the enzymes required to form the BER multiprotein complex. This complex is made up of XRCC1, LIG3, and the DNA polymerase POLβ (Wood and Doublié 2016).

Briefly, PARP inhibition stalls BER machinery, which causes unrepaired SSBs to accumulate (**Figure 4**). Typically, BER machinery repairs this type of DNA damage, but if PARP is inhibited the DNA repair process is channeled to the DSB repair pathways. PARP1/2 activates XRCC1 in the HR pathway and is involved in a regulatory feedback loop with BRCA1. Simultaneously, PARP1/2 seems to inhibit the NHEJ pathway by inactivating DNA-PK_{cs} and the activity of ATM's checkpoint. Although PARP's overall contribution to the canonical

NHEJ pathway is still uncertain, collectively, PARP's actions can affect which DSB repair pathway is selected (Brenner et al. 2011; Bryant and Helleday 2006).

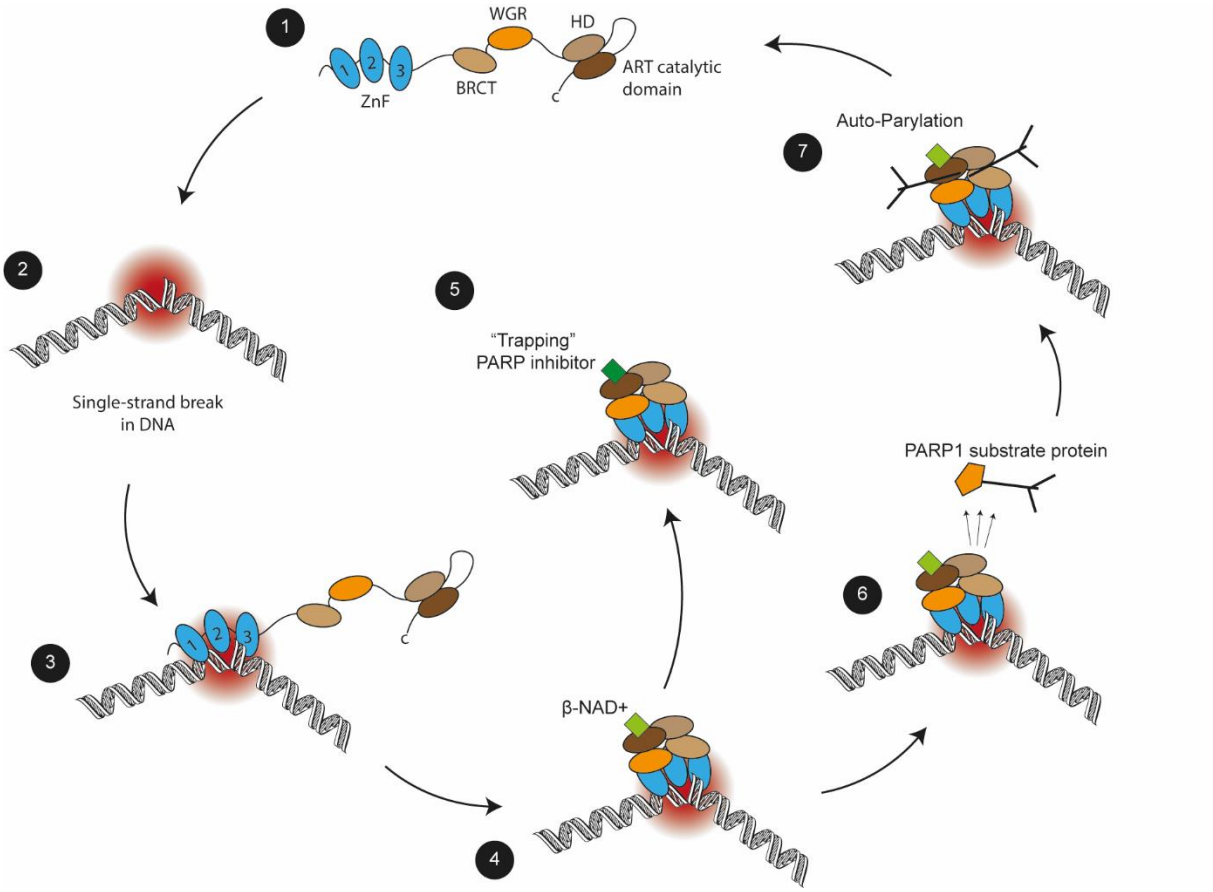

Figure 4: A model describing the PARP catalytic cycle. Schematic overview of PARP processing. Step (**1**) illustrates the non-DNA bound state of PARP1. It exists in a relatively disordered conformation, commonly referred to as "beads on a string". PARP1 structure entails three zinc finger–related domains (ZnF 1, 2, and 3): the BRCA1 C-terminus domain (BRCT); the tryptophan-, glycine-, arginine-rich domain (WGR); and the catalytic domain, which encompasses two subdomains; a helical domain (HD) and an ADP-ribosyltransferase (ART) catalytic domain. In this non-DNA bound state, HD acts as an autoinhibitory domain preventing binding of the PARP-superfamily cofactor, β-NAD^+, to its ART binding site. (**2**) Damage of the DNA double helix often causes the formation of SSBs that change the normal orientation of the double helix and provides a binding site for DNA binding PARP1 ZnF domains (**3**). The interaction of ZnF 1, 2, and 3 with DNA initiates a stepwise assembly of the remaining PARP1 protein domains onto the PARP1/DNA nucleoprotein structure (**4**). During this process leads to a change in HD conformation results in the loss of its autoinhibitory function, thus allosterically activating PARP1 catalytic activity. In step (**6**) the ART catalytic activity drives the PARylation of PARP1 substrate proteins, mediating the recruitment of DNA repair effectors, chromatin remodeling, and eventually DNA repair. In step (**7**) PARP1 auto-PARylation causes the release of PARP1 from DNA and the restoration of a catalytically inactive state. In step **5**, PARP is trapped on DNA and blocks the replication fork to progress and requires HRR for repair. Several clinical PARPi, each of which binds the catalytic site, prevent the release of PARP1 from DNA, "trapping" PARP1 at the site of damage, potentially removing PARP1 from its normal catalytic cycle. Figure adapted from (Lord and Ashworth 2017).

Cells that are missing both alleles of BRCA1 or BRCA2 have no HR functionality, which leaves repairs in the hands of NHEJ. Its limited ability to repair extensive DSB damage leads to cell death. Poly ADP-ribose polymerase (PARP) inhibitors are the first clinically approved drugs that exploit the concept of synthetic lethality (Hengel, Spies, and Spies 2017; Konstantinopoulos et al. 2015; Minchom, Aversa, and Lopez 2018). Almost 40 years ago, it was shown that small nicotinamide analogs inhibit PARylation and enhance the cytotoxicity of dimethyl sulfate, a DNA damaging agent (Durkacz et al. 1980; Purnell and Whish 1980; Terada et al. 1979). Subsequent efforts to the development of clinical PARP inhibitors led to the first generation of compounds, such as Rucaparib (Pfizer/Clovis), Niraparib (Merck & Co./Tesaro), Olaparib (KuDOS Ltd/AstraZeneca plc.), and Veliparib (Abbvie) (Lord and Ashworth 2017). A second more potent generation of PARP inhibitors was developed recently, Talazoparib (Lead/Biomarin/Medication/Pfizer) (Hopkins et al. 2015).

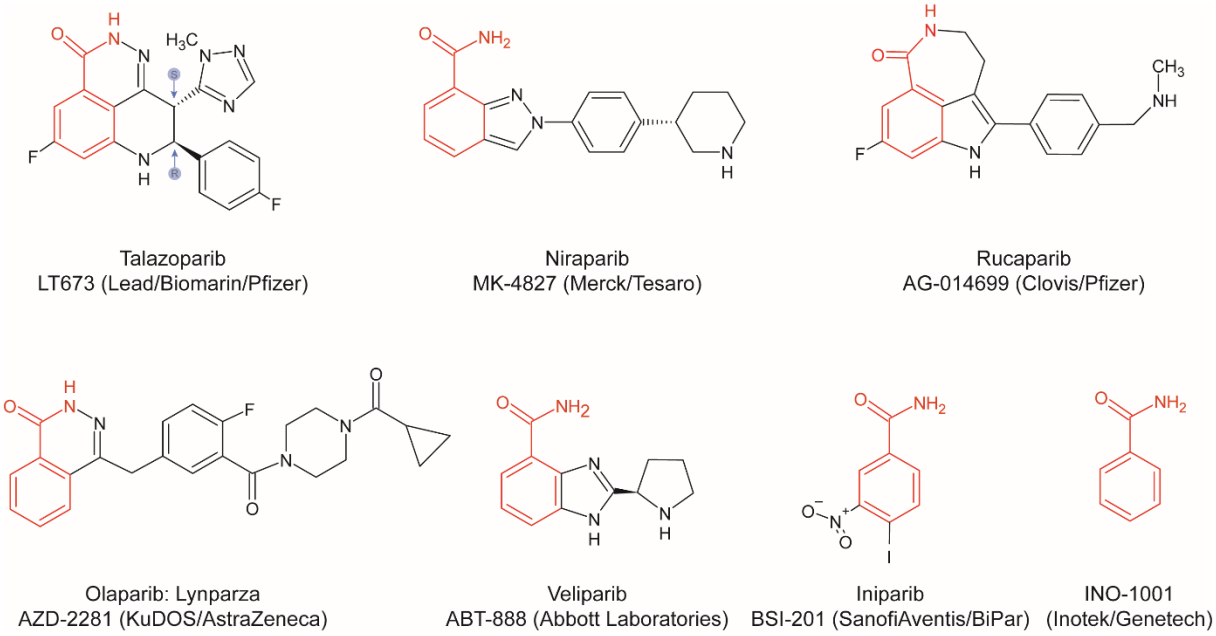

Figure 5: Clinical PARP inhibitors. Structures of seven clinical PARP inhibitors are shown. The ability of each PARPi to trap PARP1 on DNA differs and broadly correlates with cytotoxic potency. The nicotinamide moiety common to PARPi is shown in red. The blue arrows indicated the racemic centers for Talazoparib, explaining the selectivity of the active enantiomer. Figure adapted from (Pommier, O'Connor, and De Bono 2016).

All PARP inhibitors interact with the binding site of the PARP enzyme cofactor, β nicotinamide adenine dinucleotide (β-NAD+), in the catalytic domain of PARP1 and PARP2 (**Figure 5)**. However, clinically used PARP inhibitors have different abilities to trap PARP1/2 on DNA. It has been shown that a group of compounds that are among the first developed PARP inhibitors (INO-1001, Iniparib, Veliparib) do not possess any PARP trapping activity and therefore they are no longer considered potent PARP inhibitors (Lord and Ashworth 2017). Overall, PARP inhibition shows promising results in clinical studies as monotherapy for cancers with homologous recombination defects (Aly and Ganesan 2011; Carney et al. 2018; Minchom et al. 2018).

Chapter 3

Genome engineering and DNA repair assays

3.1. Genome engineering

Since the 1970s, genome engineering is used as a method to insert (or remove) genetic elements into organisms. It uses engineered nucleases to target specific DNA sequences generating a double-strand break (DSB) or guide effector molecules to DNA locations, in a precise and site-specific manner. For modifying the DNA sequence, a DSB needs to occur so that the cell's endogenous repair mechanism can be activated and once manipulated can result in the desired sequence change (Doudna and Charpentier 2014). This methodology allows scientists to disrupt or modify genes with extraordinary precision and has been implemented for several years.

In the late 1950s, Rich and colleagues described the idea of a triple helix formation (RICH 1958; Varshavsky 2006), that inspired the early approaches of gene editing. Typically, oligonucleotides coupled to chemical cleavage or cross-linking reagents like bleomycin or psoralen were used to induce site-specific modifications (Faruqi, Egholm, and Glazer 1998;

Sandor and Bredberg 1995; Strobel et al. 1991; Strobel and Dervan 1990). Other methods used peptide nucleic acids or polyamides to enable targeted binding to chromosomal loci (Cho, Parks, and Dervan 1995; Faruqi et al. 1998; Gottesfeld et al. 1997). Another strategy was to use self-splicing introns to change sequences at the DNA or RNA level (Sullenger and Cech 1994; Yang et al. 1996; Zimmerly et al. 1995). All these approaches demonstrated the effectiveness of base pairing for site-specific genome modification. However, none of them was able to lead to robust methods.

Over the following years, homing endonucleases were emerged that were capable of site-specific DNA cleavage and allow the integration of a desired exogenous sequence (Chevalier et al. 2002; Jacquier and Dujon 1985; Pavletich and Pabo 1991). This stimulated the creation of modular DNA recognition proteins that could function as site-specific nucleases when coupled to the sequence-independent nuclease domain of the restriction enzyme FokI (Bibikova, M., Beumer, K., Trautman, J.K., Carroll 2003; Boch et al. 2009; Frank, Skryabin, and Greber 2013; Moscou and Bogdanove 2009). Nowadays, two main groups of enzymes are used to introduce the DSBs, the FokI, and the Cas9 enzymes (Ran et al. 2013).

The FokI is a DNA-cutting enzyme derived from the bacterium *Flavobacterium okeanokoites*, and it is fused with proteins to create programmable endonucleases such as zinc-finger nucleases (ZFNs) and transcription activator-like effector nucleases (TALENs). The first-generation genome editing tool (ZFN) and later the next-generation genome editing tool (TALENs) that offered precision and control lead the way for functional studies in the era of genome engineering (Kim and Kim 2014; Ramirez et al. 2012; Zhang et al. 2014). However, these approaches required the generation of custom-tailored proteins for each targeting event, limiting their range of use on both practicality and cost.

Clustered Regularly Interspaced Short Palindromic Repeats (CRISPR)/Cas9 is the most recent addition to the arsenal of genome engineering tools that a scientist can use. It is an RNA-mediated adaptive immune system found in several species of bacteria and archaea, and functions to protect host cells from invasion by foreign DNA elements (Sontheimer and Barrangou 2015). CRISPR technology enables scientists to target the genome accurately, for a variety of purposes, generally either cutting the DNA to induce changes in the DNA sequences or to precisely deliver molecules, for example, effector or visualization molecules, to the sites of DNA.

3.2. The CRISPR toolkit

The introduction of the CRISPR/Cas9 system offered an unprecedented opportunity to the researcher's toolkit in designing experiments with the scope of determining the role of genes at the cellular level mechanistically (Jinek et al. 2013; Mukherjee-Clavin, Tomishima, and Lee 2013). Although still not trivial, this technology provides an opportunity to understand the genetic basis of complex diseases like cancer.

In this Ph.D. thesis, we are using CRISPR/Cas9 among other tools like TALENs, ZFN or meganucleases (e.g., I-SceI) because it provides efficiency, flexibility and cost-effectiveness to work in a high-throughput manner across different cell lines (Belhaj et al. 2013), (Sternberg et al. 2015).

3.1.1. CRISPR/Cas9 system

Cas9 is an RNA-guided endonuclease whose mechanism was clarified in 2012 (Doudna and Charpentier 2014), (Ran et al. 2013). It induces a targeted double-strand DNA break with the help of a small ~ 20 nucleotide RNA sequence termed the 'guide RNA' (gRNA) that is complementary to the target sequence (Jinek et al. 2012) and binds to it through Watson - Crick base pairing (Cong et al. 2013; Sternberg and Doudna 2015) (**Figure 6 A**). The gRNA sequence can bind up to 22-23 base pairs (Hsu et al. 2013), (Ran et al. 2013). The simplicity of the target design, the high efficiency of this system and the ability to multiplexing have made CRISPR the preferable choice of cell line engineering (Perez-Pinera, Ousterout, and Gersbach 2012), (Cox, Platt, and Zhang 2015).

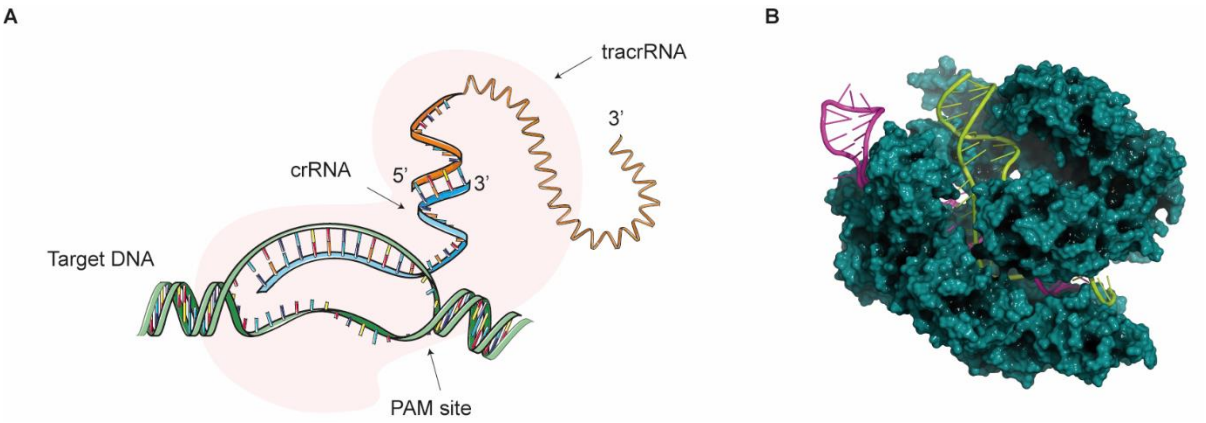

Figure 6. The CRISPR/Cas9 system. (**A**) Schematic representation of the CRISPR/Cas9 system in complex with guide RNA and target DNA. crRNA is matched to the complementary target DNA sequence and is also bind to the tracrRNA. (**B**) Crystal structure of Streptococcus pyogenes Cas9 endonuclease in complex with guide RNA and target DNA (Nishimasu et al. 2014).

For genome editing, the most commonly used and extensively characterized system is type II derived from *S. pyogenes* (SpCas9) (**Figure 6 B**). Two RNA elements (crRNA & tracrRNA) are combined into a single chimeric molecule termed the guide RNA (gRNA) that can be simultaneously expressed alongside the Cas9 nuclease (Cho and Chang 2015; Ran et al. 2013;

Walsh and Hochedlinger 2013). It has been shown that maintaining the RNA as two separate molecules (crRNA:tracrRNA) can enhance cutting efficiency, and may well be desirable for some study designs, for example developing a system whereby only the small crRNA is changed to affect different outcomes (Aida et al. 2015). The simplicity of this approach is that by altering the first 20 nucleotides of the gRNA, Cas9 nuclease can be directed to any DNA sequence, adjacent to necessary, short DNA sequences (Protospacer adjacent motif (PAM)) (Ran et al. 2013; Sander and Joung 2014).

3.1.2. The features of Cas9 cleavage

Three significant steps define the function of the CRISPR/Cas9 system: (1) initially the RNA-guided Cas9 nuclease (RGN) scans the genome to find the complementary DNA sequence to the gRNA, (2) then the induction of a DNA double-strand break by Cas9 takes place, and lastly (3) DNA repair cellular machinery repairs the DSB (Hsu, Lander, and Zhang 2014). It is well established that after a Cas9-mediated DSB, DNA mutations are generated by the cellular machinery. Those mutations determine Cas9 phenotypic efficiency (Allen et al. 2019) with the repair process to be in the majority of the cases error-prone at a rate similar to the transfection efficiency (Brinkman et al. 2018). Still, the kinetics of a Cas9-mediated DSB and repair are not fully understood. However, it is believed that they differ from the kinetics of a natural DSB repair presumably because Cas9 remains bound to the target sequence following cleavage (Agrotis and Ketteler 2015). Over the past years, several studies have provided insights into the mechanisms affecting Cas9-mediated DSB repair and provided useful understandings of the process (Brinkman et al. 2018; van Overbeek et al. 2016; Tsai and Joung 2016).

The Cas9-mediated cut and repair process

In a recent study, Brinkman *et al*. measured the kinetics of a DSB repair after a Cas9-mediated cleavage and concluded that during the process of a Cas9-DSB the DNA enters a reversible ‘‘broken’’ state (Brinkman et al. 2018). They suggest that this state may be repaired correctly, or an error-prone repair mechanism can introduce small InDels at the cleavage site. The latter state fallouts in an irreversible ‘‘InDel’’ state that can no longer be adequately recognized by the gRNA and therefore cannot be cut again by Cas9. Moreover, several other studies (Sternberg et al. 2014), (Richardson, Ray, DeWitt, et al. 2016), (A. Shibata et al. 2017) indicate that Cas9 remains tightly bound to one or both DNA ends after cutting, and the detachment can only happen by protein denaturation. Additional studies have shown that also the catalytically inactive Cas9 (“dead” Cas9) is tightly bound to its target DNA *in vivo* with a dwell time of about 2 h (Knight et al. 2015). Overall, data suggest that the rate of DSB repair is variable, relatively slow and that the repair process tends to be error-prone (Brinkman et al. 2018; Rose et al. 2017). In comparison, a natural occurring double-strand break is generally repaired within 10 to 60 min.

Cas9-mediated DSB profile

Multiple studies have analyzed short-range sequencing data by NGS from the cleavage site following a Cas9 mediated gene editing to characterize the repair process. The summary of these efforts is the evident accumulation of InDels in the cleavage site of the cells indicating an erroneous repair (Brinkman et al. 2018; Cullot et al. 2019).

More specifically, in a recent study by So and Martin 2019, it was shown that DSBs with 5’ and 3’ overhangs lead to increased processing of DNA during end-joining compared to blunt DSBs (So and Martin 2019). 5’ overhangs are removed, and 3’ are filled in at recombination

junctions, implying that different subsets of enzymes are required for repair based on Cas9 mediated DSB. These findings, together with other results, explain the prevalence of single-nucleotide insertions homologous at the cleavage site.

Furthermore, in a study by Chakrabarti *et al*. they show that the editing precision of Cas9 is an inherent feature of the target site that depends on four nucleotides located around the cleavage site within the PAM. Specifically, they highlight the importance of the -4 nucleotide position, from the PAM site, as the most influential position. In that position, possibly an overhanging nucleotide is created that can be used as a template of single-nucleotide insertions homologous since it can be used as a template before the broken DNA ends are rejoined (Anob M. Chakrabarti et al. 2019).

Multiple repair pathways active at one locus

CRISPR/Cas9 has been successfully used to Knock-Out (KO) or Knock-In (KI) genes of interest in cells and zygotes of different species (Rezza et al. 2019). During this process two repair mechanisms prevail; c-NHEJ which produces small insertions or deletions (InDels) at the cleavage site, or Homologous Directed Repair (HDR) that induces the specific insertion of an exogenous DNA fragment at the cut site.

Apart from these two main repair pathways, recent studies show the implication of additional pathways to be active at one DSBs locus (van Overbeek et al. 2016), (Bothmer et al. 2017). However, the interplay and relative contributions have remained mostly uncharacterized (Allen et al. 2019). Except for HR and c-NHEJ, recent findings also implicate alt-EJ in the process of DNA repair after a Cas9-mediated DSB that is thought to be highly mutagenic (Brinkman et al. 2018), (So and Martin 2019). Alternative end-joining (alt-EJ), uses short sequence

homologies near the two ends, which leads to specific small deletions (McVey and Lee 2008). Therefore it is believed that both classical and alternative end-joining pathways contribute to the erroneous repair (Brinkman et al. 2018), (Allen et al. 2019). In an attempt to measure the kinetics of the Cas9 cut and repair process, Brinkman *et al.* showed that alt-EJ has slower repair kinetics than c-NHEJ (Brinkman et al. 2018). They observe that mainly the lower rate is because alt-EJ exhibits a delayed onset compared to c-NHEJ rather than a reduced activity. Most likely, the c-NHEJ system initially prevents the access of the alt-EJ pathway to the DSB; only after several hours if c-NHEJ has failed to repair the break, the alt-EJ pathway is allowed to engage (Brinkman et al. 2018).

Applications of CRISPR/Cas9

Recently, the prokaryotic immune system, CRISPR/Cas9 has been adapted for genetic editing in a variety of systems or organelles including bacteria (J.-S. Kim et al. 2016), (Barrangou et al. 2013), fungi (Liu et al. 2015), plants (Belhaj et al. 2013), insects (Alphey 2016), (Bassett and Liu 2014), worms (Friedland et al. 2013), zebrafish (Blackburn et al. 2013), mouse (Yin et al. 2016) and mammals (Bachu, Bergareche, and Chasin 2015). CRISPR has already transformed the field of genome engineering and will likely continue to do so, forming the basis of future research and clinical strategies.

The expansion in CRISPR research is mainly due to the simplicity of targeting; instead of using custom *in vitro* generated proteins, the Cas9 nuclease can be targeted to specific genomic regions by a single guide RNA, which is comparably easy to produce. The CRISPR technology has rapidly evolved over the past few years, and it seems that several of the drawbacks have been mitigated with off-target effects (OTE) to represent an important issue that hinders the

use of CRISPR/Cas9 in *in vivo* applications. (Biagioni et al. 2017; Cho et al. 2014; Kleinstiver et al. 2016; Ricci et al. 2019; Tsai and Joung 2016; Zhang et al. 2015). Some possible solutions that have been described in the literature are first to evolve the gRNA design algorithms to minimize the OTE. Secondly, to use shorter gRNA sequences to decrease the potential mismatch tolerance. Thirdly, the concentration of the Cas9/gRNA complex needs to be maintained at minimal levels since it influences the OTE. Another possible solution is the use of paired Cas9 nickases that increases significantly the target specificity.

Overall, CRISPR fulfils the criteria that an ideal genome-editing tool should possess (Cong et al. 2013): low or negligible off-target mutations (Tan et al. 2015), (Veres et al. 2014), (Yang et al. 2014), (Sander and Joung 2014), (Anderson et al. 2015), rapid and efficient assembly of the nuclease and in high occurrence (1 per 8 bp) of the desired sequence in the targeted cell population. In summary, it is this availability and simplicity that allowed genome editing to become so attractive.

3.3. Reporter assays for DNA repair

The cell's DNA repair mechanisms try to restore the original DNA sequence after encountering DNA damage. Sometimes it repairs without a change or sometimes with mutagenic alterations or even recombination events (Gunn and Stark 2012). Over the past decades to detect these changes scientists have developed several *in vitro* reporter assays in various model systems (**Figure 7**) (Bennardo et al. 2008; Bervoets and Charlier 2018; Certo et al. 2011; Gomez-Cabello et al. 2013; Iliakis et al. 2008; Johnson, Liu, and Jasin 1999; C. Ren et al. 2015; A. Shibata et al. 2017; Stark and Jasin 2003). There are assays for DNA damage and repair that

can trace and quantify the DNA repair pathway activity, examine the consequences of the processing of chromosome rearrangements, and evaluate the repair process of induced DNA damage, most frequently of a DSB (Adamson et al. 2012; Certo et al. 2012; Choe, Guo, and van den Engh 2005; Kuhar et al. 2016; Rakauskait et al. 2011; Ramirez et al. 2012; Q. Ren et al. 2015; A. Shibata et al. 2017). These assays are powerful tools, and each comes with its particular advantages and limitations (Klein et al. 2019).

The first implementation of an *in vitro* assay was made with the SCneo reporter in 1999 (Johnson et al. 1999). Roger *et al.* developed a recombination reporter that contains two non-functional copies of the neomycin phosphotransferase (*neo*) gene (**Figure 7 A**). After the induction of a DSB with the I-SceI endonuclease the system allows for the detection of two recombination products; short tract gene conversion (STGC) or long-tract gene conversion (LTGC). I-SceI endonuclease generates a defined DSB within its 18 base-pair (bp) recognition sequence, resulting in DSB ends with 4 nucleotides (nt) 3' cohesive overhangs. This approach helped to identify the involvement of XRCC2 and XRCC3 to DSB by HR (Johnson et al. 1999; Pierce et al. 1999) and that sister chromatid gene conversion is a prominent DSB repair pathway in mammalian cells (Johnson and Jasin 2000).

In the years to follow several GFP-based reporters assays with recognition sites for the rare-cutting endonuclease I-SceI, have been developed to examine the distinct repair outcomes of mammalian DNA DSB repair (Gunn and Stark 2012) (**Figure 7 A-E**). Depending on the design, reporters can be used to assess homology-directed repair, single-strand annealing, or alternative end-joining. Beginning with DR-GFP, DRins-GFP, SA-GFP, and EJ2-GFP, these reporters are designed to examine a series of repair outcomes that utilize homology. DR-GFP and DRins-GFP are used to quantify two distinct homology-directed repairs (HDR) events,

whereas SA-GFP and EJ2-GFP are used to measure single-strand annealing (SSA) and alternative end-joining (alt-EJ) events, respectively. These efforts revealed the importance of Nbs1 and CtIP in the initiation of end-resection (Sartori et al. 2007; Stracker and Petrini 2011).

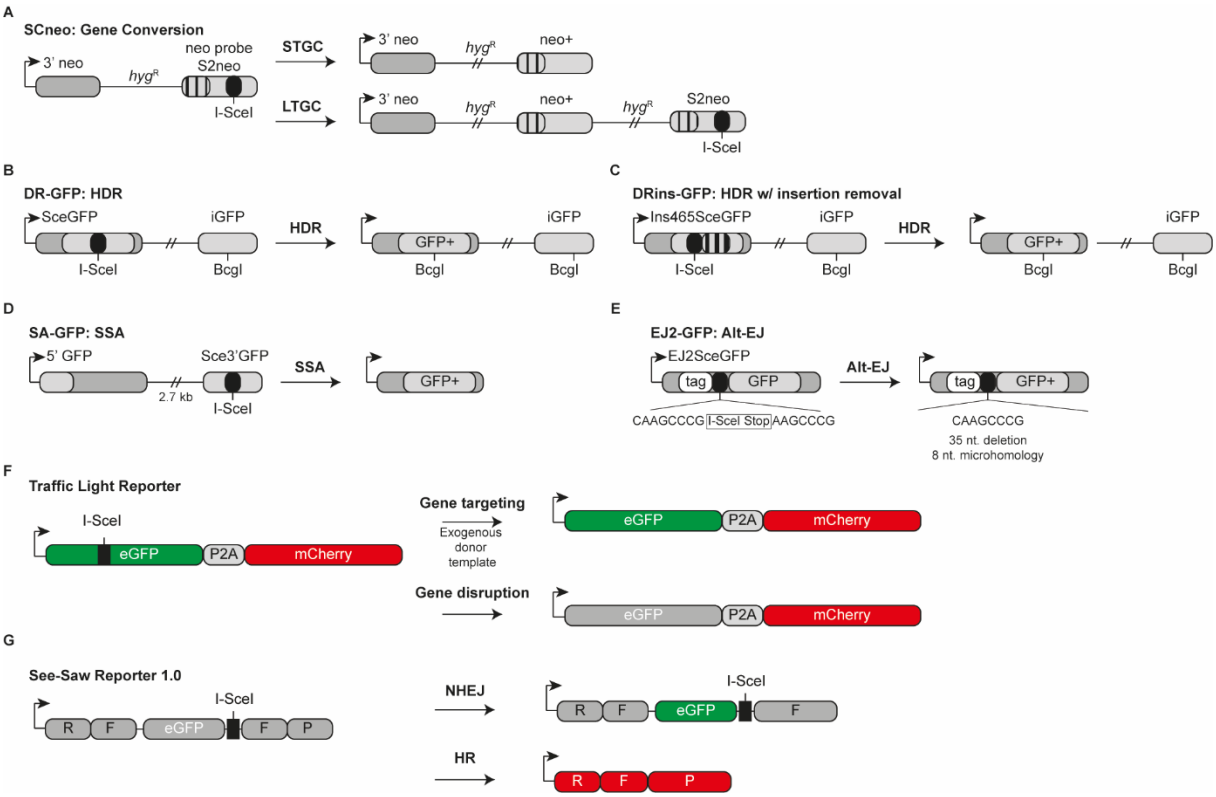

Figure 7: Development of DNA repair assays. (**A**) Structure of SCneo and predicted HR products. (**B**) The DR-GFP contains the SceGFP cassette that is interrupted by a single I-SceI site, along with 5' and 3' truncated fragment of GFP. iGFP is used as a template to lead to a GFP+/BcgI+ product. (**C**) Similar to DR-GFP, with the addition of a 464 nt insertion that has to be removed during HDR. (**D**) SA-GFP contains a 5' fragment of GFP and a 3' fragment of GFP that contains an I-SceI site. The GFP fragments are separated by 2.7 kb and share 266 nt of homology. (**E**) EJ2-GFP contains an expression cassette for a tagged version of GFP that is interrupted by an I-SceI site and a series of stop condos, which is flanked by 8 nt of homology. (**F**) Schematic of the Traffic Light reporter showing the different engineering outcomes after the induction of DSB by I-SceI. (**G**) In the See-Saw Reporter, a GFP gene is flanked by two truncated parts of the RFP gene (RF and FP) that share 302 bp of homologous sequence. Figures adapted from (Johnson and Jasin 2000), (Certo et al. 2011), (Gunn and Stark 2012), (Gomez-Cabello et al. 2013).

Apart from these specific reporters some researchers also established reporters to measure the activity of specific proteins like the kinase C, CKAR reporter that monitors the activity of ATM or other specific proteins in living cells (Johnson, You, and Hunter 2007).

So far, these methods have only been focusing on the study of specific DDR pathways and were driven by the target design, failing to provide an overall understanding of the complexity of double-strand break repair. In 2011 Certo *et al.* developed the Traffic Light Reporter (Certo et al. 2011) implementing a reporter assay for the first time to a high-throughput genetic screen (**Figure 7 F**). Several studies followed this approach in an effort to identify novel target genes involved in DNA-damage response with great success (Adamson et al. 2012; Bervoets and Charlier 2018; Goglia et al. 2015; Gong et al. 2015; Kojima and Borisy 2014; López-Saavedra et al. 2016; Q. Ren et al. 2015; A. Shibata et al. 2017).

The recent expansion of genome engineering have recently brought the CRISPR/Cas9 system (Ran et al. 2013), (Doudna and Charpentier 2014), in the footsteps of reporter systems to induce highly site-specific DSBs instead of I-SceI (He et al. 2016; Q. Ren et al. 2015; Wen et al. 2017). In this Ph.D. thesis, we describe the development of a dual-fluorescent reporter coupled to CRISPR/Cas9 technology, providing an opportunity to advance our knowledge of DSB repair and study the interplay among DNA DSB repair pathways.

Theoretical framework

Chapter 4

Aims

To study the DNA double-strand break repair choices *in vitro*, we developed and employed Colour Assay Tracing Repair (CAT-R) as a dual-fluorescence reporter-based system. This study is conducted at the DNA Damage in Cancer group at BioMed X Innovation Centre.

The main aims of this research are to:

- Develop a novel method to trace the DNA repair status after a Cas9-mediated DSB.
- Establish a platform to screen small pharmacological compounds related to DSB.
- Evaluate the importance of individual DNA repair components on DSB repair choice.
- Estimate the impact of the genetic background in DNA repair choice.

Results

Chapter 5

CAT-R fluorescent reporter

This chapter describes the development of the tandem fluorescent reporter (CAT-R) that takes advantage of the highly efficient and precise CRISPR/Cas9 based double-strand break (DSB) induction to assess *in vitro* the different DNA repair outcomes.

Custom model cell lines were engineered with the Flp recombinase to integrate the fluorescent reporter as a single stable copy to the cell's genome. Besides, the cells were engineered to express the enzymatically active Cas9 endonuclease in a doxycycline-inducible format. Furthermore, the transfection conditions and the timing of analysis were optimized to ensure high reproducibility in both model cell lines achieving an unparalleled resolution of the DSB events.

CAT-R distinguishes small insertions or deletions (InDels) from large deletions allowing the simultaneous measurement of the rates of end-protection and end-resection DNA repair mechanisms in human cell lines. In this chapter, it is shown that DNA repair deficiencies can alter the rate between InDels and large deletions by directing the repair of the DSBs to either end-protection or end-resection based mechanisms.

5.1. Custom cell line engineering

Expressing vectors designed for use with the Flp-In™ System

Transformed human embryonic kidney (Flp-In™ HEK293, Life technologies) and human telomerase reverse transcriptase (hTERT)-immortalized retinal pigment epithelial (hTERT T-Rex™ RPE-1, a kind gift from Jonathon Pines) mammalian cell lines were used as model systems to integrate the custom-made DNA fluorescent reporter as a single stable copy to the cell's genome with the use of Flp-In™ system. The Flp recombinase-mediated integration approach (Flp-In™, Invitrogen™) has been used widely to generate stable mammalian expression cell lines (Callesen et al. 2016; Ji et al. 2017; Sabath and Shim 2000; Theodosiou and Xu 1998). It uses the flippase (Flp) recombinase to recombine DNA sequences between short flippase recognition target (FRT) sites.

According to the manufacturer's protocol (Flp-In™ System), cells were transfected and expanded for one week. Since the integrated gene of interest contains fluorescent proteins, FACS sorting was used as an application for the selection of positive cells.

Generating stable cell lines expressing Cas9 endonuclease

The Edit-R inducible lentiviral Cas9 particles (Horizon™ Dharmacon) were used to generate Cas9 expressing cell lines that employ the Tet-On 3G induction system allowing for a robust Cas9 induction at doxycycline doses between 100 ng/ml and 1 μg/ml. The lentiviral Cas9 particles confer Blasticidin resistance in transduced cells, therefore it is important to determine the minimum required Blasticidin concentration that kills the un-transduced cell lines.

Therefore, concentrations ranging from 2.5-20 µg/ml of Blasticidin were tested in both HEK293 and RPE-1 cell lines. Within 3-15 days after the addition of Blasticidin (0, 2.5, 5, 10, 15, 15, 20 µg/ml) both cell lines exhibit resistance to the highest dose of Blasticidin (**Figure 8 A**).

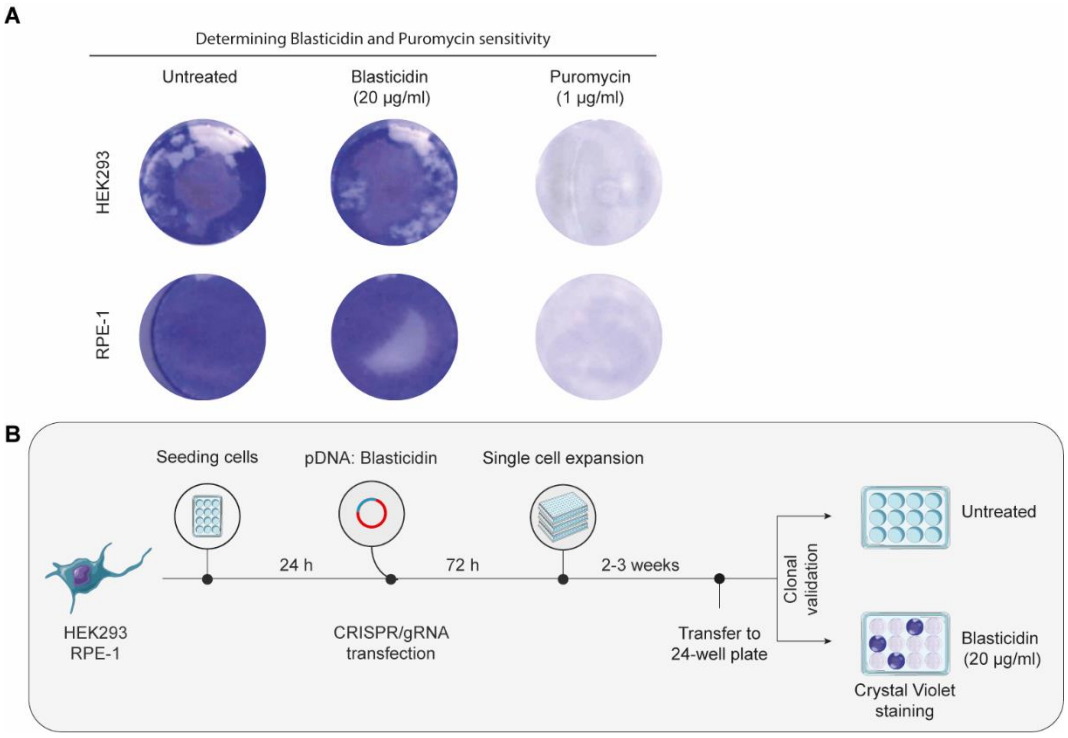

Figure 8: Determining Blasticidin sensitivity and schematic representation on the workflow for knocking it out. (**A**) Raw pictures of HEK293^{CAT-R} and RPE-1^{CAT-R} cell lines after applying crystal violet. The cells were tested at increasing concentrations of Blasticidin (2, 2.5, 5, 10, 15, 20 µg/ml). Both cell lines are resistant to Blasticidin. (**B**) Workflow scheme. Cell lines were individually treated with an all-in-one vector to knockout the Blasticidin gene. Then cells were single-cell expanded for 2 - 3 weeks. Subsequently, approximately 10 clones were transferred to a larger plate and allowed to reach confluency. Colonies were split 1:2 and Blasticidin was applied to the medium. After one-week crystal violet was used to visualize the colonies. Images were taken for each plate.

To disrupt the Blasticidin sequence and generate single knock-out (KO) clones sensitive to Blasticidin, the CRISPR/Cas9 system was used. Specific gRNAs targeting the Blasticidin sequence were designed and cells were transfected with an all-in-one vector (**Figure 8 B**). Overall, ten monoclonal cell lines sensitive to Blasticidin were generated that could be used with the Edit-R inducible lentiviral Cas9 particles.

After transducing the cell lines with the Edit-R inducible lentiviral Cas9 particles (hereafter referred to as HEK293^{CAT-R} and RPE-1^{CAT-R} cells), cells were cultured for seven days in selection medium supplemented with 1 µg/ml Blasticidin. Protein extracts from mixed cell populations were used to determine the expression levels of Cas9 protein in an inducible manner in the presence of doxycycline by western blotting using an anti-Cas9 antibody (**Figure 9**).

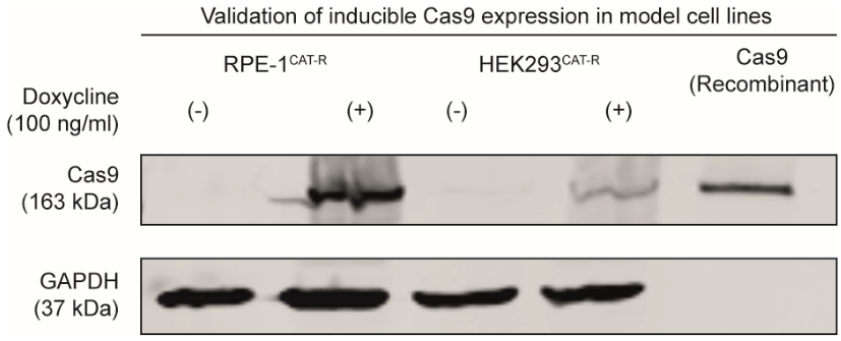

Figure 9: Western blot detecting Cas9 expression. Western blot from a mixed cell population from both cell lines (HEK293^{CAT-R}, RPE-1 $^{CAT-R}$) shows that under Doxycycline induction the expression of the Cas9 protein is induced. Blots were incubated with antibodies directed against Cas9 and GAPDH.

5.2. Optimizing transfection and Cas9 cutting efficiency

To establish and optimize the conditions of the double-strand break (DSB) induction are described to ensure high reproducibility in HEK293^{CAT-R} and RPE-1^{CAT-R} cells (**Figure 10 A)**, several conditions have been considered such as (1) the effect of cell population density on transfection efficiency, (2) the type and optimal concentration of transfection reagent, and lastly (3) the ideal time point of analysis.

It is widely acknowledged that some "cargo" types such as longer pieces of DNA or proteins are difficult to get into cells. Therefore, the transfection efficiency of both cell lines was evaluated by quantifying the levels of eGFP expression three days post-transfection with the

same pDNA vector (LentiGuide puro eGFP), lipid-mediation reagent (Lipofectamine™3000) and lipid to DNA ratio (1:3). The maximum transfection efficiency achieved in normal HEK293 was approximately 80%, whereas for normal RPE-1 the efficiency had a maximum of 55% (**Figure 10 B)**. Even though 55% of transfection efficiency is can be considered high under certain conditions, our experimental pipeline requires higher rates since a build-in cell-based assay is developed for large-scale screens with several gene-edited transgenic cell lines to be used and a robust phenotype needs to occur every time.

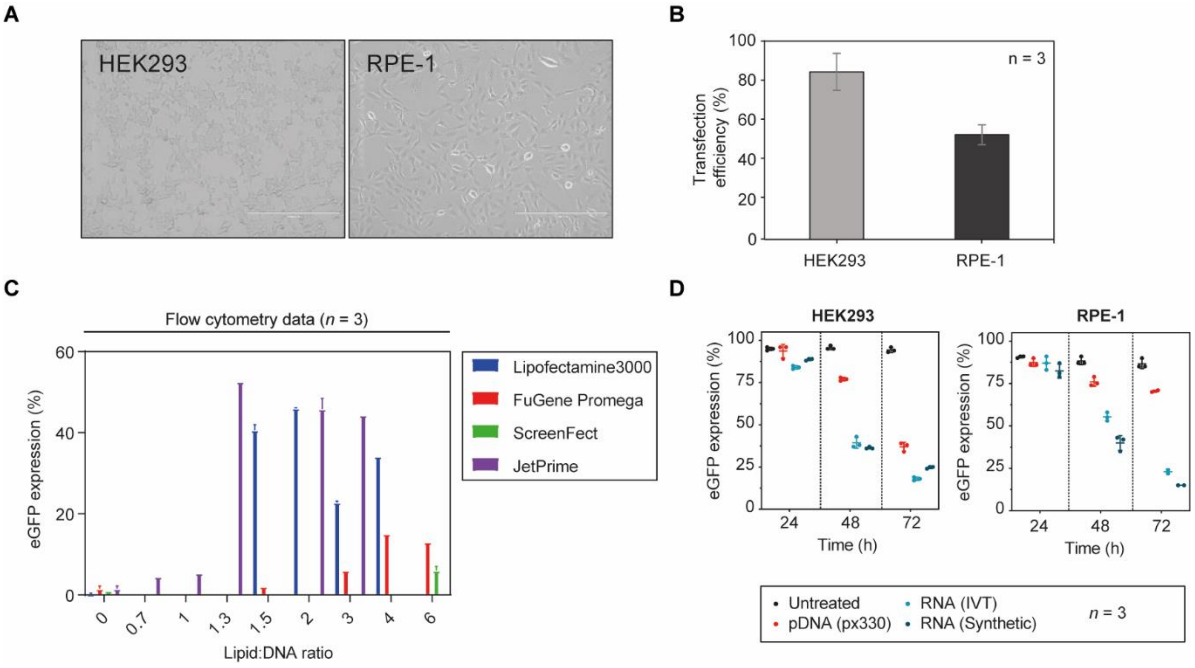

Figure 10: Ensuring system quality performance. (**A**) Ideal cell confluency 24 h after seeding 20.000 cells HEK293 and 8.000 cells RPE-1 in a 96 well plate intended for a liquid transfection. (**B**) Transfected wild type RPE-1 and HEK293 with the same eGFP expressing vectors (LentiGuide puro eGFP) with Lipofectamine™3000 in 1:1.3 DNA to lipid ratio. The effect of Cationic lipid-DNA complex ratio on lipid-mediation transfection efficiency in RPE-1 cell lines. (**C**) The pDNA vector (LentiCRISPR eGFP) is used to transfect RPE-1 cells with different lipid-mediation reagents (JetPrime®Polyplus, FuGene®Promega, ScreenFect®, Lipofectamine™2000, Lipofectamine™ 3000) at various lipid: DNA ratios. The pDNA vector expresses the eGFP protein and is used to quantify the expression levels of it with flow cytometry. (**D**) The efficiency of different gRNA format is tested in a time-dependent manner (24, 48, and 72 hr) in HEK293^{CAT-R} and RPE-1^{CAT-R} cells. The eGFP reduction is checked with flow cytometry. The same gRNA sequence is used in all formats. A standard student t-test is used to calculate the *P-values* between untreated and treated samples. pDNA: px330), RNA: *in-vitro* transcribed (IVT) or synthetic crRNA:tracrRNA gRNA.

The efficient delivery of the CRISPR reagents into the cells ensures a higher probability of success for any downstream application. For this reason, we examined several transfection

reagents such as Lipofectamine™ 3000, JetPrime®Polyplus, FuGene®Promega, ScreenFect®, at different concentrations, and formats (pDNA, RNA) to further boost the transfection efficiency of the CRISPR reagents into the model cell lines. To optimize the delivery of pDNA vectors to HEK293 and RPE-1 cell lines we tested different lipid-reagent (µl) to DNA concentration (µg) ratios in ranges from 0.7 to 6 with several transfection reagents (**Figure 10 C**). Lipofectamine™ 3000 and JetPrime®Polyplus exhibit the highest transfection efficiencies (approximately 55%) in RPE-1 with lipid:DNA ratio to range from 1.3 up to 3, whereas FuGene®Promega and ScreenFect® displayed signs of transfection at much higher lipid:DNA ratios (3 to 6). Among all transfection reagents, Lipofectamine™ 3000 and JetPrime®Polyplus had the least cytotoxic effects after three days of transfection. Probably the higher amount of lipid-reagent that was needed in the case of FuGene®Promega and ScreenFect® reagents was the causal for the severe cytotoxicity.

As defined above, the maximum transfection efficiency of a pDNA for normal HEK293 and RPE-1 was measured at 80% and 55% respectively. However, transfection efficiency may not necessarily translate into similar levels of a functional read-out. Therefore, to maximize the Cas9-mediated DSB read-out, two different gRNA formats (pDNA, RNA) of the same gRNA sequence were examined by comparing the levels of *eGFP* reduction in a time-course manner (**Figure 10 D)**.

The use of a pDNA vector reduces the expression levels of eGFP 48 h post-transfection on average only by 25% in both cell lines (**Figure 10 D)**. While 72 h post-transfection the reduction of eGFP expression was about 60% for HEK293$^{CAT\text{-}R}$ and still 35% for RPE-1$^{CAT\text{-}R}$. Subsequently, the pDNA vector format cannot carry adequate CRISPR reagents to the cells for the induction of an effective phenotype.

Instead, when transfecting the gRNA sequence in an RNA format significantly higher results are achieved. Even at 48 h post-transfection the reduction of eGFP expression for HEK293^{CAT-R} was about 75% and 55% for RPE-1^{CAT-R} (**Figure 10 D)**. Those numbers were further increased 72 h post-transfection with both cell lines achieving a reduction to the levels of eGFP at about 85%, with similar efficiencies to have been reported before (Agrotis and Ketteler 2015).

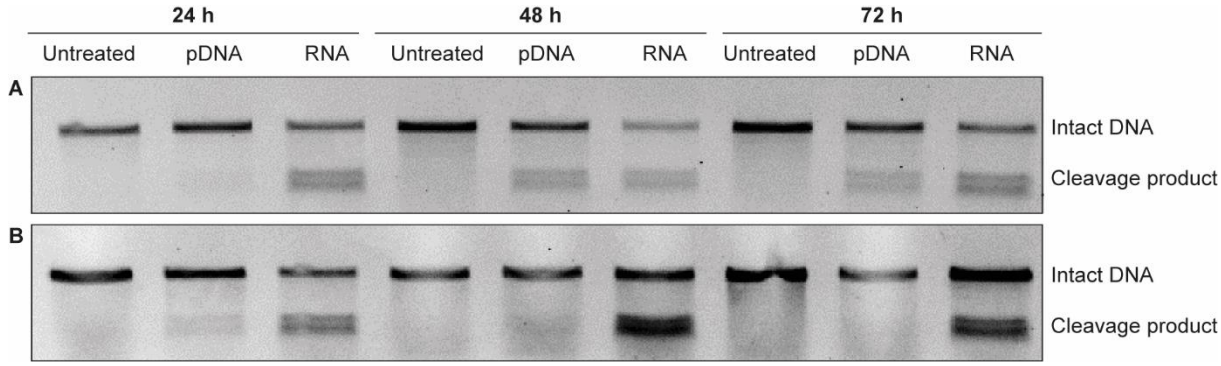

Figure 11: The cutting efficiency is examined with the SURVEYOR assay. Genomic cleavage analysis of the eGFP genomic loci targeted with the synthetic gRNA in (**A**) HEK293^{CAT-R} and (**B**) RPE-1^{CAT-R} cells. The efficiency of the gRNA is studied for 24 to 72 h post-transfection with the SURVEYOR assay. Products from untreated control cells and cells transfected with the CRISPR system were analyzed in a 1.5% agarose gel electrophoresis.

Moreover, to further investigate the optimal conditions for a Cas9-mediated DSB read-out, we evaluated the genome editing efficiency based on an enzymatic mismatch cleavage assay (Langhans and Palladino 2009) in a time-course manner for both cell lines of interest (**Figure 11**). A successful editing event can already be detected 24 h post-transfection with the RNA format in both cell lines. Whereas signs of an efficient double-strand break were visible with the pDNA only 48 h post-transfection. In addition, the intensity ratio between intact DNA and cleavage products between pDNA and *in vitro* transcribed (IVT) RNA at 48 h was much higher for the RNA format compared to the pDNA, indicating a better double-strand break induction. Overall, the cutting efficiency measured by the Surveyor nuclease showed similar results in terms of efficiency and timing as with our previous efforts.

Collectively, the data suggest that to maximize the Cas9-mediated DSB read-out the synthetic (crRNA:tracrRNA) gRNA format should be used, in lipid to RNA ratio 1:2, with Lipofectamine™RNAiMAX as a transfection reagent in the model cell lines HEK293^{CAT-R} and RPE-1^{CAT-R}. In addition, the optimal time point of analysis varies between three- to four-days post-transfection for a robust phenotype.

5.3. Color assay tracing repair

We designed an *in vitro* reporter assay named the Color-assay tracing repair (CAT-R). It consists of two coding sequences for the fluorescent proteins *mCherry* and *eGFP* linked with a self-cleaving P2A peptide and is integrated at a single genomic locus in human HEK293 and RPE-1 cells, engineered to express the doxycycline-inducible Cas9 endonuclease (**Figure 12 A)**. To generate a single site-specific DNA double-strand break, we used a gRNA targeting the eGFP coding sequence in doxycycline-induced HEK293^{CAT-R} cells. Three days post-transfection the repair outcome is analyzed with flow cytometry and plotted as a density plot of *mCherry* and *eGFP* expression (**Figure 12 B)**. The repair of this double-strand break can potentially give rise to three populations with distinct fluorescent signals: (**i**) in the first case, a frameshift mutation places only the eGFP coding sequence out of frame (*mCherry*$^{+}$/*GFP*$^{-}$) due to repair by small insertions/deletions (InDels); (**ii**) in the second case, deletions larger than approximately 250 bps leads to loss of both *mCherry* and *eGFP* sequences (*mCherry*$^{-}$/*GFP*$^{-}$) and (**iii**) in the third case if the repair is error-free, then both *mCherry* and *eGFP* sequences remain intact (*mCherry*$^{+}$/*GFP*$^{+}$). Comparing the phenotypes observed upon gRNA targeting eGFP with a non-targeting (scrambled) gRNA, indeed we could observe three different populations, two of which correspond to error-prone and one to error-free repair of

the double-strand break. Even though we achieve very high transfection efficiencies (greater than 80%) in HEK293^{CAT-R} cells, this third population likely represents a combination of untransfected cells and cells underwent an error-free repair (**Figure 12 B)**.

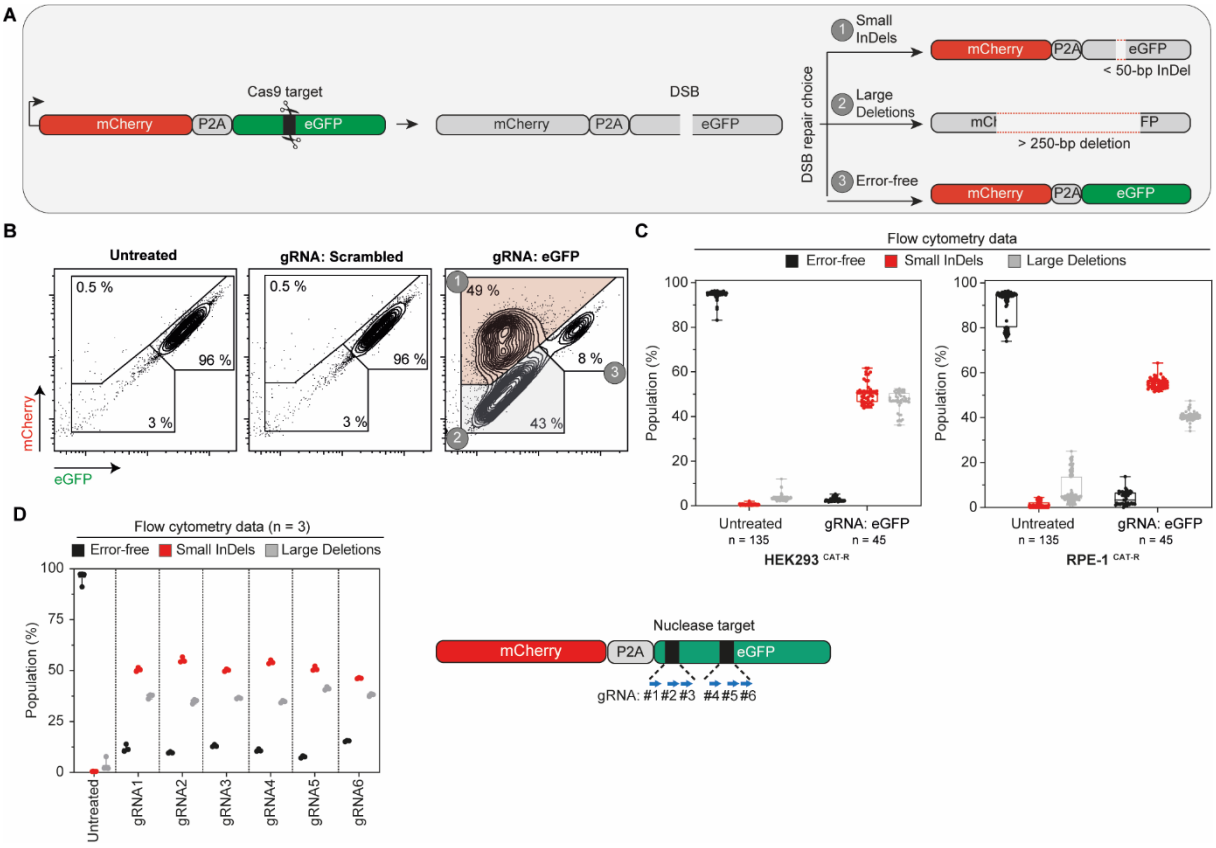

Figure 12: The Color Assay Tracing repair (CAT-R) reporter. (**A**) Schematic representation of CAT-R reporter illustrating the different DNA repair outcomes after a Cas9-mediated site-specific double-strand break (DSB). Arrow represents promoter and initial mCherry start codon. The CRISPR/Cas9 site is indicated at the eGFP loci 355 bp downstream of P2A. If the break is resolved through end-protection pathways, small insertions/deletions (InDels) will form at the break site that will translate eGFP out of frame, and only the mCherry will be expressed; if the break is resolved through end-resection pathways, both mCherry and eGFP sequence will be translated out of frame due to the formation of large InDels. (**B**) Flow cytometry analysis plot of HEK293^{CAT-R} cells 72 h post-transfection with the synthetic crRNA:tracrRNA complex. Comparing the phenotypes between a non-targeting (scrambled) gRNA to a gRNA targeting the eGFP sequence, we observe three fluorescent populations to form. Numbers inside plots indicate percentages of live cells. Axes report relative fluorescence intensity in arbitrary units. (**C**) Quantification box and whisker plot (min to max) of flow cytometry analysis for HEK293^{CAT-R} and RPE-1^{CAT-R} cell line 72 h post-transfection with the synthetic crRNA:tracrRNA complex. A standard student t-test is used to calculate the *P-values* between untreated and treated samples per population. (**D**) Flow cytometry analysis of HEK293^{CAT-R} cells 72 h post-transfection with six different synthetic gRNA complexes targeting the eGFP sequence. All gRNAs induce a double-strand break with a similar effect. Numbers inside plots indicate percentages of live cells. Axes report relative fluorescence intensity in arbitrary units.

The population frequency suggests that the DNA repair choice is on average 1.1 (±0.2) for HEK293^{CAT-R} between InDel formation and large deletions with error-free repair to be very

rare (**Figure 12 C**). This result is not specific to HEK293^{CAT-R} cells, as RPE-1^{CAT-R} cells also showed an equal representation of these two error-prone populations. In RPE-1 cells, however, the formation of the small InDels was slightly higher than that of HEK293 cells in a ratio of small InDels to large deletions to be on average 1.4 (±0.1) (**Figure 12 C)**. To confirm that the choice of gRNA did not affect the relative frequencies of these two populations, we additionally designed five more gRNAs targeting different regions of the eGFP sequence. In all cases, we observed similar results, with an average ratio of small InDels to large deletions to be 1.4 (±0.2). Collectively, our results suggest that upon CRISPR/Cas9 mediated DSB, both small InDels, and large deletions can occur at similar frequencies (**Figure 12 D)**.

Integrating cell cycle with the DNA damage repair

To gain more insights into the kinetics of a Cas9-mediated DSB, we monitored for four days the repair process with a live cell imaging system (IncuCyte, Sartorius) (**Figure 13 A**). The results demonstrate that after a Cas9-mediated DSB the repair process commences as early as 12 ±2 hours post-transfection, agreeing well with similar outcomes of recent studies (Brinkman et al. 2018; Anob M Chakrabarti et al. 2019; Kosicki, Tomberg, and Bradley 2018). Furthermore, to confirm that these populations are indeed products of erroneous DSB-repair and are stably maintained, we monitored the cell division for seven days following a DSB induction. We observed that the fluorescence intensity of mCherry and eGFP reduces over time without drastically changing the ratios among these populations (**Figure 13 B**).

Moreover, the control of DNA repair by the cell cycle checkpoints has been well described (Ghelli Luserna di Rora', Iacobucci, and Martinelli 2017; Hustedt and Durocher 2017; Mjelle et al. 2015; Stracker et al. 2009). Typically, the cell cycle is arrested at specific points to give

cells the necessary time to repair the DNA damage before proceeding to division. Certain cell cycle points involve different DDR pathways that give rise to distinct DNA repair outcomes. For instance, c-NHEJ, which is a major contributor to small InDels, is active throughout the cell cycle, whereas end-resection, that leads to large deletions or error-free repair, is generally restricted during late S and G2 phase.

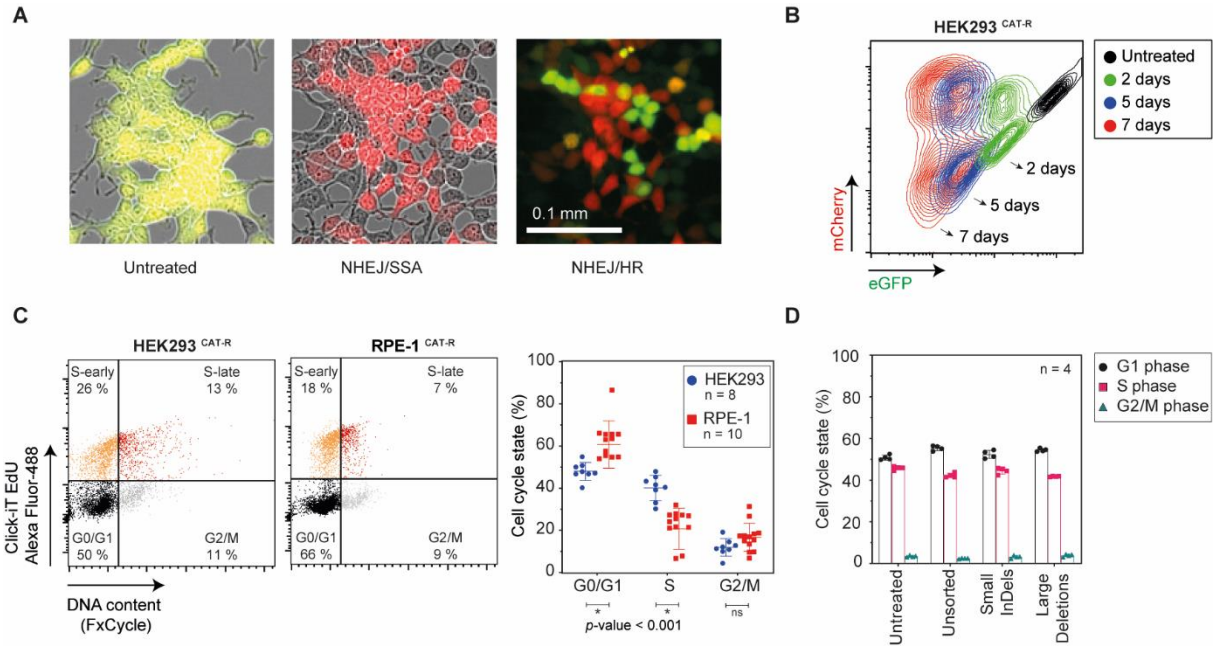

Figure 13: The control of DNA repair by the cell cycle. (**A**) Fluorescent images are showing the different repair outcomes 72 h post-transfection. Only red fluorescent cells indicate an end-protection repair, whereas no fluorescence cells refer to end-resection repair. Green & red fluorescence cells indicate the untransfected or cells that underwent error-free repair. (**B**) Time course tracking for HEK293^{CAT-R} cells following a DSB induction throughout 2, 5, and seven days. (**C**) Cell cycle profile of untreated HEK293^{CAT-R} and RPE-1^{CAT-R} cells. A standard student t-test is used to calculate the *P-values* between cell lines in every cell cycle phase. (**D**) Cell cycle profile of sorted HEK293^{CAT-R} cells populations.

Therefore, we evaluated the cell cycle profile of the HEK293^{CAT-R} and RPE-1^{CAT-R} to better explain the slight differences in the ratio of small InDels to large deletions. When compared the cell cycle profiles of both cell lines, we observed that RPE-1 cells spend relatively less time in the S and G2 phase comparing to HEK293 (**Figure 13 C**). That could explain why RPE-1 cells have a lower frequency of large deletions than HEK293. Moreover, we questioned whether the two DNA repair outcomes are a product of cell cycle stalling. Therefore we sorted

cells based on their DNA repair profile outcome, small InDels or large deletions, and compared their cell cycle profile (**Figure 13 D**). No significant differences occurred, suggesting that both cell populations are indeed products of erroneous DSB-repair and not products of cell cycle stalling. Overall, these results imply that the Cas9 cut and repair process is not profoundly affected by the cell cycle.

Regulation of DNA repair pathway choice by homologies

Long-homology and micro-homology sites are used by the DNA repair sensor complexes, like PARP1, to influence the outcome of the DNA repair in terms of pathway choice (Ceccaldi et al. 2016; Ray Chaudhuri and Nussenzweig 2017). Therefore, it is crucial to understand the homology sites and their frequency at the loci of interest. To do so, we used the basic local alignment search tool (BLAST) (https://blast.ncbi.nlm.nih.gov/Blast.cgi), which allows the identification of regions with local similarity across the FRT integration site (a 14.673 bp DNA sequence). Two regions of long homologies (LHM; > 100 bp) are located at the S40 poly(A) signal, and at the ampicillin resistance sequence that could possibly justify for long DNA losses after a DNA double-strand break (**Figure 14**). This type of DNA repair would result in an increase of the *mCherry*$^-$/*GFP*$^-$ population.

Furthermore, focusing more on the region of the CAT-R system (a 2.586 bp DNA sequence) we identified three potential microhomology sites (MHM; 20 – 50 bp) between the mCherry and eGFP sequence. Those microhomologies theoretically could be sensed by PARP1 to enable alternative end-joining pathway (alt-EJ) that would lead to the loss of both fluorescence proteins function in this locus.

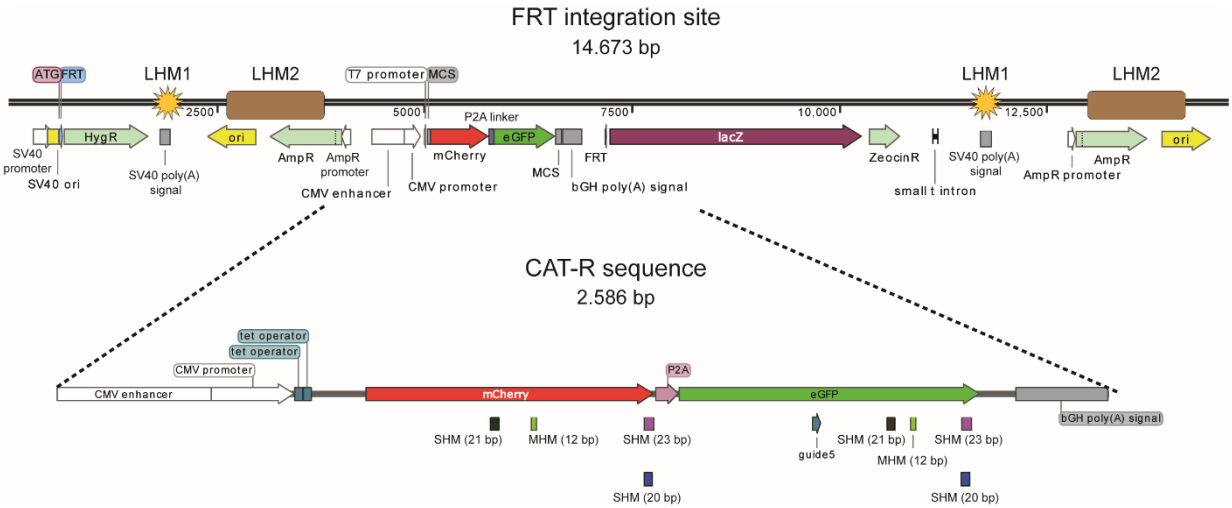

Figure 14: Schematic representation of the entire FRT integration site in the model cell lines. At the entire FRT integration site, two sites of long-homologies (> 100 bp) are identified, one at the SV40 poly(A) signal and another at the Ampicillin resistance sequence. In addition, at the CAT-R system, a 2.586 bp length DNA sequence, three potential microhomologies sites are identified across the double-strand break site (guide5). LHM: Long-homology, SHM: Microhomology, MHM: Microhomology.

Additionally, more than 50 small microhomologies (SHM; 1 - 10 bp) of different base-pair length and type are identified across the double-strand break site (guide5) with the use of an online available tool (www.rgenome.net). If in this case, small microhomologies are used during the repair process after a DSB, then only the eGFP sequence would be translated out of frame resulting in an increase of the *mCherry*$^{+}$/*GFP*$^{-}$ population.

Mutational profile of small InDels

To further understand the repair patterns and outcomes of a Cas9-mediated DSB, we performed targeted next-generation sequencing (NGS) to detect the frequency of the InDels at the affected site. Genomic DNA was harvested from cells 72 h post-transfection and a two-step PCR protocol was employed to prepare the PCR products for amplicon sequencing.

The analysis of the amplicons showed that the maximum length of deletion that we detected was 171 bps, and for the majority of the cases (99%) the size of InDels was less than 50 bps

when counting events with more than 1% frequency (**Figure 15 A**). The most common type of event was 1 bp deletions and 1 bp insertions, with 1 bp insertions to exclusively consist of an adenine "A" at the repair site supporting the idea of templated insertions (Shen et al. 2018) at the DSB site (**Figure 15 B**). Interestingly, microhomology-mediated end repair deletions of 11 and 24 bps were also often (5.7% and 3.1% frequency, respectively) (**Figure 15 C**). An in-depth analysis revealed seven different microhomology (MH) patterns supporting deletions of various bps length, with the "AC" and "GG" MH patterns to be the most common.

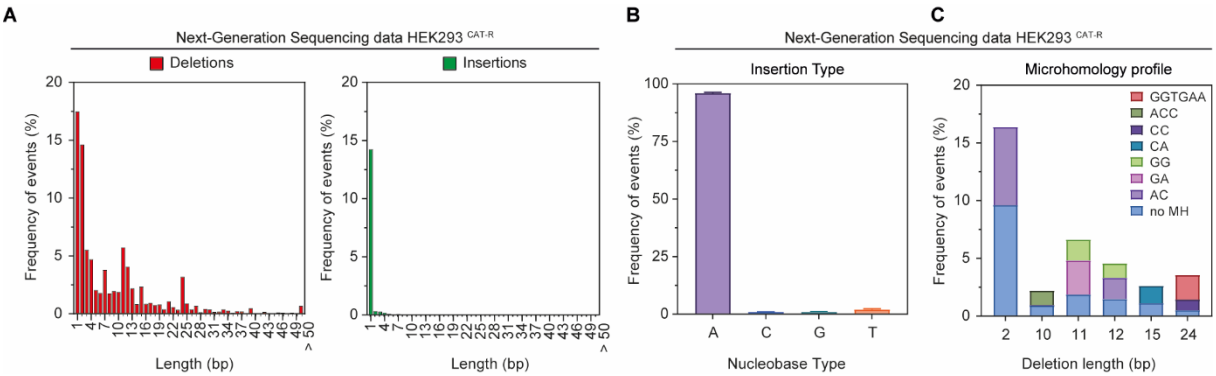

Figure 15: Mutational profile of InDels (**A**) Deep targeted next-generation sequencing to detect InDels at the targeted site from genomic DNA harvested 72 h after transfection. The frequency of events that occur after a Cas9-mediated DSB in almost all cases (~ 99%) are InDels smaller than 50 bps. The most common events were 1 bp deletions and 1 bp insertions, with 1 bp insertions to exclusively consist of an A at the repair site supporting templated insertions at the DSB site. (**B**) Profile of the inserted nucleobase type. (**C**) The pattern of microhomologies supporting deletion length.

The findings from the CAT-R and recent studies suggest that large deletions occur frequently after a Cas9-mediated DSB (Cullot et al. 2019; Gasperini et al. 2017; Kosicki et al. 2018). However, since larger deletions are technically challenging to observe by short-read NGS, their contribution to the DSB repair is less studied.

CAT-R as a Homologous Recombination reporter

Recently it was reported (Glaser, McColl, and Vadolas 2016) that the green fluorescent protein (GFP) could be converted to a blue fluorescent protein (BFP) by a change of a single amino

acid: from Proline (CCT) to Alanine (GCC). This simple modification allowed us to accurately measure the single-strand template repair (SSTR) by providing a single strand oligodeoxynucleotide (ssODN) as a donor template together with the gRNA targeting the eGFP sequence. Previous studies have implemented this approach to quantify knock-in events with the conversion rate to be around 3% when lipid-mediation transfection is used (Janssen et al. 2019; Y. et al. 2017). With this adaptation, CAT-R could be used as a homologous directed repair (HDR) reporter, and the repair of the Cas9-mediated DSB could give rise to an additional population with distinct fluorescent signals: $mCherry^{+}/BFP^{+}$ which corresponds to an SSTR event (**Figure 16 A**). We optimized our reporter with the use of a sense and an anti-sense gRNA in combination with symmetric and an asymmetric ssODN (**Figure 16 B**). We tested two asymmetric donors' designs with their length to vary from 123 to 136 bps. The ssODN(L) bares the extended homology arm on the 5' end, and the ssODN(R) has the extended homology arm on the 3' end. In overall, the use of the ssODN(L) overperforms the ssODN(R), and the symmetric ssODN in terms of SSTR frequency (**Figure 16 C**). This indicates that there is a preference in ssODN symmetry to designs baring extended 5' homology arms. In $HEK293^{CAT\text{-}R}$, the highest SSTR frequency that we achieved was 4.9% (±1.2) with the combination of the ssODN(L) asymmetric donor and a sense gRNA (**Figure 16 D**).

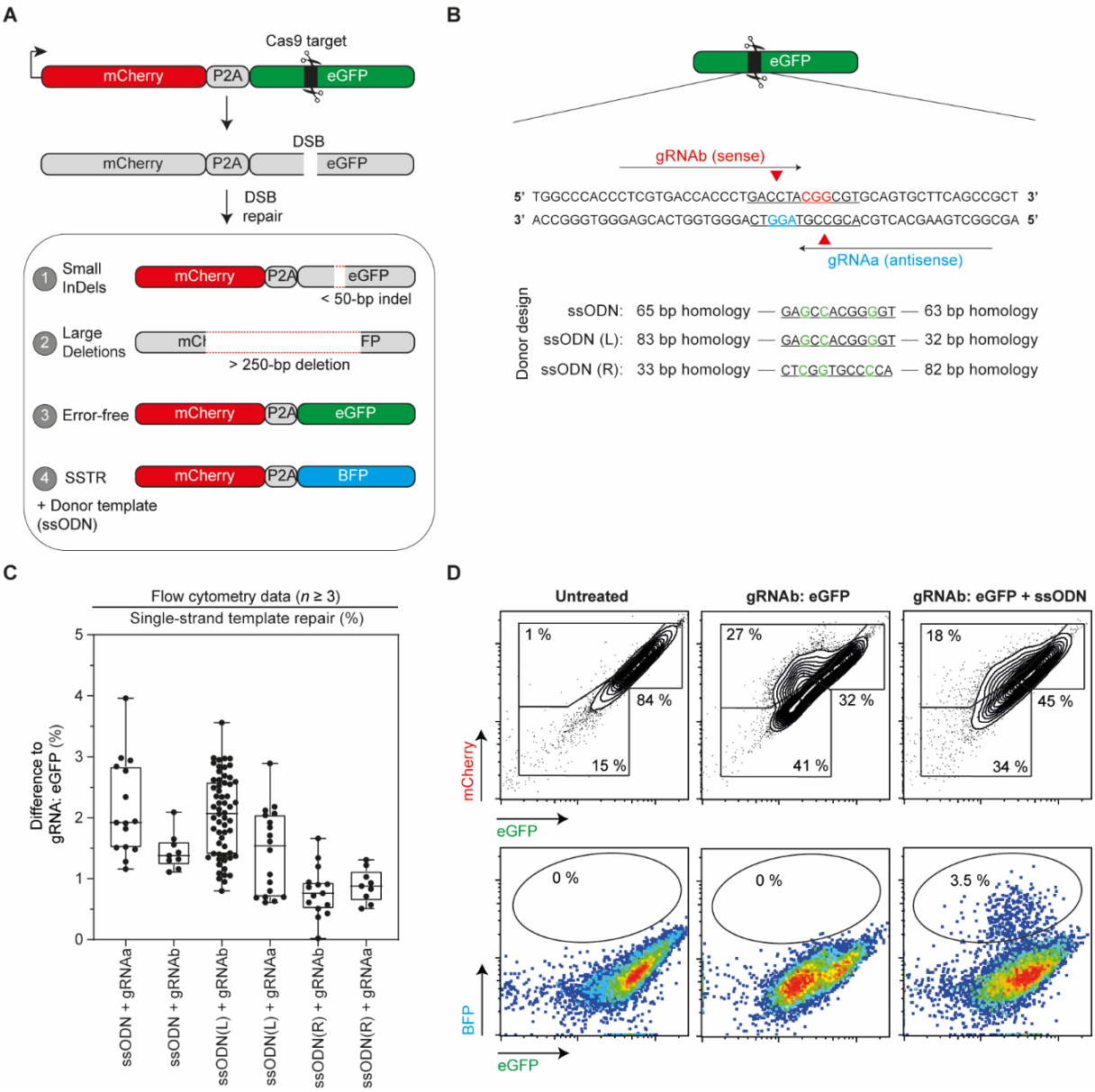

Figure 16: CAT-R as a Homologous Recombination reporter. (**A**) Representation of the CAT-R reporter with the supply of an external donor template as a single-stranded oligodeoxynucleotide (ssODN). The ssODN bears the necessary nucleotide changes to convert a Green fluorescent sequence to a Blue fluorescent sequence indicating a homologous recombination event. (**B**) The ssODN bares 2 mutations that change the amino acid from Proline to Alanine so that instead of the GFP the BFP is produced indicating a knock-in event via the single-strand template repair pathway. The asymmetric design of donor templates is also illustrated. (**C**) A box and whiskers plot (min to max) showing the frequency of conversion of GFP to BFP with the use of an asymmetric ssODN template in cells that are transfected with the gRNAs that are depicted. A minimum of three biological replicates is used. (**D**) Representative flow cytometry analysis plots of HEK293^{CAT-R} cells 72 h post-transfection with the synthetic gRNA and the ssODN. Numbers shown inside plots indicate percentages of live cells. Axes report relative fluorescence intensity in arbitrary units. The conversion from GFP to BFP is quantified based on the control.

5.4. DNA repair deficiencies influence the CAT-R response

We hypothesized that DNA repair deficiencies could modulate the frequency of the two error-prone populations. Since DSB repair choices can alternate between end-protection and end-resection based mechanisms, we examined the response of CAT-R reporter, without the use of a ssODN, to specific defects in DSB response.

Deficiency in end-protection decreases small InDels

Using the CRISPR/Cas9 system we first generated single knock-out (KO) clones of *PRKDC* and *XRCC4*, which are two of the most critical components of the c-NHEJ pathway, mediating end-protection based DSB repair (Davis and Chen 2013). For each gene of interest one gRNA is used to transfect the HEK293^{CAT-R} cells (**Figure 17 A**). Afterward, monoclonal cell lines are generated by limiting dilution and once fully-grown clones are selected for validation. The KO efficiency is validated by immunofluorescence for PRKDC (**Figure 17 B**), and by immunoblotting for XRCC4 (**Figure 17 C**).

In these two custom-made cell lines, we evaluated the phenotype of the CAT-R reporter in response to defects in end-protection pathways (**Figure 17 D**). In agreement with our hypothesis, we observed the involvement of c-NHEJ in the formation of small InDels, in both cell lines upon DSB induction we observe a substantial reduction in the formation of small InDels on average by 31% (±7) together with an increase in the formation of large deletions (**Figure 17 E**). More specifically, loss of XRCC4 decreases the frequency of small InDels by 37% (±2), whereas the loss of PRKDC results in a reduction of small InDels by 25% (±1) (**Figure 17 F**). This slight difference might be explained by the fact that PRKDC is involved

during the early steps of c-NHEJ, whereas XRCC4 is involved during the last steps. Therefore, cells might have not fully committed to this type of end-joining repair and possibly they have repaired alternatively, hence the higher frequency of small InDels population.

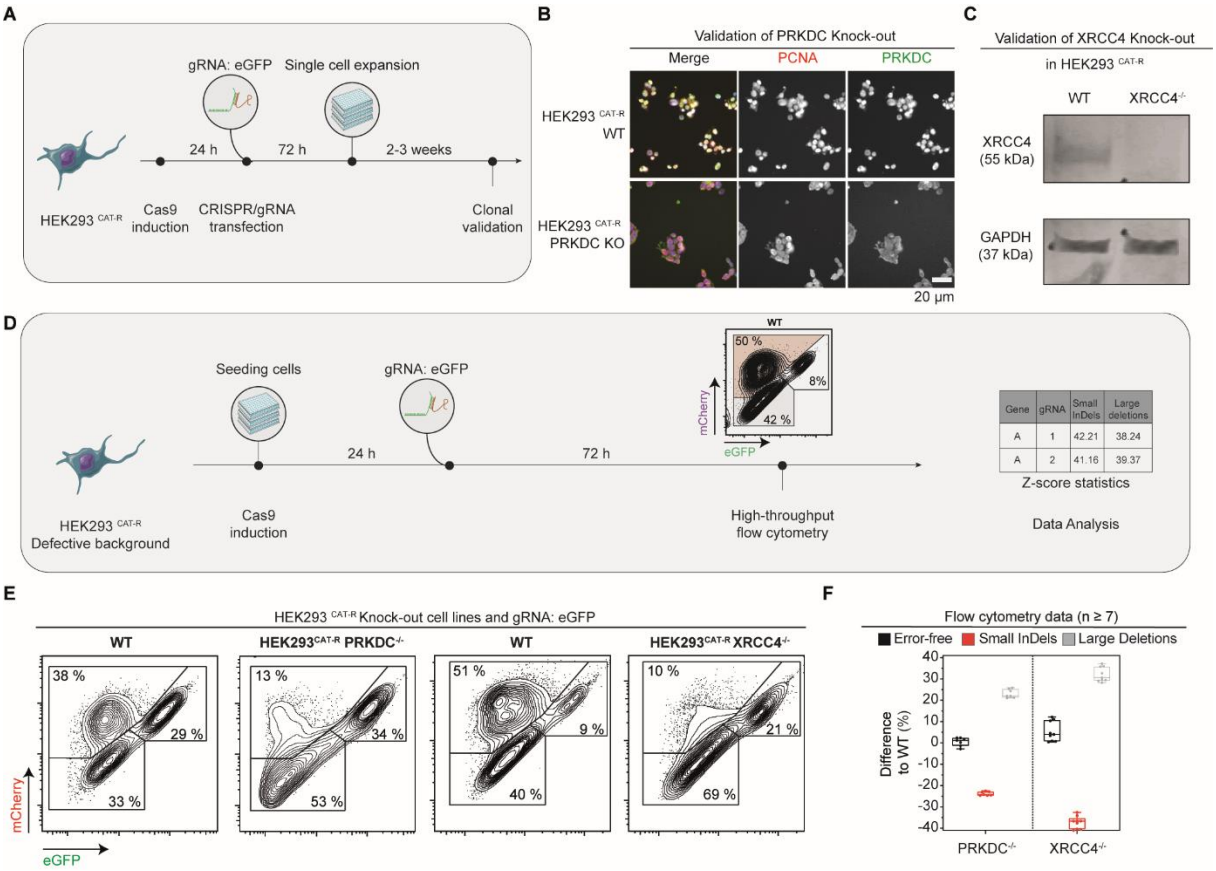

Figure 17: DNA repair deficiencies in end-protection influence CAT-R response. (**A**) Schematic workflow of generating custom deficient cell lines. (**B**) Validation of custom made PRKDC$^{-/-}$ HEK293^{CAT-R} cell line by immunofluorescence (IF). IF against PCNA and PRKDC in wild type and KO cells. (**C**) Validation of custom made XRCC4$^{-/-}$ HEK293^{CAT-R} cell line by western blot. Western blot against XRCC4 and GAPDH. (**D**) Schematic workflow of KO cell lines evaluating the CAT-R response to DDR deficient background. Representative flow cytometry analysis plot of HEK293^{CAT-R} cells 72 h post-transfection with the synthetic gRNA targeting the eGFP coding sequence in (**E**) PRKDC and XRCC4 KO cells. Numbers inside plots indicate percentages of live cells. Axes report relative fluorescence intensity in arbitrary units. Quantification plots of flow cytometry analysis for HEK293^{CAT-R} deficient cells are shown in (**F**). Data presented in box and whiskers (min to max) with 7 biological replicates.

Deficiency in end-resection decreases large deletions

Next, we tackle end-resection based repair pathways by targeting some of the critical molecules of homologous recombination (HR) and Fanconi anemia (FA) such as BRCA1, BRCA2,

USP1, and several FANC genes. The generation of KO cell lines in critical genes in this class may not be possible supporting the notion of essentiality of some of these genes for cell survival (Pearl et al. 2015). Therefore, in this case, we transfected cells with synthetic gRNA complexes targeting these genes (**Figure 18 A**) to generate a pool of cells with a defective end-resection background.

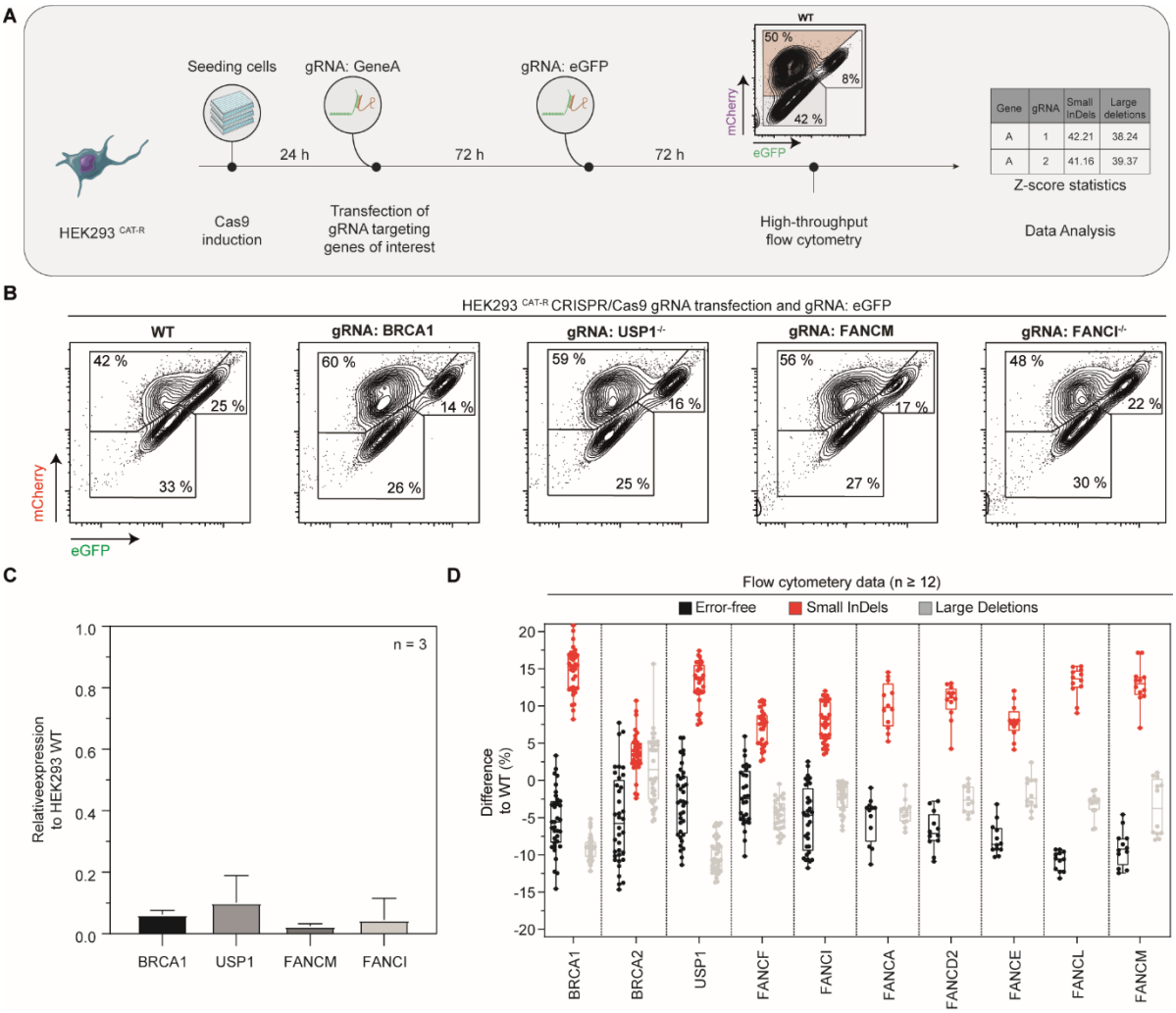

Figure 18: DNA repair deficiencies in end-resection influence CAT-R response. (**A**) Schematic workflow of a pool of CRISPR/gRNA transfected cell lines evaluating the CAT-R response to DDR deficient background. (**B**) Representative flow cytometry analysis plot of HEK293^{CAT-R} cells 72 h post-transfection with the synthetic gRNA targeting the eGFP coding sequence in a pool of CRISPR/gRNA transfected cells. Numbers inside plots indicate percentages of live cells. Axes report relative fluorescence intensity in arbitrary units. (**C**) Validation of RNA levels reduction by RT-qPCR expression analysis in HEK293^{CAT-R} 72 h after crRNA:tracRNA transfection. Quantification plots of flow cytometry analysis mixed pool CRISPR/gRNA transfected cells are shown in (**D**). Data presented in box and whiskers (min to max) with a minimum of 12 biological replicates.

Consistent with the idea that end-resection can lead to large deletions, knocking out essential genes involved in end-resection led to an increase in the formation of small InDels on average by 10% (±5) and a decrease in the formation of larger deletions (**Figure 18 B**). The level of KO efficiency is controlled by measuring the RNA levels of the transfected cells three days post-transfection by quantitative polymerase chain reaction (RT-qPCR) (**Figure 18 C**). The strongest phenotype is observed when BRCA1 and USP1 are KO. Both proteins are collaborating when chromatin remodelers unwind the DNA structure allowing for end-resection based repair. The role of BRCA1 and USP1 is to further support the end-resection by activating ATR, CHK1, and APC (Brown and Jackson 2015; Mjelle et al. 2015; Murai et al. 2011). The absence of BRCA1 and USP1 increases the frequency of small InDels by 15% (±3), and 13% (±3) respectively with the simultaneous reduction of large deletions as well as the frequency of error-free repair (**Figure 18 D**).

ATM deficiency increases the frequency of large deletions

We also wanted to analyze how ATM deficiency affects CAT-R response. On the one hand, ATM is stimulating DSB end-resection through phosphorylation and activation of the nuclease enzymes such as CtIP, MRE11, EXO1, and BLM. On the other hand, ATM also mediates end-protection through phosphorylation of DNA-PK_{cs} and the recruitment of Artemis (Jiang et al. 2015). In order to delineate the potential role of ATM in resolving DSBs, we generated an *ATM* KO cell line (**Figure 19 A**) and validated the KO efficiency of each single-cell clone by western blot. More specifically, the levels of ATM protein along with the levels of phospho-CHK2 protein, a downstream target of ATM, were detected in the presence of 1μM of

doxorubicin, a DNA damage reagent. In half of the tested clones, the ATM was successfully KO since the protein of both ATM and p-Chk2 was not present.

Next, we analyzed the repair upon a single double-strand break with CAT-R (**Figure 19 B**). In this case, ATM deficiency caused a decrease in small InDels on average by 3% (±1) and an increase in larger deletions presumably affecting end-protection based repair (**Figure 19 C**).

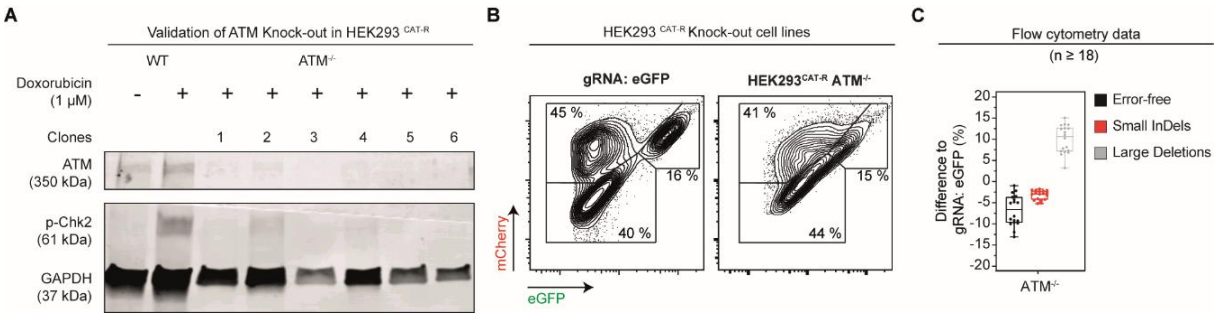

Figure 19: ATM deficiency influences DNA repair choice. (**A**) Validation of custom-made *ATM*$^{-/-}$ HEK293^{CAT-R} cell line by immunoblotting. Western blot against *ATM* and p-*CHK2* after incubation with 1 µM of Doxorubicin for 1.5 h. (**B**) Representative flow cytometry analysis plots of HEK293^{CAT-R} cells 72 h post-transfection with the synthetic gRNA targeting the eGFP coding sequence in *ATM* KO cells. Numbers inside plots indicate percentages of live cells. Axes report relative fluorescence intensity in arbitrary units. Box and whisker plots (min to max) of flow cytometry analysis for HEK293^{CAT-R} deficient cells are shown in (**C**). Data presented with a minimum of 18 biological replicates.

PARP1 deficiency reduces the frequency of small InDels

Next, we analyzed how CAT-R can respond to PARP1 deficiency. PARP1 plays an integral part during the repair of single-strand breaks. However, how it contributes to the repair of DSBs is less well defined, although it was suggested to play diverse roles in the repair of DSBs (Wei and Yu 2016). On the one hand, it is suggested to play a role during end-resection by rapid recruitment of MRE11 nuclease to the sites of DNA DSBs as well as later stages of HR presumably by limiting the amount of end-resection (Hengel et al. 2017). By recruitment of MRE11, PARP1 may also be involved in alternative end-joining.

On the other hand, it is also reported to stimulate c-NHEJ by interacting with and activating DNA-PK$_{cs}$. To delineate the potential role of PARP1 in resolving DSBs, a *PARP1* KO cell line is generated (**Figure 20 A**) and the repair upon a single double-strand break was analyzed (**Figure 20 B**). In this case, *PARP1* deficiency caused a decrease in small InDels on average by 6% (±1) and an increase in larger deletions, suggesting a more prominent role of PARP1 in either end-protection mediated repair or alt-EJ (**Figure 20 C**).

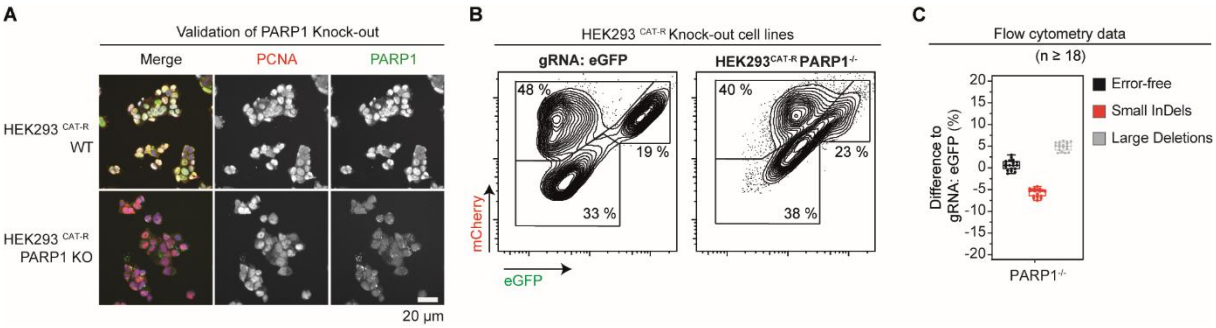

Figure 20: PARP1 deficiency influences DNA repair choice. (**A**) Validation of custom made *PARP1*$^{-/-}$ HEK293^{CAT-R} cell line by immunofluorescence (IF). IF against *PCNA* and *PARP1* in wild type and KO cells. (**B**) Representative flow cytometry analysis plots of HEK293^{CAT-R} cells 72 h post-transfection with the synthetic gRNA targeting the eGFP coding sequence in *PARP1* KO cells. Numbers inside plots indicate percentages of live cells. Axes report relative fluorescence intensity in arbitrary units. Box and whisker plots (min to max) of flow cytometry analysis for HEK293^{CAT-R} deficient cells are shown in (**C**). Data presented with a minimum of 18 biological replicates.

Deficiency in PRKDC and PARP1 reduces the frequency of small InDels by alternative types of repair

We have established so far that the loss of function of either *PRKDC* or *PARP1* is decreasing the formation of small InDels (**Figure 21 A**). More specifically, the results from CAT-R show that in a *PRKDC* KO background small InDels are heavily reduced by 25% (±1), whereas in a *PARP1* KO background small InDels are reduced by 4% (±4) (**Figure 21 B**). Even though both genes show a similar phenotype, the underlying mechanism of DNA repair differs. It is known

that microhomologies (MH) are the designated pattern of repair for alt-EJ, a pathway in which PARP1 is a prominent member. Therefore, to detect the different types of InDels that are generated when PRKDC and PARP1 are absent we performed deep targeted next-generation sequencing (NGS). Genomic DNA was harvested from cells 72 h post-transfection and a two-step PCR protocol was employed to prepare the PCR products for amplicon sequencing.

First of all, the data show that once PRKDC is lost, there is a significant reduction in the diversity of the various length types (**Figure 21 C**) such as deletions of 7-, 8-, 9-, 10-bp which are completely missing. Whereas at the same time, in a PARP1 deficient background a notable increase (13%) in the frequency of 1 bp insertions is observed with the simultaneous reduction of the 2-, 11-, and 24-bp deletions frequency, that as we have seen, are supported by MH (**Figure 21 C**). A closer look at the NGS data regarding the PRKDC deficient background shows a significant increase by 14% of the 2 bp length insertion frequency (**Figure 21 D**). Simultaneously the frequency of 11-, and 24-bp deletions is significantly increased since in most cases they are supported by MH of 2-8 bp length.

Moreover, NGS data shows that in a PARP1 deficient background, the frequency of 2-, 11-, and 24-bp deletions that are supported by microhomologies is decreased. Our findings demonstrate how alt-EJ is involved during the DNA repair process (**Figure 21 D**) and are consistent with the current literature. Collectively our data suggest that in the absence of major components of c-NHEJ then a convergent pathway (alt-EJ) takes over the DNA repair process by increasing the rates of MH.

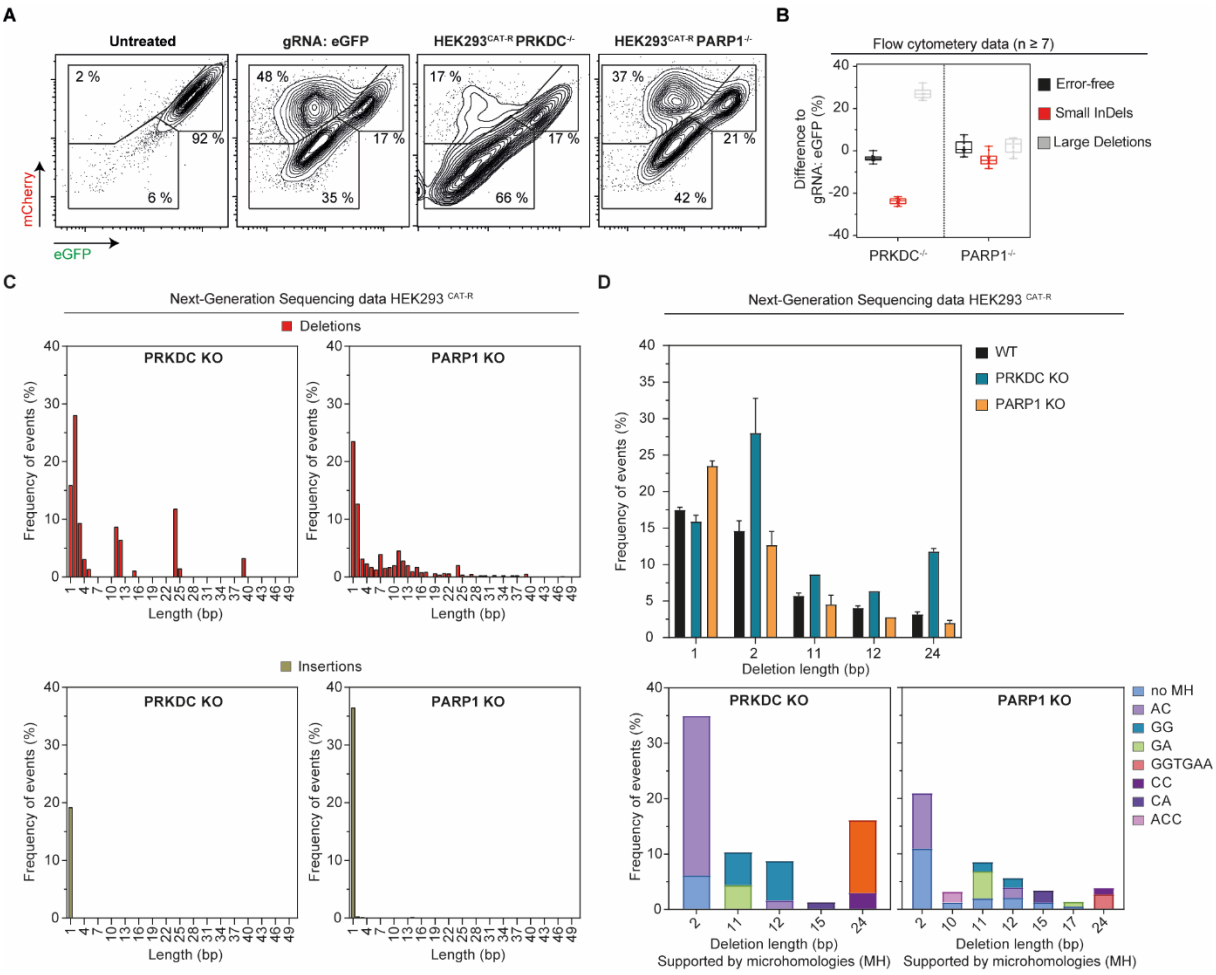

Figure 21: Mapping the impact of DNA repair deficiency by sequencing. (**A**) Representative flow cytometry analysis plot of HEK293^{CAT-R} cells 72 h post-transfection with the synthetic gRNA targeting the eGFP coding sequence in *PRKDC* and *PARP1* KO cells. Numbers inside plots indicate percentages of live cells. Axes report relative fluorescence intensity in arbitrary units. (**B**) Quantification of flow cytometry analysis for HEK293^{CAT-R} deficient cells. Data presented in box and whiskers (min to max) with a minimum of 7 biological replicates. A standard student t-test is used to calculate the *P-values* between untreated and treated samples. (**C**) Deep targeted next-generation sequencing to detect InDels at the targeted site from genomic DNA harvested 72 h after transfection in *PRKDC* and *PARP1* KO cells. (**D**) Profile of the various bp length types in WT, *PRKDC* and *PARP1* KO cells.

The impact of genetic background in DNA repair choice

Next, we wanted to assess how the genetic background (*PRKDC*$^{-/-}$ and *PARP1*$^{-/-}$) influences the actions of 13 prominent DNA repair genes (*ATM*, *ATR*, *BRCA1*, *BRCA2*, *CHK1*, *NHEJ1*, *PARP1*, *PARP2*, *PARP3*, *POLQ*, *PRKDC*, *RAD51B*, *XRCC4*) involved in end-protection and end-resection pathways.

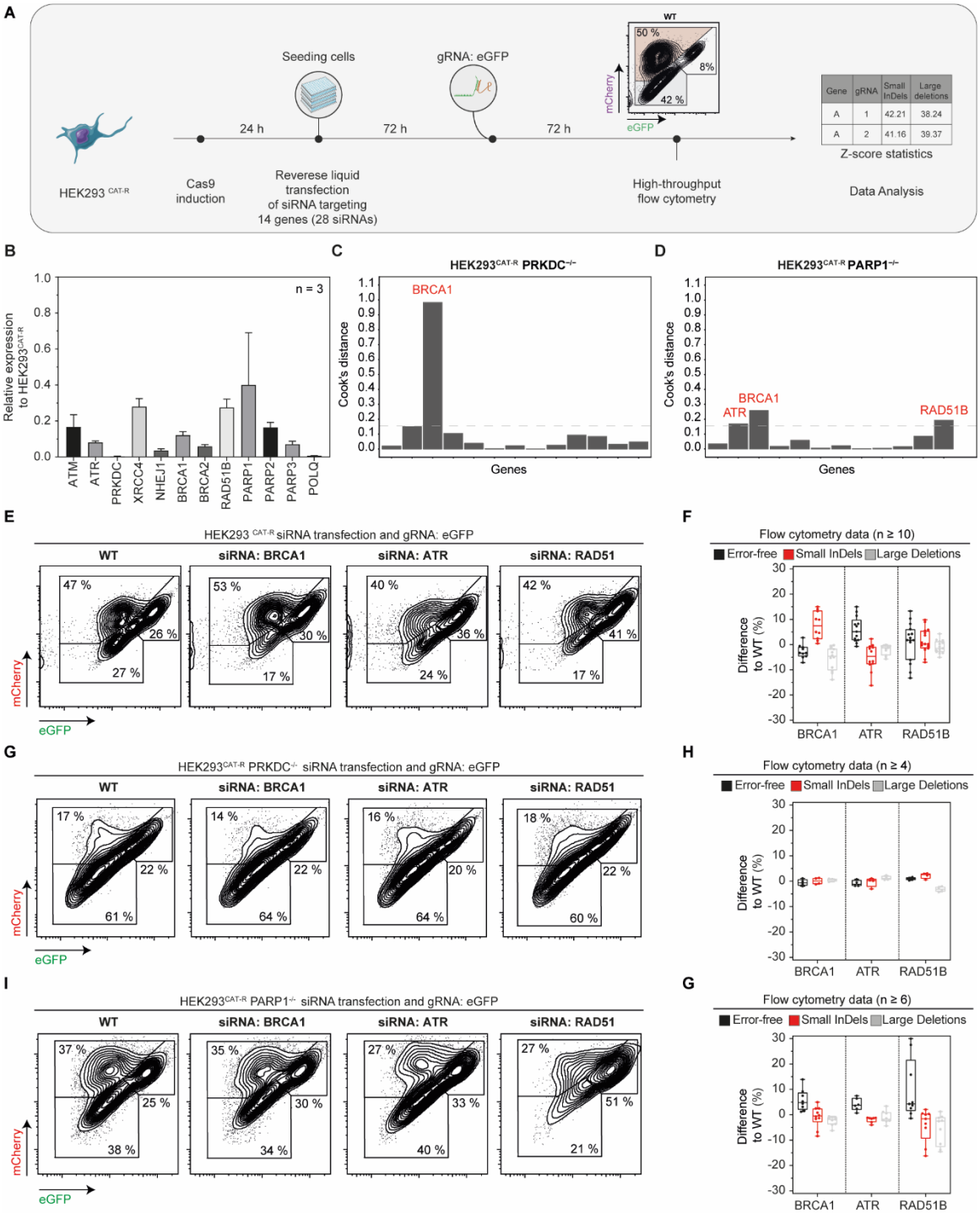

Figure 22: The impact of genetic background in DNA repair choice. (**A**) Schematic workflow of the mini siRNA screen. (**B**) Gene expression levels measured by RT-qPCR three days post-transfection with siRNA. Cook's distance bar plots in a (**C**) *PRKDC*, and (**D**) *PARP1* deficient background. Representative flow cytometry analysis plots of HEK293^{CAT-R} cells 72 h post-transfection with the synthetic gRNA targeting the eGFP sequence in (**E**) WT, (**G**) *PRKDC*, *and* (**I**) *PARP1* KO cells. Numbers inside plots indicate percentages of live cells. Axes report relative fluorescence intensity in arbitrary units. Box and whisker plots (min to max) of flow cytometry analysis for HEK293^{CAT-R} KD cells are shown in (**F**) WT, (**H**) *PRKDC*, (**G**) *PARP1* background. Data presented with 16 biological replicates.

Therefore, we used a small-scale arrayed RNAi screen, with every gene to be targeted by a set of 2 independent siRNAs. In total, we transfected 28 siRNAs, including negative controls to the cells by reverse liquid transfection and three days post-transfection, we delivered the gRNA targeting the eGFP sequence. At day 6, we assessed the eGFP and mCherry ratios by high-throughput flow cytometry, and we calculated Z scores of all three populations per gene based on non-targeting (scrambled) controls (**Figure 22 A**). The level of KD efficiency is controlled by measuring the RNA levels of the transfected cells three days post-transfection by RT-qPCR (**Figure 22 B**). In order to detect the genes with the highest impact, we used a standard outlier diagnostic tool (Cook's distance) for each of the three genetic backgrounds (WT, *PRKDC*$^{-/-}$, and *PARP1*$^{-/-}$) (**Figure 22 C, D**).

In a *PRKDC* KO background, we observe a change in the DDR response of the tested genes mostly in the frequency of large deletions. In this background, small InDels are a minor population that presumably points to repair by alt-EJ. In contrast, the *PARP1* KO background deregulates more genes, and especially genes that are involved in end-resection pathways, such as *BRCA1*, *ATR*, and *RAD51*. The impact of *PRKDC* loss is so prominent that none of the tested genes were able to influence significantly the small InDel phenotype (**Figure 22 E**). The results show that in a *PRKDC* deficiency, the effect of BRCA1 is minimized, implying that BRCA1 is no longer in the driving force of dictating the pathway choice since the burden of repair relies solely on end-resection pathways.

In the *PARP1* deficient background, the most affected genes are *RAD51B*, *BRCA1*, and *ATR*; with all three to be implicated in end-resection mechanisms. In PARP1_RAD51B deficient cells, the error-free repair is favored substantially with the simultaneous reduction of small InDels and large deletions. Similar results are observed also in the PARP1_BRCA1 and

PARP1_ATR deficient cells (**Figure 22 E,F,G**). Interestingly, cell viability remains intact throughout the seven days of analysis, with a minor reduction in the RAD51 deficient cells.

Recent studies have shown that in a PARP1 KO background, there is an increase in Rad51 foci formation (Ronson et al. 2018), suggesting that RAD51 might have a progressive role in dictating the fate of end-resection. Our results indicate a direct or indirect PARP1 association to RAD51 in restoring HR (**Figure 22 I**). In addition, previous studies have shown that in the absence of PARP1, Ku70/Ku80 dimer, 53BP1, and RIF1 are no longer localized to the DNA damage site effectively (Ray Chaudhuri and Nussenzweig 2017). Therefore, the presence or absence of BRCA1, which acts as the opposing side to maintain the balance of end-protection vs. end-resection, might not be so crucial in a PARP1 deficiency. A remark that can be highlighted from our data, since the loss of BRCA1 in a PAPR1 deficient background does not affect the DNA repair choice as much as it did in a wild-type background (**Figure 22 I**).

Chapter 6

Drug compound screening

Using genetic deficiencies in key molecules involved in DNA DSB repair, we established that CAT-R could dynamically respond to changing conditions in DSB repair choice. This chapter describes how CAT-R can be used to assess the level of engagement of a drug compound to DNA repair choice. Since the high efficiency of DSB induction in our system potentially allows us to detect even minor changes in DSB repair choice, we tested whether we can utilize this fluorescent reporter as a platform to assess the *in vitro* potencies of different DDR inhibitor classes. To this end, we selectively targeted the key enzymes of DNA repair that are in preclinical and clinical trials in a concentration-dependent manner. We first screened 13 inhibitors that target three significant classes of PI3 Kinase related protein kinase (PI3KK) family members that are involved in DNA damage signaling and repair: DNA-PK, ATM, ATR as well as the CHK1 and Wee1 kinase and analyzed their response by high-throughput flow cytometry. Next, we expanded our screening approach to 11 additional compounds targeting histone deacetylase (HDAC) and poly (ADP-ribose) polymerase (PARP) inhibitors. In this chapter, we present how CAT-R can be used as a platform to screen small pharmacological compounds.

Table 1: List of small pharmacological compounds used in this study

Compound name	Target	Cancer target type/ Indications	Development stage	Company
KU-0060648	DNA-PK	N/A	Phase I	KuDOS Ltd
M3814	DNA-PK	Rectal cancer, advanced solid tumors	Phase I/II	Merck KGaA
NU7026	DNA-PK	N/A	N/A	KuDOS Ltd
NU7441	DNA-PK	N/A	N/A	KuDOS Ltd
AZD0156	ATM	Advanced Solid Tumors	Phase I	AstraZeneca plc
KU-55933	ATM	N/A	N/A	KuDOS Ltd
KU-60019	ATM	N/A	N/A	KuDOS Ltd
M3541	ATM	Solid Tumors	Phase I	Merck KGaA
AZD6738	ATR	Small Cell Lung Cancer	Phase II	AstraZeneca
M1774	ATR	N/A	N/A	Merck KGaA
M4344	ATR	Advanced solid tumors	Phase I	Merck KGaA
M6620	ATR	Advanced solid tumors	Phase I	Merck KGaA
GDC-0425	CHK1	Refractory Solid Tumors	Phase I	Genetech Inc.
AZD1775	Wee1	Adenocarcinoma of the Pancreas	Phase II	AstraZeneca plc
Talazoparib	PARP	Locally Advanced Breast Cancer, Metastatic Breast Cancer	Phase III	Biomarin/Pfizer Inc.
Niraparib	PARP	Fallopian Tube Cancer, Ovarian Epithelial Cancer, Primary Peritoneal Cancer	Phase III	Tesaro/Merck & Co.
Rucaparib	PARP	Advanced Ovarian Cancer	Phase II	Clovis/Pfizer
Olaparib	PARP	Fallopian Tube Cancer, Metastatic Breast Cancer (MBC), Ovarian Epithelial Cancer, Refractory Advanced Ovarian Cancer	FDA approved	KuDOS/AstraZeneca plc
Veliparib	PARP	Ovarian Cancer	Phase II	Abbott Laboratories/ AbbVie
Iniparib	PARP	Solid Tumors	Phase III	Sanofi S.A.
INO-1001	PARP	Heart Diseases	Phase II	Inotek/Genetech

ATM, ataxia telangiectasia mutated; ATR, AT and rad-3 related; CHK1, checkpoint kinase 1; DNA-PK, DNA-dependent protein kinase; PARP, poly adenosine diphosphate-ribose polymerase.

6.1. DNA repair & small pharmacological compounds

We used a selective DNA-activated protein kinase catalytic subunit (DNA-PK$_{cs}$) inhibitor KU-0060648 (500 nM), a potent ataxia telangiectasia mutated (ATM) inhibitor AZD0156 (500 nM), and an ataxia telangiectasia and Rad3-related (ATR) inhibitor M4344 (100 nM) with our reporter to trace the impact on DNA repair choice after a Cas9-mediated DSB. From our data it is clear that inhibition of DNA-PK$_{cs}$ and ATM reduces the frequency of small InDels on average by 28% and 34% respectively (**Figure 23 A)**. On the other hand, ATR inhibition increases the frequency of small InDels by 5%, suggesting an opposing role in DSB repair choice.

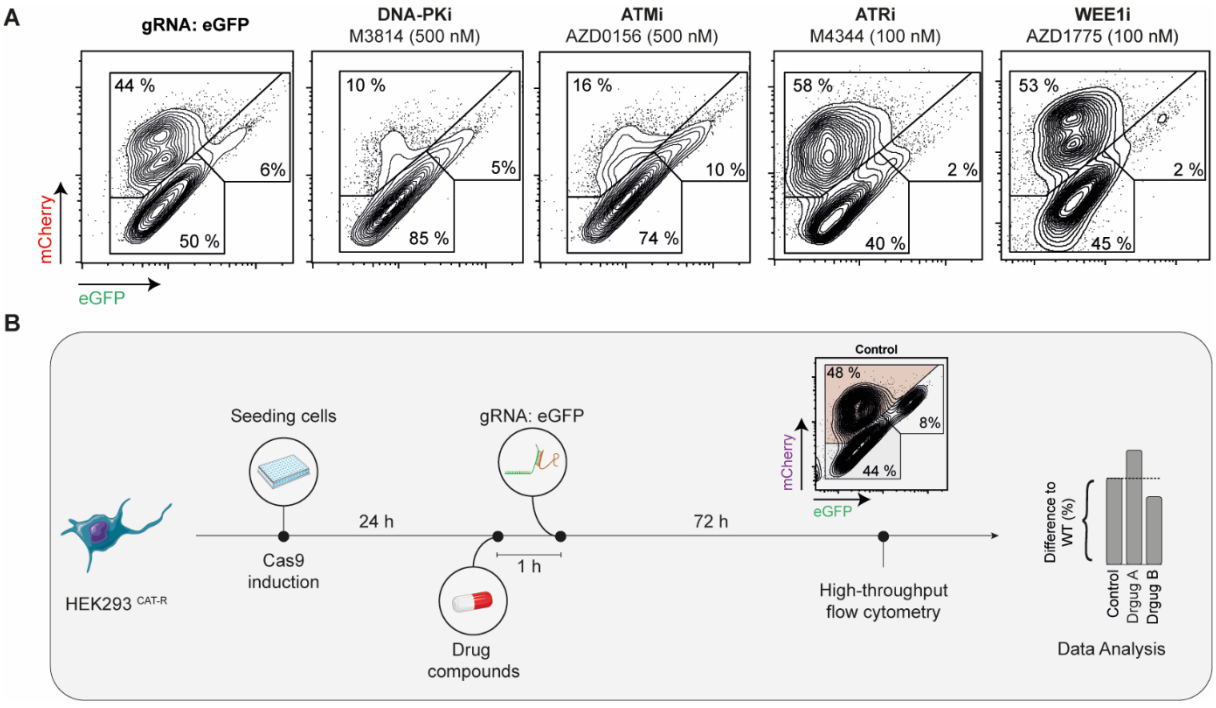

Figure 23: A platform to screen important DDR inhibitors. (**A**) Representative flow cytometry analysis plots of HEK293^{CAT-R} cells 72 h post-transfection with the synthetic gRNA in the presence of the inhibitors: DNA-PKi (KU-0060648), ATMi (AZD0156), ATRi (M4344) and WEE1i (AZD1775). Numbers shown inside plots indicate percentages of live cells. Axes report relative fluorescence intensity in arbitrary units. (**B**) Workflow schematic of the small pharmacological compound screen. HEK293^{CAT-R} cells induced with doxycycline (1 µg/ml) are seeded on a 96-well plate, and 24 h later, the cell culture medium is supplemented with the drug compounds. An hour afterward, the synthetic gRNA complex is transfected to the cells. Three days post-transfection, cells are analyzed in a high-throughput flow cytometer.

We coupled CAT-R with high-throughput flow cytometry to provide for the first time a head-to-head comparison of 24 pharmacological compounds, using CAT-R as a platform to screen small pharmacological compounds (**Figure 23 B**). Cells were seeded on a 96-well plate and 24 h later the cell culture medium was supplemented with the appropriate drug compound. An hour afterward, the synthetic gRNA complex targeting the eGFP sequence was transfected to the cells. Three days post-transfection, cells were analyzed in a high-throughput flow cytometer.

DNA-PKi acts in favor of end-resection

We compared four different DNA-PK_{cs} compounds that inhibit the major kinase responsible for the cellular c-NHEJ activity and DSB repair (Adamo et al. 2010) at 8 different concentrations from 1–500 nM. On average, the reduction of small InDel formation was 19% (±4) with the simultaneous increase of large deletions by 18% (±4) at 250 nM, coming in agreement with the phenotype we observed with the knock-out of *PRKDC* (**Figure 24 A**). These results follow the fact that in the presence of DNA-$PK_{cs,}$ the DSBs are repaired by the c-NHEJ pathway, which contributes to the $mCherry^{+}/GFP^{-}$ population.

Interestingly, there were no significant differences in DNA repair choice when the small-molecule inhibitor NU7026 was tested at concentrations lower than 500 nM. However, an improved analog of NU7026, the NU7441, performed slightly better by reducing the frequency of small InDels by 8% (±0.7) and increasing the large deletions formation by 5% (±0.5) at concentrations higher than 250 nM (**Figure 24 A**). However, when the DNA-PK_{cs} inhibitor KU-0060648 and M3814 were compared, there was no significant difference. The results show that both compounds have a similar pharmacodynamic profile, acting at concentrations as early

as at 50 nM by reducing the formation of small InDels on average by 18% (±4) and increasing large deletions by 19% (±4) (**Figure 24 A**).

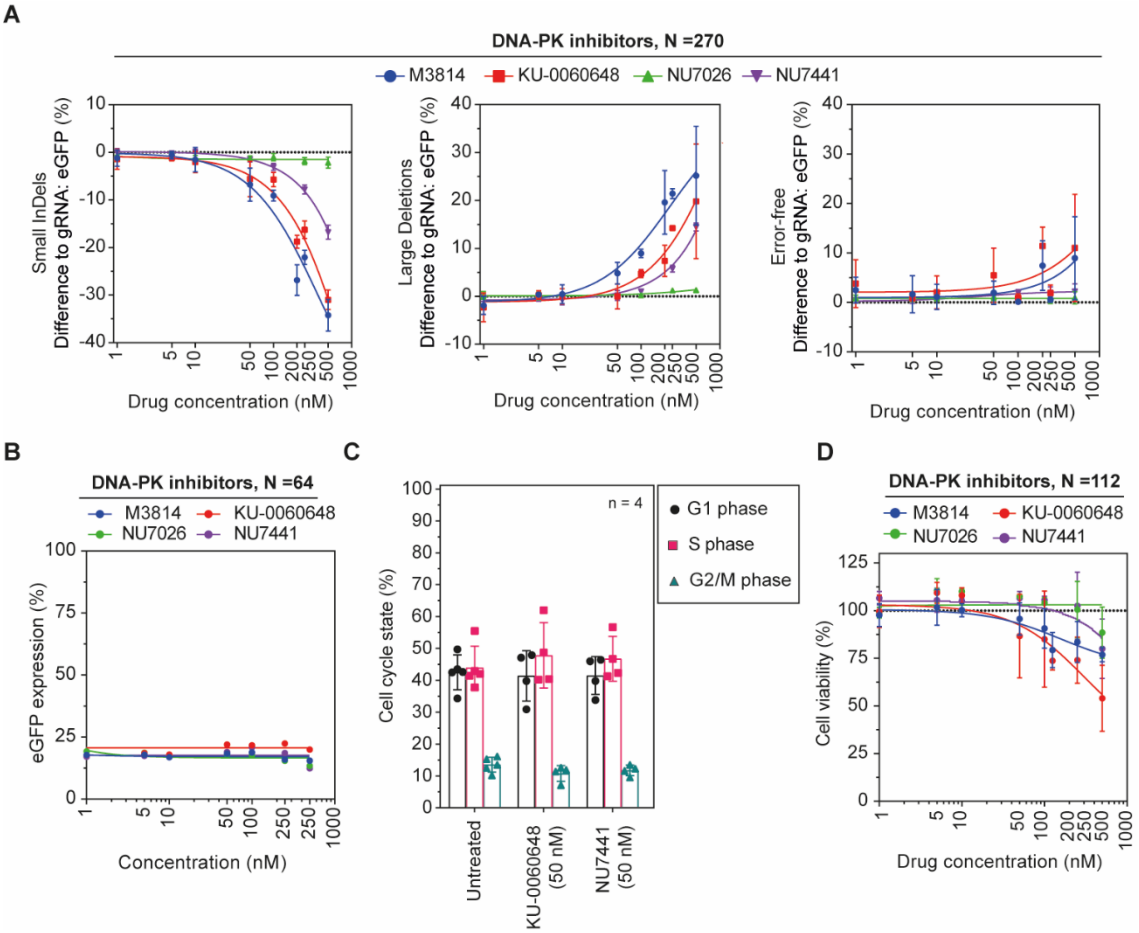

Figure 24: Effect of DNA-PK inhibitors in DNA repair choice. (**A**) Scatter plots (mean and SD error) of flow cytometry analysis for HEK293^{CAT-R} cells are showing the effect of DNA-PK$_{cs}$ inhibitors on the DNA repair choice, with sample size to be annotated. Additionally, a scatter plot (**B**) serves as a control to lipid-mediation in which a siRNA against eGFP is transfected in the presence of the inhibitors. The sample size is annotated, and the values are normalized to untreated control. (**C**) Cell cycle profile of DNA-PK$_{cs}$ inhibitors upon three days of treatment. (**D**) Cell viability assay in HEK293^{CAT-R} in the presence of DNA-PK$_{cs}$ inhibitors. The analysis is performed three days after treatment.

Meanwhile, we investigated whether compounds as standalone drugs, affect cell proliferation or have a prominent effect on cell cycle or transfection. We report that neither of the compounds exhibits any cell cycle or transfection de-regulation (**Figure 24 B,C**). However, we report that at concentrations between 200-500 nM, KU-0060648 slows down cell proliferation approximately by 50% during three days of incubation (**Figure 24 D**), findings

that are supported by other studies too (Chen et al. 2016). Overall, inhibition of DNA-PK$_{cs}$ acts in favor of end-resection by strongly decreasing the frequency of small InDels and increasing the formation of large deletions as well as the error-free repair.

ATMi phenocopies DNA-PKi profile

We wondered how ATM inhibition could affect DNA repair choice. To answer this question, we selected a series of ATM inhibitors to screen for their *in-vitro* influence in the choice of DNA repair at concentrations from 1–500 nM. We report several similarities with DNA-PK$_{cs}$ inhibition profile since the DNA repair choice after ATM inhibition leads to increased rates of large deletions by 24% (±2.6) and simultaneously to the reduction of small InDels formation by 26% (±2.8) at 250 nM (**Figure 25 A**).

It is clear that the AZD0156 compound achieves a robust change to the phenotype at concentrations as low as 5 nM, consistent with it is *in vivo* reported potency (Tse, Carvajal, and Schwartz 2007). Additional selective ATM inhibitor compounds such as M3541, and KU-60019, exhibit a similar profile by reducing small InDels formation and increasing large deletions on average by 25% (±2.6) at 200 nM (**Figure 25 A**). The compound KU-55933 appears to have a very week potency at concentrations lower than 500 nM. Additionally, we investigated the cell growth inhibition of individual compounds, and the findings indicate that only AZD0156 stalls cell growth almost by 50% at concentrations higher than 200 nM after three days of incubation (**Figure 25 B,C**). The most potent ATM inhibitor AZD0156 slightly increases the time cells spent in S phase (**Figure 25 D**), however, this effect is not substantial enough to explain the drastic decrease in the formation of small InDels observed upon ATM inhibition at similar concentrations.

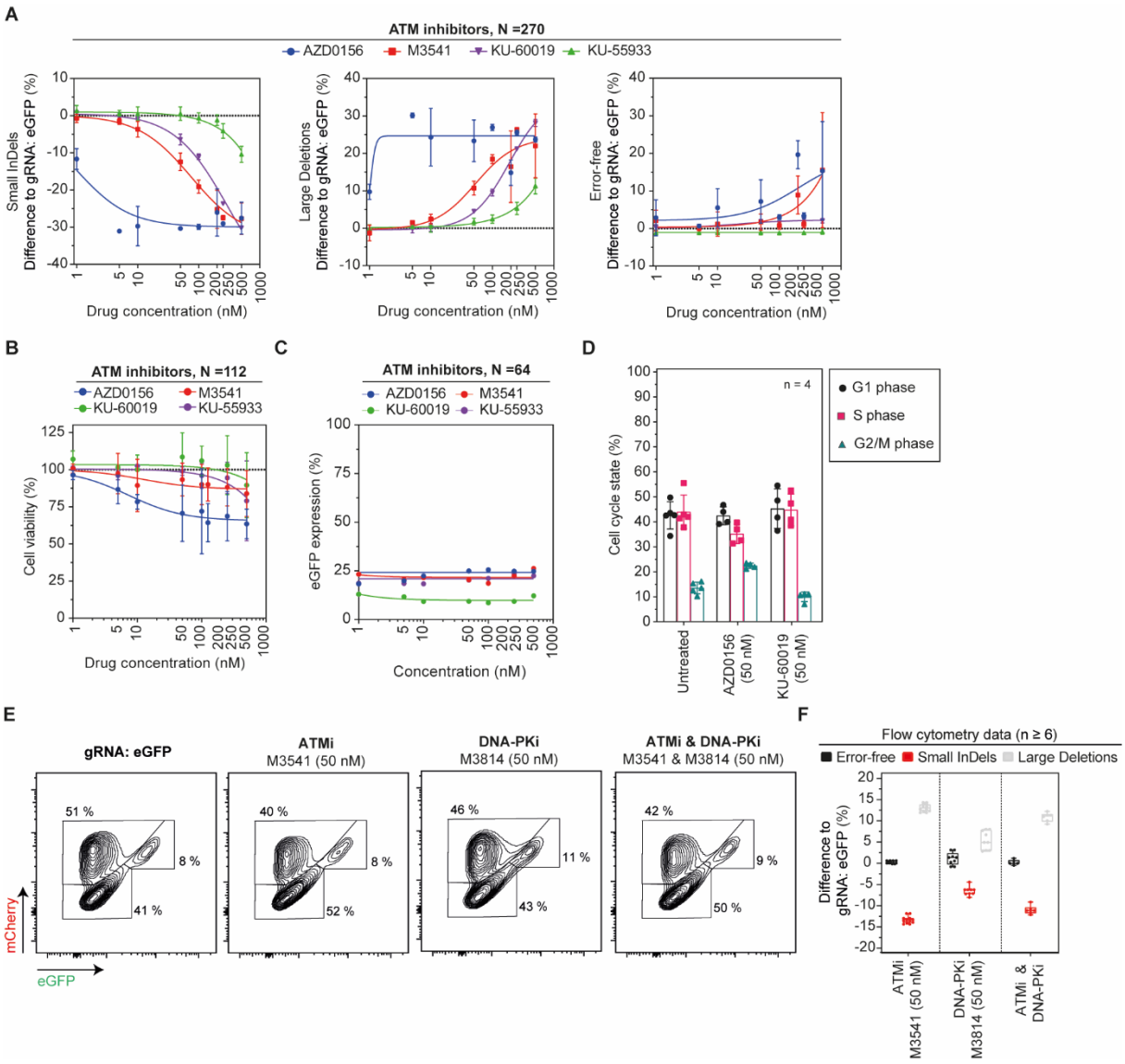

Figure 25: Effect of ATM inhibitors in DNA repair choice. (**A**) Scatter plots (mean and SD error) of flow cytometry analysis for HEK293^{CAT-R} cells are showing the effect of ATM inhibitors on the DNA repair choice, with sample size to be annotated. (**B**) Cell viability assay in HEK293^{CAT-R} in the presence of ATM inhibitors. The analysis is performed three days after treatment. Additionally, a scatter plot (**C**) serves as a control to lipid-mediation in which a siRNA against eGFP is transfected in the presence of the inhibitors. The sample size is annotated, and the values are normalized to untreated control. (**D**) Cell cycle profile of ATM inhibitors upon three days of treatment. (**E**) Effect of dual ATM and DNA-PK inhibition on DNA repair choice. Representative flow cytometry analysis plot of HEK293^{CAT-R} cells 72 h post-transfection with the synthetic gRNA targeting the eGFP HEK293^{CAT-R}. Numbers shown inside plots indicate percentages of live cells. Axes report relative fluorescence intensity in arbitrary units. (**F**) Box and whiskers plot (min to max) of flow cytometry analysis for HEK293^{CAT-R} cells in the presence of ATM and DNA-PK inhibitors. Data presented with a minimum of 6 biological replicates.

We also tested whether inhibition of ATM has off-target effects and directly impacts on DNA-PK$_{cs}$ activity. To this end, we compared the effect of DNA-PK$_{cs}$ inhibition, alone to combined inhibition of ATM and DNA-PK (**Figure 25 E**). Using 50 nM concentration of

DNA-PK$_{cs}$ inhibitor M3814, we have observed a 6.6% (±1.1) reduction in the formation of small InDels. This effect was exacerbated by the combined inhibition of ATM and DNA-PK$_{cs}$, leading to an 11% (±0.9) decrease in the formation of small InDels, arguing that ATM acts as the first responder at the ATM-DNA-PK$_{cs}$ signaling cascade (**Figure 25 E**).

Targeting the ATR-CHK1-WEE1 axis creates a dependency on end-protection

A large body of preclinical data supports the further development of ATR, CHK1, and Wee1 inhibitors that are currently being investigated in clinical trials as monotherapy or in combination with standard of care agents. Given their standing to clinical research a series of ATR inhibitors were used to evaluate their influence on DNA repair choice at concentrations from 1–100 nM.

The primary phenotype of the ATR inhibition was the reduction of large deletions and simultaneous increase of small InDels frequency on average by 3% (±2) at 100 nM (**Figure 26 A**). A pair of highly selective and potent small-molecule inhibitors of ATR, M4344, formerly known as VX803 & AZD6738 were used with CAT-R reporter assay. M4344 showed the most robust phenotype by influencing predominantly the end-resection pathways. It reduced the frequency of large deletions by 10% (±4.2) at 50 nM and channeled the DNA repair choice towards the formation of small InDels (**Figure 26 A**). The most surprising finding was the profile of the highly selective and potent ATR kinase inhibitor, AZD6738. The profile of AZD6738 differed among the other ATR compounds by reducing the formation of small InDels and increasing the formation of large deletions by 2% (±0.7) at 50 nM.

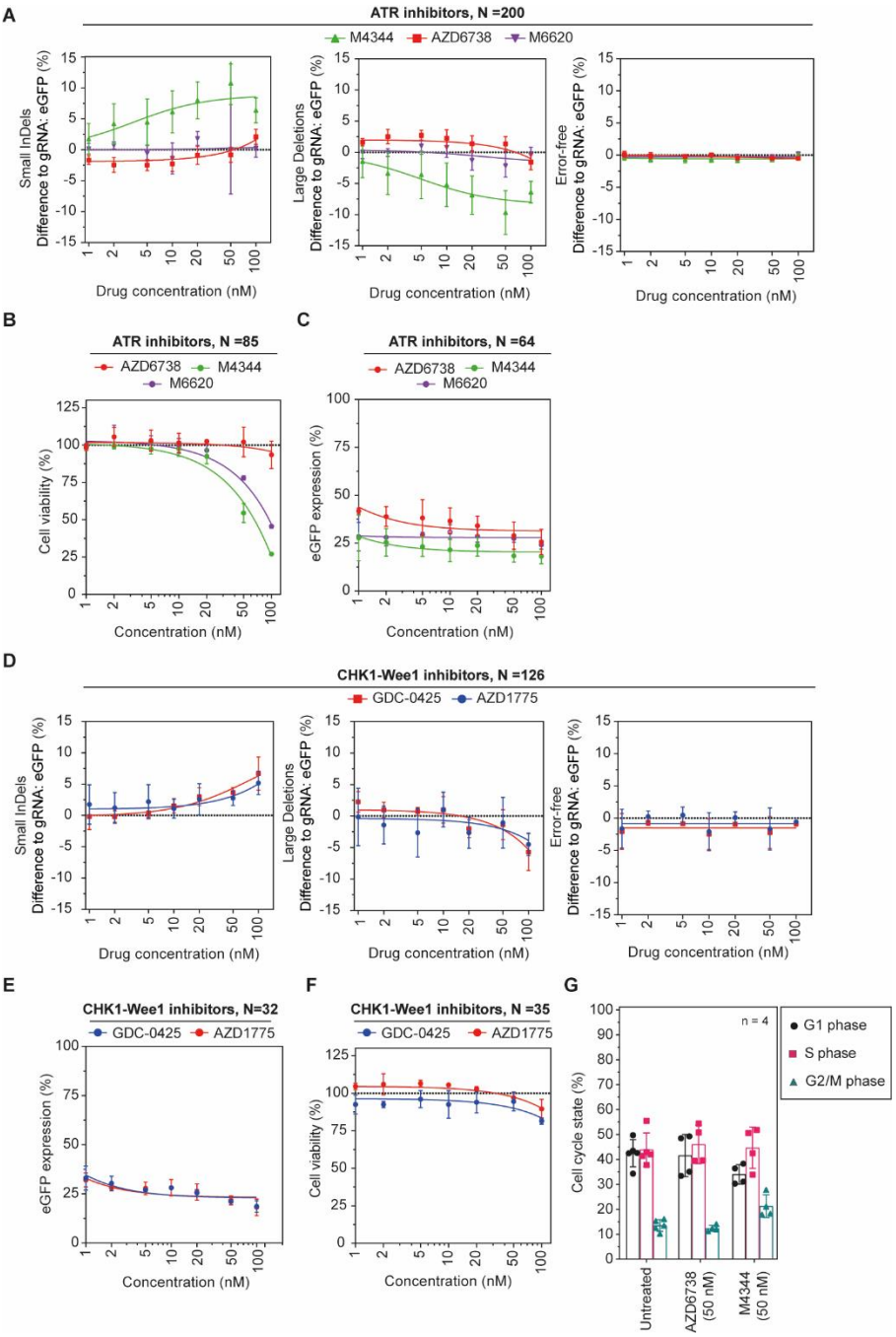

Figure 26: Effect of ATR-CHK1 inhibitors in DNA repair choice. Scatter plots (mean and SD error) of flow cytometry analysis for HEK293^{CAT-R} cells are showing the effect of (**A**) ATR, (**B**) CHK1-WEE1 inhibitors on the DNA repair choice, with sample size to be annotated. Cell viability assay in HEK293^{CAT-R} in the presence of (**C**) ATR, (**E**) CHK1-WEE1 inhibitors. The analysis is performed three days after treatment. Additionally, a scatter plot (**E, F**) serves as a control to lipid-mediation in which a siRNA against eGFP is transfected in the presence of the inhibitors. The sample size is annotated, and the values are normalized to untreated control. (**G**) Cell cycle profile of DNA-PK$_{cs}$ inhibitors upon three days of treatment.

Additionally, we investigated the cell growth inhibition of individual compounds, with M4344 and M6620 compounds to show signs of severe cell toxicity at concentrations higher than 50 nM that can reach up to 75% in 100 nM concentration. On the contrary AZD6738 compound exhibits no signs of cell proliferation stalling or any type of cytotoxic effects (**Figure 26 B**).

We also evaluated the inhibition of CHK1, which is a downstream target of ATR, with a selective compound (GDC-0425). The profile of GDC-0425 showed a similar phenotype with the ATR inhibitors since it reduces the frequency of large deletions and increases the formation of small InDels on average by 8% (±2) at 100 nM (**Figure 26 D**). In addition, we evaluated Wee1 inhibition, which is an inhibitor of CDK1 and plays a role in the ATR-CHK1 pathway in multiple ways. We used a potent and selective small-molecule inhibitor of Wee1, the AZD1775 compound (formerly known as MK-1775). Inhibition of Wee1 with AZD1775 showed a similar phenotype to ATR-CHK1 inhibition. Collectively our data suggest that by targeting the ATR-CHK1-Wee1 axis the DNA repair is channeled to end-protection pathways.

HDAC inhibitors in DNA repair choice

We tested four broad-spectrum histone deacetylase (HDAC) inhibitors to understand their effect on DDR choice. HDAC proteins remove acetyl groups from a lysine amino acid of a histone allowing them to wrap the DNA more tightly. Therefore, HDAC inhibitors promote the acetylation of histones potentially favoring end-resection based mechanisms. In contrast to what was expected, all compounds show a similar profile by increasing the formation of small InDels on average by 7.6% (±5.7) at 1 μM concentration and a simultaneous decrease in large deletions (**Figure 27 A**). The most substantial effect on DNA repair choice belongs to Abexinostat, and Panobinostat, a pair of pan-spectrum HDAC inhibitors. Abexinostat

increases the formation of small InDels on average by 10% (±2.3) at 500 nM, whereas Panobinostat shows a similar effect on average by 6.8% (±2.3) at a lower concentration (20 nM) (**Figure 27 B**). We also used another well-studied pan-spectrum HDAC inhibitor, Vorinostat (or else known as SAHA), in a concentration from 100-1000 nM but we were not able to detect a prominent swift in the DNA repair choice at those concentrations. From our data, we can suggest that Panobinostat has a higher *in vitro* drug potency than Abexinostat and other HDAC inhibitors.

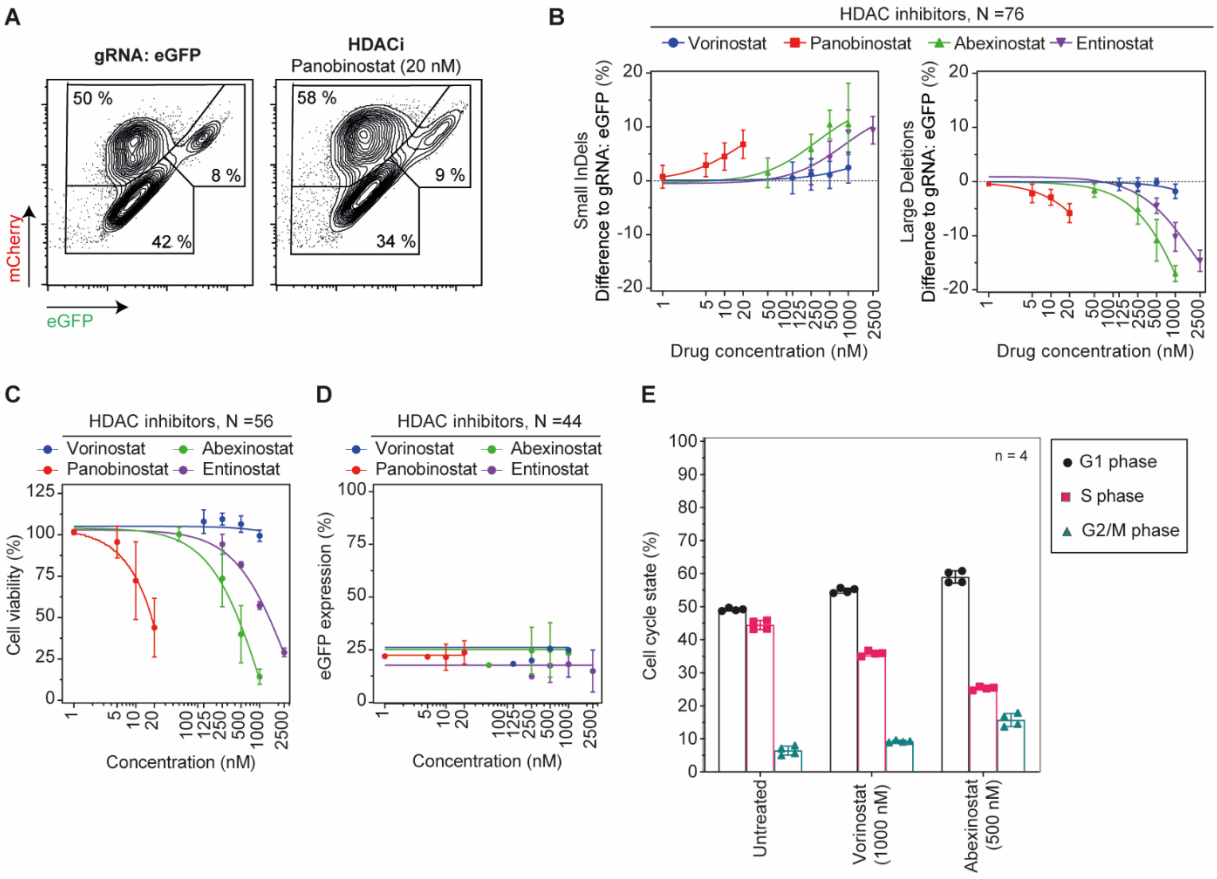

Figure 27: Comparing the *in vitro* activity of HDAC inhibitors. (**A**) Representative flow cytometry analysis plots of HEK293^{CAT-R} cells 72 h post-transfection with the synthetic gRNA in the presence of the inhibitor HDAC (Panobinostat). Numbers shown inside plots indicate percentages of live cells. Axes report relative fluorescence intensity in arbitrary units. (**B**) Scatter plots (mean and SD error) of flow cytometry analysis for HEK293^{CAT-R} cells are showing the effect of HDAC inhibitors on the DNA repair choice, with sample size to be annotated. (**C**) Cell viability assay in HEK293^{CAT-R} in the presence of HDAC inhibitors. The analysis is performed three days after treatment. Additionally, a scatter plot (**D**) serves as a control to lipid-mediation in which a siRNA against eGFP is transfected in the presence of the inhibitors. The sample size is annotated, and the values are normalized to untreated control. (**E**) Effect of HDAC inhibitors on the cell cycle profile.

Furthermore, we evaluated the effect of HDAC inhibitors on cell viability. In general HEK293^{CAT-R} cells were affected by HDAC inhibitors especially at high concentrations where cell viability was reduced up to 50% (**Figure 27 C**). Furthermore, to better understand the DNA repair outcome, we examined the effect of HDAC inhibition on cell cycle profile. Both Abexinostat and Panobinostat compounds affect the cell cycle, by increasing the time cells spent in G1 phase (**Figure 27 E**). This difference might be enough to explain the increase in the formation of small InDels, attributing the phenotype of HDACi mostly to the cell cycle stalling and not to DDR manipulation.

PARP inhibitors in DNA repair choice

Inhibition of poly (ADP-ribose) polymerase (PARP) shows promising results in preclinical studies and clinical trials. For some cancer types, PARPi is used either as a monotherapy or in combination therapy. In this study, we compared 7 PARP inhibitors sharing a similar architecture and evaluated their effect on DNA repair choice at concentrations from 0.5 nM up until 3 μM. In addition to our high throughput flow cytometry-based assessment of repair choices, we also evaluated the toxicity of each compound based on ATP measurements. The general phenotype of PARP inhibitors was the reduction of small InDels formation and the increase of large deletions on average by 4% (±1.6) at 50 nM (**Figure 28 A**). These results agree well with the idea that in the presence of PARP, the DSBs are repaired by the alternative EJ pathway, which contributes to the mCherry^{+}/GFP^{-} population.

Comparing the potency of all these PARP inhibitors, consistent with the literature, we found that Talazoparib performs much better than other inhibitors even at concentrations as low as 10 nM. Talazoparib reduces the formation of small InDels by 5% (±2.4) and slightly increases

the formation of large deletions at 50 nM (**Figure 28 B**). Increasing concentrations of Talazoparib higher than 50 nM exhibit a different phenotype, possibly due to the toxic effects of the drug in this cell line (**Figure 28 C**). Unexpectedly, in addition to the reduction of cell proliferation, we noted that at concentrations higher than 50 nM, Talazoparib also blocks lipid-mediated transfection; thus, they are excluded from our analyses (**Figure 28 D**).

The next group of inhibitors that are slightly less efficient than Talazoparib is Niraparib, Rucaparib, and Olaparib. At 200 nM concentration, the average reduction of these three compounds in the formation of small InDels is 4% (±1.7). These effects were exacerbated when we increased the compound concentration to 1 μM.

Interestingly, when we tested Veliparib, Iniparib, and INO-1001, a group of compounds that are among the first PARP inhibitors that were later shown not to possess any PARP-trapping activity, none of these three compounds exhibited any prominent effect in the repair of Cas9-induced DSB. Moreover, this group of compounds has a positive effect on cell proliferation at concentrations higher than 200 nM potentially due to the off-target drug effects on metabolic pathways (**Figure 28 E**).

Altogether these results suggest that CAT-R can measure not only differences in compound activities that directly affect DSB repair such as DNA-PK but also PARP trapping activity and can be used as a screening platform for a rapid *in vitro* assessment of DDR compound efficiencies.

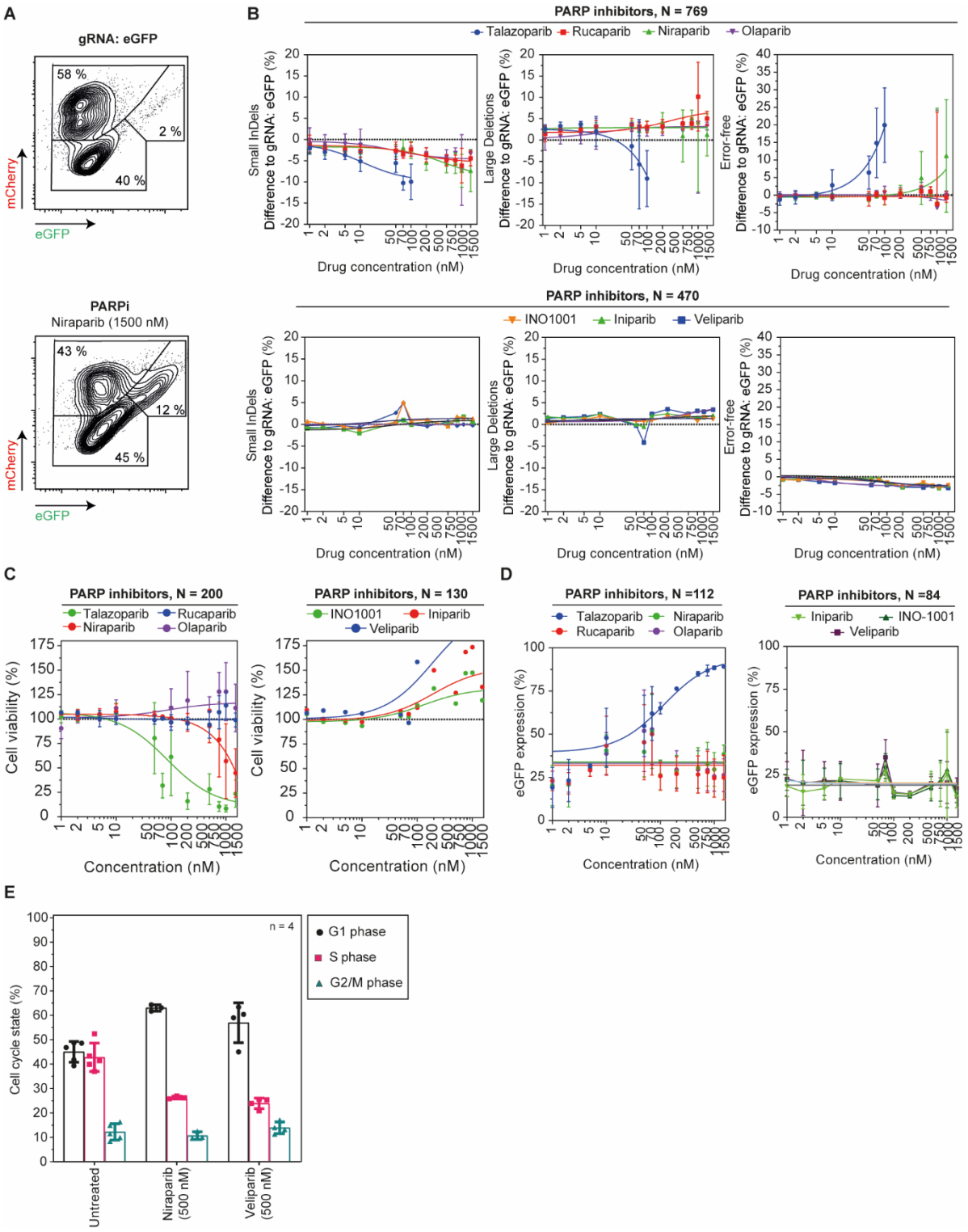

Figure 28: Comparing the *in vitro* activity of clinical PARP inhibitors. (**A**) Representative flow cytometry analysis plots of HEK293$^{CAT\text{-}R}$ cells 72 h post-transfection with the synthetic gRNA in the presence of the inhibitor PARP (Niraparib). Numbers shown inside plots indicate percentages of live cells. Axes report relative fluorescence intensity in arbitrary units. (**B**) Scatter plots (mean and SD error) of flow cytometry analysis for HEK293$^{CAT\text{-}R}$ cells are showing the effect of PARP inhibitors on the DNA repair choice, with sample size to be annotated.

(**C**) Cell viability assay in HEK293^{CAT-R} in the presence of PARP inhibitors. The analysis is performed three days after treatment. Additionally, a scatter plot (**D**) serves as a control to lipid-mediation in which a siRNA against eGFP is transfected in the presence of the inhibitors. The sample size is annotated, and the values are normalized to untreated control. (**E**) Effect of PARP inhibitors on cell cycle profile.

6.2. Predicting drug-likeness response with a machine learning model

Thanks to the high efficiency of the CAT-R system, even small differences in DSB repair choices can be evaluated, and different classes of compounds can be identified. To adapt this system for potential compound screening purposes, I collaborated with Dr. Salvatore Benfatto to build a machine-learning-based model that can predict the type of compounds based on their phenotype from the CAT-R assay.

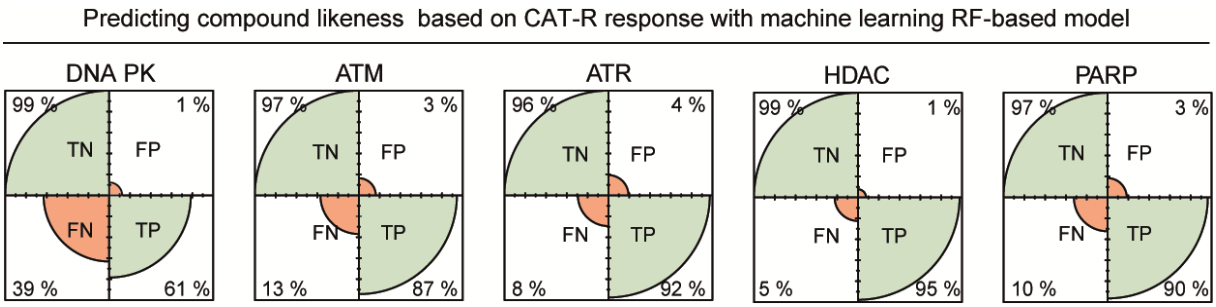

Figure 29: Machine learning model to predict drug-likeness response to DSB: Four-dot plots are showing the accuracy of the Random-Forest generated model for the different classes of compounds. TN: True Negative, FP: False Positive, TP: True Positive, and FN: False Negative.

A random forest (RF) model is generated to predict the classes of the compounds starting from the data in output from the CAT-R assay. A pre-filtering step is required to remove samples that do not show a significant change from the initial DSB phenotype. Of the 2624 initial samples, 434 are filtered out since they do not show significant changes from the control phenotype generated by the gRNA targeting the eGFP sequence without any treatment. From the remaining data, 80% was used to train an RF model, and the other 20% was used as a test

set to assess the model performance (**Table 2)**. The final RF model showed an overall accuracy of 83%, and the statistical measures for almost all the compound classes were generally high (**Figure 29)**. Notably, the model showed excellent ability to discriminate against the true negatives (high specificity) and to predict the classes of the DNA-PKi, ATMi, ATRi, and PARPi compounds in the test set correctly. Moreover, some ATMi and DNA-PKi compounds showed very similar phenotypes; however, we were able to predict accurately the right class the 68% and 65% of the times, respectively (**Figure 29**, **Table 2**). Overall the RF model exhibited great performances suggesting its potential future employment to predict the classes of unknown compounds, in terms of phenotype similarity with the trained classes, starting from the data in output from the CAT-R assay.

Table 2: Random Forest model analysis.

RF-based classification models

Class	Sample size (*n*)	Sensitivity%	Specificity (%)	PPV (%)	NPV (%)	Accuracy (%)
DNA-PKi	190	65%	95%	60%	96%	95%
ATMi	259	68%	97%	76%	95%	96%
ATRi	343	89%	96%	82%	98%	96%
HDACi	132	95%	99%	96%	99%	99%
PARPi	589	85%	94%	85%	94%	95%

N = 2190, CI: confidence intervals, PPV: Positive predictive value, NPV: Negative predictive value.

Validation data set - Confusion matrix

Prediction	Total	DNA-PKi	ATMi	ATRi	HDACi	PARPi
DNA-PKi	37	25	11	1	0	0
ATMi	46	11	35	0	0	0
ATRi	71	0	4	61	0	6
HDACi	25	0	0	0	25	0
PARPi	107	2	0	5	0	100

Accuracy: 83%, 95% CI: (79%, 86%), Kappa: 79%

ATM, ataxia telangiectasia mutated; ATR, AT and rad-3 related; CHK1, checkpoint kinase 1; DNA-PK, DNA-dependent protein kinase; HDAC. Histone deacetylase; PARP, poly adenosine diphosphate-ribose polymerase.

Chapter 7

CRISPR/Cas9 arrayed genetic screen

At present, little is known about the interplay of the DNA repair pathways during the decision of DNA repair choice. In the previous chapter, we established that CAT-R can respond to even minor genetic deficiencies during the DNA repair choice. In this chapter, we explore the effects of individual DNA repair genes on DSB repair and identify the major regulators of Cas9-mediated double-strand break repair.

7.1. An arrayed screen for regulators of DSB repair

The DNA damage response is a multifactorial process; therefore, we designed an arrayed CRISPR/gRNA library targeting 417 genes involved in DNA repair to investigate the effects of individual components during the DNA DSB repair. Each gene is targeted by two individual gRNAs, and in total, we transfected 932 gRNAs, including four positive (POLR2A) and six negative (Scrambled, non-targeting gRNA) controls to the cells by solid-phase transfection.

Three days post-transfection, we transfected the gRNA targeting eGFP, and three days later assessed the eGFP and mCherry ratios by high throughput flow cytometry. We calculated Z scores of all three populations based on non-targeting (scrambled) controls. We removed 48 genes whose KO resulted in a dramatic decrease in viability after five days from the subsequent analyses (**Figure 30 A**). Among 369 genes after this initial filtering step, we formed clusters based on the three populations applying a K-Means clustering method. Estimating the optimal number of clusters to be 5, we then performed pathway enrichment analysis on these 5 clusters.

A scatter diagram depicts the landscape of the fundamental mechanisms that regulate and promote the DNA repair choice after a Cas9-mediated DSB (**Figure 30 B**). As expected, c-NHEJ was enriched in the cluster with low Z scores of small InDels and high Z scores of large deletions, consistent with their phenotype of reduced formation of small InDels. In this cluster, loss-of-function of essential genes for end-protection, such as *RNF168*, *TP53BP1*, *ATM*, *SETX*, *PRKDC*, *XRCC4* displayed the most considerable differences as compared to the scrambled (**Figure 30 B**). On the other hand, loss-of-function of essential genes for end-resection, such as the FA components *BRCA1*, *USP1*, *COPS4*, *BARD1* significantly increased the formation of small InDels and reduced the formation of large deletions. In addition, loss of HRR components reduces the formation of large deletions primarily and channels the repair to small InDels formation. Several HRR components are positively affecting the formation of small or large InDels, suggesting that in the absence of these genes, a more efficient KO can take place (**Figure 30 C**).

In order to identify the most active influencers of Cas9-mediated DSB repair, we used a standard outlier diagnostic tool (Cook's distance) for each of the 369 genes (**Figure 30 D**). We found 25 genes that are identified as outliers.

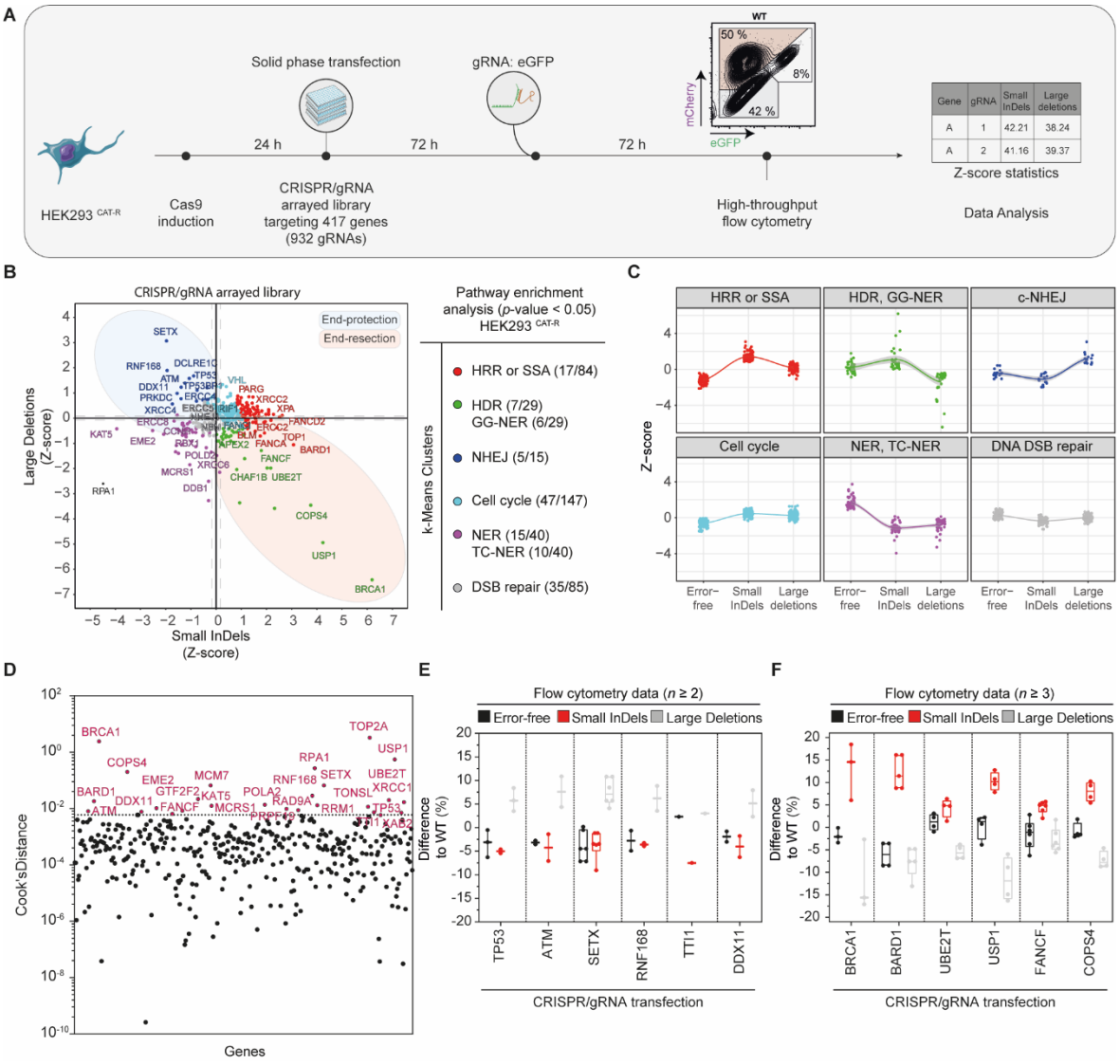

Figure 30: The landscape of Cas9-mediated double-strand break repair. (**A**) Workflow schematic of the CRISPR/gRNA genetic screen. In total, 417 genes are targeted with two different gRNA sequences. HEK293^{CAT-R} cells are induced with doxycycline (1 μg/ml) and then transfected with the solid-phase methodology in pre-coated 96-well plates to deliver the gRNA arrayed library. At 96 h, the cells are transfected with the gRNA: eGFP and at 7-day analyzed in a high-throughput flow cytometer. Data points are averaged, and the Z-score values are calculated per 96-well plate. (**B**) A scatter diagram showing the effect of 417 genes upon Cas9-mediated DSB. In the x-axis, the regulation of small InDels and in the y-axis, the regulation of the large InDels are presented. K-Means clustering is applied with the "elbow point" to be 6 clusters. Pathway enrichment analysis of the 6 clusters reveals the implication of end-resection, end-protection, and nucleotide excision repair (NER) related genes. (**C**) Individual k-Means clusters profile in terms of DNA DSB repair choice with the use of the CAT-R system. Each dot represents a gene. (**D**) Cook's distance bar plot identifies genes with the most robust phenotype upon Cas9-mediated DSB. Box and whiskers plots (min to max) of flow cytometry analysis for the HEK293^{CAT-R} cells are shown in (**E**), and (**F**). Values are normalized to control gRNA: eGFP.

Consistent with our clustering approach, we identified several known genes of the c-NHEJ (such as RNF168 and TP53) to be essential for decreasing the rate of small InDels formation

and increasing the rate of large deletions along with potentially new regulators of this process such as TTI1 and DDX11 (**Figure 30 E**). TTI1 was identified from a genetic screen as a part of a triple complex and is required for DNA damage signaling to stabilize ATM and ATR (Hurov, Cotta-Ramusino, and Elledge 2010). It controls the G2/M and Intra S-phase DNA damage checkpoints by regulating PIKK proteins (Ciccia and Elledge 2010). Here we confirm these discoveries and suggest that TTI1 acts in favor of the end-protection mechanism to an equal extent as the loss of ATM function.

Furthermore, DDX11 (also known as ChlR1) is a DEAH-box DNA helicase essential in DNA repair, chromosome structure, and genome integrity (Abe et al. 2016). It has been shown that DDX11 is vital to unwind the DNA with a 5' to 3' directionality, behaving similar to ERCC2 (XPD) (Bharti et al. 2014). Its action creates a 5' flap structure which resembles an intermediate step of the lagging strand synthesis and therefore DNA repair pathways such as base excision repair is required. Pearl *et al.* characterize DDX11 as a gene with probable DDR role (Pearl et al. 2015), and our data suggest that it is a strong influencer of small InDels formation (**Figure 30 E**).

Overall, loss of end-protection components decreases the frequency of small InDels, whereas loss of end-resection components increases the rate of small InDels (**Figure 30 E, F**). In a recent study, it was shown that multiple FA components were important for a Cas9-mediated single-strand template repair (SSTR) but not for c-NHEJ (Richardson et al. 2018).

7.2. Involvement of Nucleotide Excision Repair in Double-Strand Break

Interestingly, these analyses also revealed that individual NER components (such as *RBX1*, *RAD23A*, *DDB1*, *ERCC5*, *ERCC8*, and *ERCC3*) increased the "error-free" population while reducing both small InDels and large deletions. These results suggested that targeting these genes may increase the efficiency of error-free repair in cells upon Cas9-mediated breaks.

We tested the effect of individual NER components such as *ERCC5* (XPG), *ERCC8* and *ERCC3* (XPB) in regulating SSTR (**Figure 31 A**). To this end, we first transiently transfected the HEK293^{CAT-R} cells with gRNAs targeting the *ERCC5* (XPG), *ERCC8* and *ERCC3* (XPB), along with *PRKDC* that was previously shown to increase the rate of knock-ins.

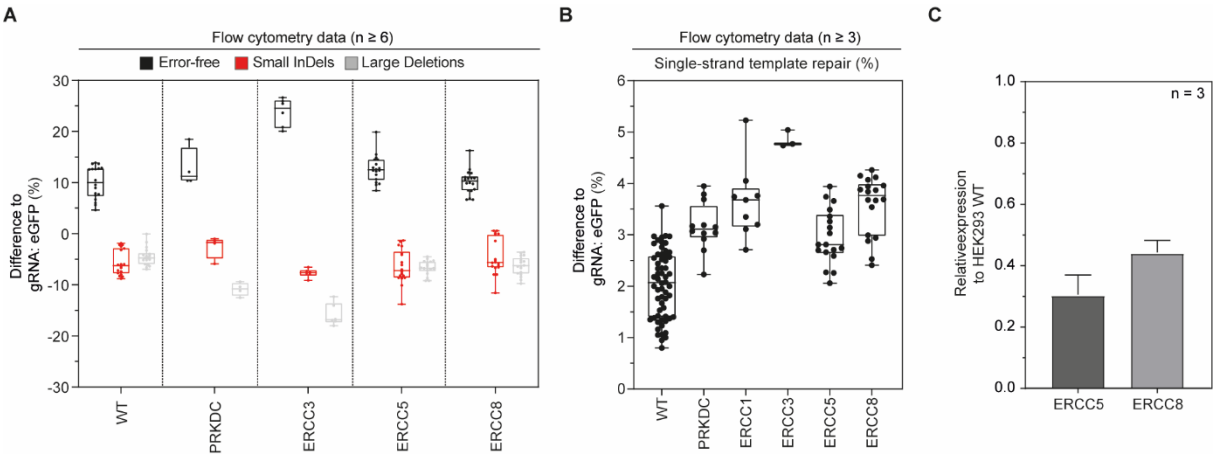

Figure 31: Deficiency in NER components increases Knock-in efficiency. (**A**) Box and whiskers plots (min to max) of flow cytometry analysis for the HEK293^{CAT-R} cells. Values are normalized to control gRNA: eGFP. (**B**) A box and whiskers plot (min to max) showing the conversion of GFP to BFP with the use of an asymmetric ssODN template. In the absence of PRKDC, the single-strand template repair (SSTR) is increased. Once essential NER genes are a knock-out, the SSTR is further increased. (**C**) The knock-out expression levels 72 h after transfection is validated by RT-qPCR.

We then transfected the gRNA targeting eGFP together with a ssODN serving as a template for GFP to BFP conversion. The efficiency of a successful conversion in normal

HEK293^{CAT-R} was, on average, 2.5% (±1.5). In the case of a genetic depletion such as *PRKDC*, the conversion efficiency was increased to 3.1% (±0.7) (**Figure 31 B**), consistent with previously reported effects of *PRKDC* KO in increasing the knock-in efficiency by blocking the c-NHEJ (Certo et al. 2011). Interestingly, when we target the NER genes that regulate the 3' flap removal such as *ERCC3*, *ERCC5*, *ERCC8*, we also observed an increase in the knock-in efficiency of up to 4.5% (±0.1). The level of KO efficiency is controlled by measuring the RNA levels of the transfected cells three days post-transfection by quantitative polymerase chain reaction (RT-qPCR) (**Figure 31 C**). Overall, the results suggest that removal of 5' to 3' flaps by the NER pathway is important for mediating SSTR and thus suggest an alternative way for increasing the rate of knock-ins in cell lines.

7.3. A proposed mechanism of Cas9-mediated DSB repair choice

Based on our results and previous reports, we propose a sequence of events that can occur upon a CRISPR/Cas9 mediated DSB (**Figure 32**). Once the Cas9 endonuclease binds to its DNA target sequence, it undergoes a massive conformational change of ~140^{o} (anti-clock-wise) that enables the dual cleavage of the loci (Zhu et al. 2019). An electron microscopy study has shown that the distal DNA end to the PAM sequence is released, whereas, in the proximal side, the Cas9 complex remains bound (M. Shibata et al. 2017). End-protection proteins will likely bind immediately to the released DNA strand stabilizing the ends and avoiding any chromosomal loss. Therefore, we hypothesize that it is less likely to have end-resection at the distal DNA side. On the other DNA side more and more studies so that a 5' to 3' flap will be generated

during the Cas9 cleavage process (Janssen et al. 2019), (Richardson, Ray, Dewitt, et al. 2016). Generally, 5' to 3' flaps can be removed by the NER mechanism. Here, we show that in the absence of crucial NER genes, most likely the 5' to 3' flap cannot be removed efficiently increasing the chances of a successful KI via SSTA/HDR event.

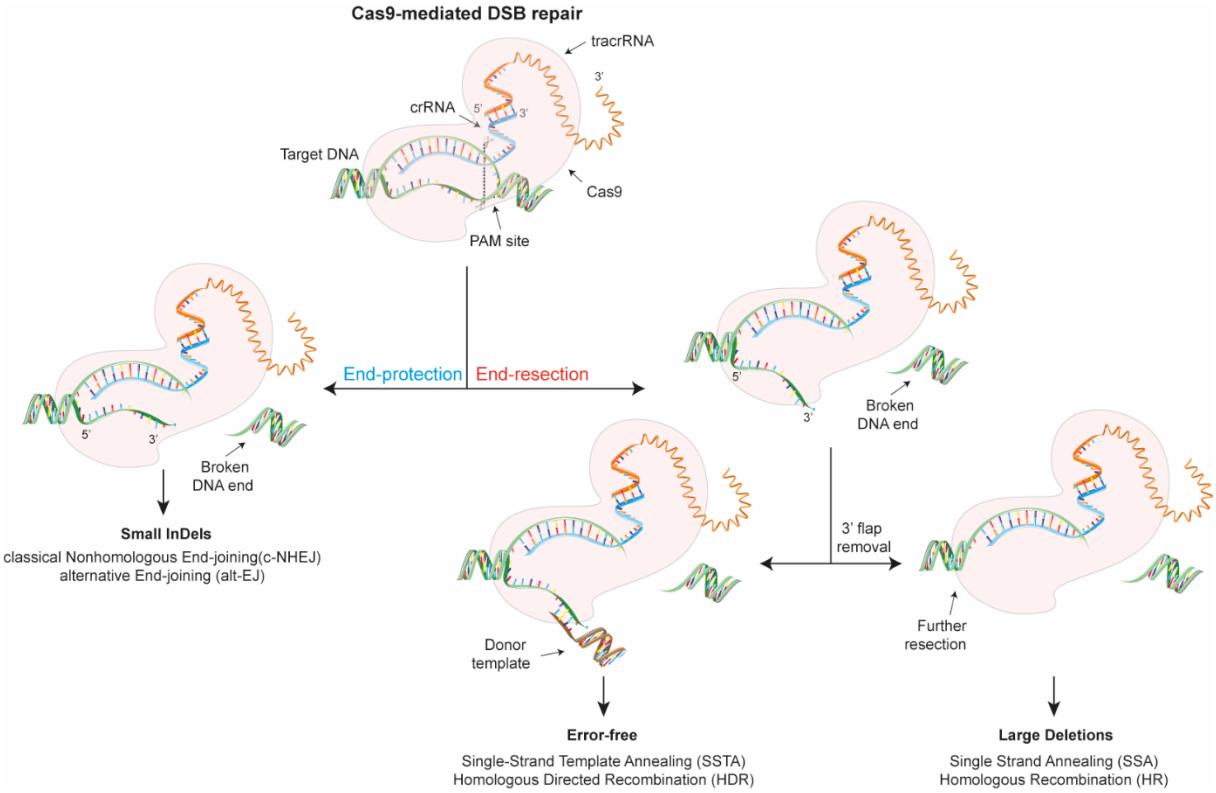

Figure 32: Proposed mechanism of Cas9-mediated DSB repair choice. Once a Cas9-mediated DSB occurs, end-protection mechanisms or alt-EJ will act to favor a quick ligation and thus form small InDels. If the damage is not repaired, then end-resection mechanisms will start resecting the region leading to large InDels. Due to the nature of Cas9-mediated DSB, a 3' flap is created and possibly it is removed with the help of NER components. If this 3' flap is not removed, then it favors a more efficient knock-in.

Chapter 8

Identifying novel PARP interactions

The impact of the genetic background in DNA repair choice is mostly understudied. In the previous chapters we showed how the loss of PARP1 deregulates several components of the DNA repair choice, and we highlighted the association of PARP1 and RAD51 in restoring the phenotype by increasing the rates of error-free repair.

In this chapter, we are using a custom arrayed genetic screen coupled to the fluorescent reporter to delve into the DSB repair landscape in a PARP inhibited background. We uncovered a gene cluster that is significantly affected by PARPi and regulates a key step during end-resection, suggesting potentially new interactions of PARP1 with DDR. Besides, we propose PARP inhibition as an alternative approach to increase the odds of a successful knock-in, since we show that PARP inhibition increases the rates of single-strand template repair to a similar extent with other well-known strategies.

8.1. PARP inhibition deregulates the DNA repair choice

At present, little is known about how DDR deficiencies influence the DNA repair choice and what is the interplay of the repair pathways during this process. Therefore, we used an arrayed genetic screen to evaluate the behavior of 417 components of DDR on DNA repair choice upon PARP inhibition (**Figure 33 A**).

We delivered the library with the solid-phase transfection approach, and three days later we transfected the gRNA targeting the eGFP sequence and supplemented the cell culture medium with 100 nM of Niraparib. Three days later, we assessed the eGFP and mCherry ratios by high-throughput flow cytometry. As anticipated from previous experiments, PARP inhibition reduced the frequency of small InDels and at the same time increased the frequency of large deletions (**Figure 33 B,C**).

Similar to the previous analysis, we calculated Z scores of all three populations, but this time based on the mean difference (ΔT) of the treated to the untreated sample and plotted their effect on a scatter plot (**Figure 33 D**). We removed 13 genes whose KO resulted in a dramatic decrease in viability after six days from the subsequent analyses. Among 404 genes after this initial filtering step, we formed clusters based on the three populations applying a Mclust clustering method. Finally, we estimated the optimal number of clusters to be 8, and then we performed pathway enrichment analysis on these 8 clusters. In order to identify the most influenced genes of PARP inhibition, we used a standard outlier diagnostic tool (Cook's

distance) for each of the 404 genes. Overall, we identified 30 genes that were recognized as outliers and showed a strong influence in their phenotype by PARP inhibition (**Figure 33 E**).

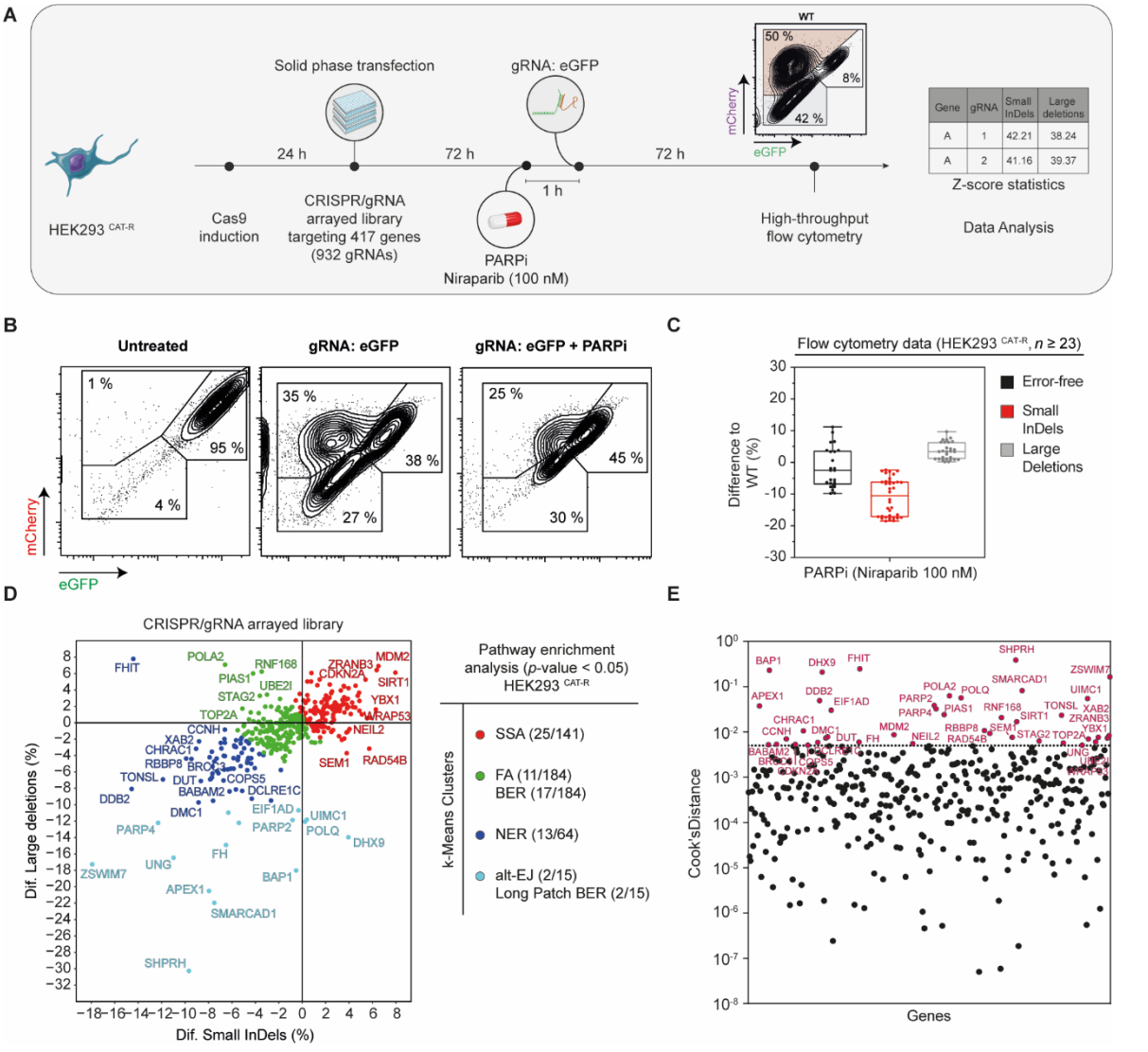

Figure 33: The impact of PARP inhibition on DNA repair choice. (**A**) Workflow schematic of the CRISPR/gRNA genetic screen. In total, 417 genes are targeted with two different gRNA sequences. HEK293^{CAT-R} cells are induced with doxycycline (1 µg/ml) and then transfected with the solid-phase methodology in pre-coated 96-well plates to deliver the gRNA arrayed library. At 96 h, the cells are transfected with the gRNA: eGFP and at 7-day analyzed in a high-throughput flow cytometer. Data points are averaged, and the Z-score values are calculated per 96-well plate. (**B**) Flow cytometry analysis plot of HEK293^{CAT-R} cells 72 h post-transfection with the synthetic crRNA:tracrRNA complex. Comparing the phenotypes between a non-targeting (scrambled) gRNA to a gRNA targeting the eGFP sequence and to a gRNA targeting the eGFP sequence in a PARPi background. Numbers inside plots indicate percentages of live cells. Axes report relative fluorescence intensity in arbitrary units. (**C**) Box and whiskers plots (min to max) of flow cytometry analysis for the HEK293^{CAT-R} cells that are shown in (**B**). (**D**) A scatter diagram showing the effect of 404 genes upon Cas9-mediated DSB in a PARPi background. In the x-axis, the regulation of small InDels and in the y-axis, the regulation of the large InDels are presented. mClust clustering is applied with the "elbow point" to be 8 clusters. Pathway enrichment analysis of the 8 clusters reveals the implication of end-resection, end-protection, chromatin organization, and RAD51 related genes. Annotated genes

exhibit the most robust phenotype upon Cas9-mediated DSB identified by a standard diagnostic tool. (**E**) Cook's distance bar plot identifies genes with the most robust phenotype upon PARP inhibition.

8.2. PARP antagonizes end-resection in double-strand break

Our clustering approach showed that several genes were significantly affected by PARP inhibition with the most important processes to be the NER pathway (*RPA1*, *RDC2*, *PCNA*, *DDB2*, *CDK7*, *RBX1*), the chromatin organization (*TOP2A*, *PRPF19*, *DDB1*) and the ATR signaling pathway (*RUVBL1*, *RFC2*, *RPA1*, *XRCC5*, *PCNA*, *RPA2*, *COPS3*). In these sets of genes, the DNA repair choice was channeled towards the error-free repair by reducing simultaneously the frequency of small InDels and large deletions (**Figure 34 A**). Evidence from recent studies describe similar associations of the multifaceted roles of PARP1 in chromatin remodeling and explain how PARP1 PARylates histone tails to relax the chromatin structure allowing for DNA repair to commence (Ray Chaudhuri and Nussenzweig 2017). In addition, PARP inhibition affected also *RAD21* that is involved in the regulation of the sister chromatin separation with studies to report that PARP inhibition down-regulates the expression levels of end-resection components that are also implicated in similar steps such as BRCA1 and RAD51 (Hegan et al. 2010; Schultz et al. 2003). Therefore, we conclude that the inhibition of PARP1 affects mostly genes that are associated with end-resection pathways.

Furthermore, we identified a gene cluster that is significantly affected by PARPi and increased the frequency of small InDels by reducing the levels of end-resection. This cluster is enriched in genes responsible for the BARD1 signaling events like the *PRBP8*, *BARD1*, and *UBE2T* genes that are interacting with EXO1, a 5' to 3' exodeoxyribonuclease, to resolve D-loop

structures that are formed during the end-resection repair (**Figure 34 A**). A recent study described how PARP1 blocks EXO1 (Caron et al. 2019) supporting our observations that PARP1 probably antagonizes end-resection based mechanisms in several steps.

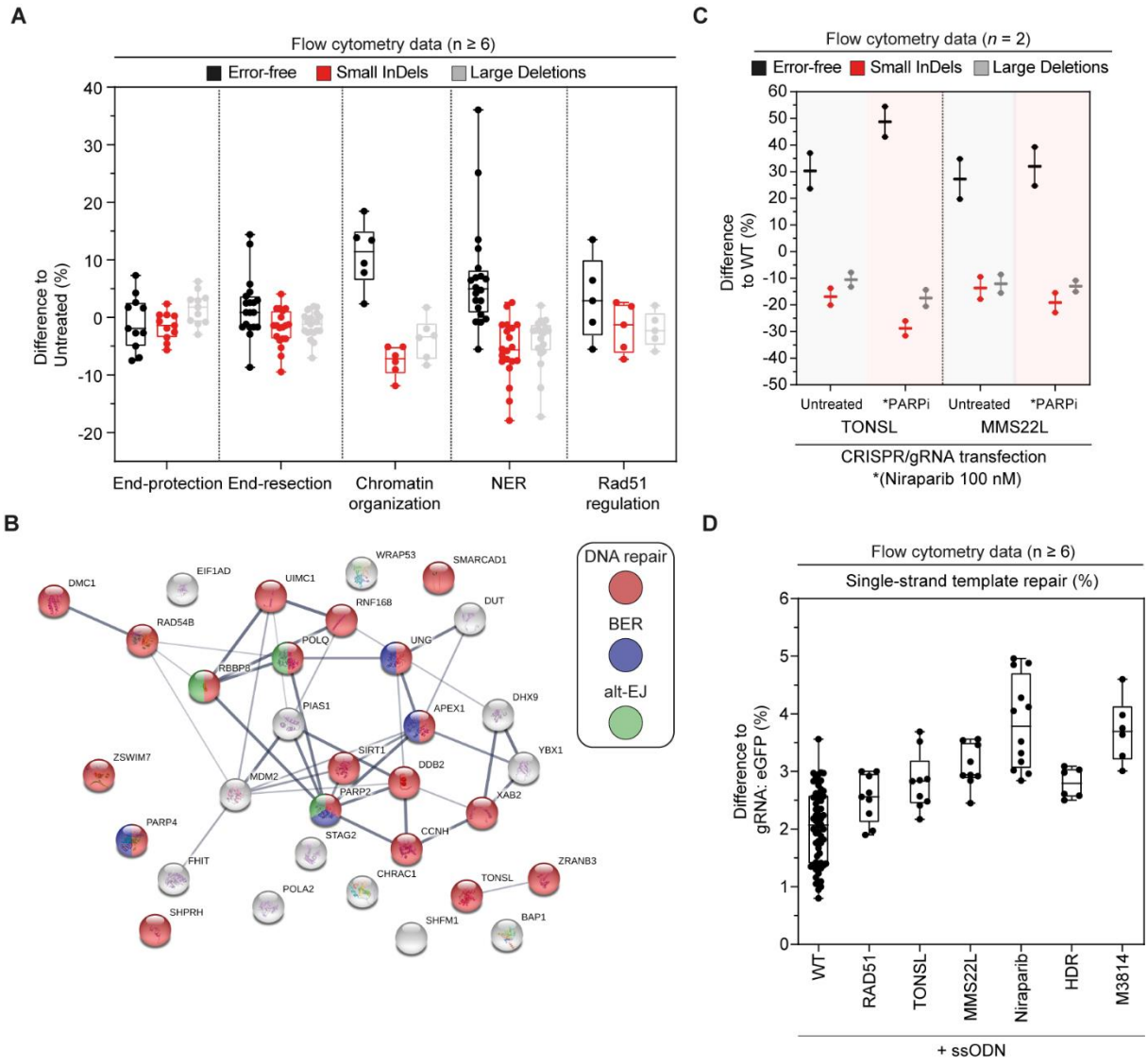

Figure 34: Identifying novel PARP interactions. Data presented in (**A**) are a cluster of genes based on relevant pathways. Values are normalized to control gRNA: eGFP. (**B**) A functional network of the most significant genes builds in StringDB. (**C**) Box and whiskers plots (min to max) showing the effect of TONSL-MMS22L complex to DSB choice. (**D**) Box and whiskers plots (min to max) showing the single-strand template repair efficiency in WT and several genetic backgrounds.

The most significant genes that are affected by PARPi create a functional network once analyzed with StringDB (**Figure 34 B**). The DNA repair was highlighted as the primary

process, and the nucleus was the cellular place where those interactions take place. The TONSL-MMS22L complex stands out with no immediate functional associations to the rest of the 28 genes. This complex reduced the frequency of both small InDels and large deletions with the simultaneous increase of the error-free repair (**Figure 34 C**). It appears that PARP inhibition regulates its activity since its effect is further enhanced upon inhibition. It is reported that this complex stimulates the recombination dependent repair of stalled or collapsed replication forks (Duro et al. 2010; Piwko et al. 2016) by promoting HR, and consequently it may act by mediating the assembly of RAD51 filaments on ssDNA. Interestingly when we targeted RAD51, and the TONSL-MMS22L complex we observed a moderate increase in the knock-in efficiency on average 2.9% (±0.4). Collectively from our observations, we suggest that PARP1 might antagonizes end-resection based repair mechanisms in more steps than already has been described and potentially it interacts with the TONSL-MMS22L complex to regulate RAD51 filament formation.

Furthermore, we wondered whether PARP inhibition influences knock-in efficiency. Therefore, we quantified its contribution and compared it with other known strategies that enhance knock-in efficiencies, such as the use of a DNA-PK_{cs} inhibitor (M3814) or the use of the commercially available HDR enhancer compound (**Figure 34 D**). Our data showed that PARP inhibition increased the knock-in efficiency by 3.9% (±0.7), whereas DNA-PK_{cs} inhibition by 3.7% (±0.5) and HDR by 2.8% (±0.2). In summary, we propose that PARP inhibition can be considered as an alternative approach to increase the odds of a successful knock-in.

8.3. A proposed role of PARP in double-strand break

The current literature suggests that PARP1/2 are one of the first responders to a double-strand break (Caron et al. 2019) and perhaps their influence in the choice of DSB repair is more significant than already presumed. PARP1/2 facilitates the recruitment of Ku70 to the DSB as well as the MRE11 nuclease (Caron et al. 2019). This dual character of PARP1/2 makes it a versatile molecule that promotes c-NHEJ but also activates limited end-resection, a step that is vital for alt-EJ (Chen et al. 2019; Muthurajan et al. 2014; Wray et al. 2013). In the meantime, it is reported that PARP1/2 blocks EXO1 (Caron et al. 2019) supporting the idea that PARP1/2 are antagonizing extended end-resection during DSB, possibly to favor limited end-resection by promoting alt-EJ.

Here we suggest that PARP1/2 interacts with another step of extended end-resection, the RAD51 filament formation (**Figure 35**). It has been shown that inhibition of PARP1 downregulates BRCA1 and RAD51 pathway (Hegan et al. 2010), but the exact mechanism of downregulation is still missing. We suggest that the TONSL-MMS22L complex is interacting with PARP1 to regulate the RAD51 filament formation step. Functional studies have already shown that the TONSL-MMSS2L complex promotes RAD51 dependent HR (Duro et al. 2010; Piwko et al. 2016) but not in the context of PARP inhibition. We suggest that loss of RAD51 in a PARP1 deficient background restores the error-free phenotype implying a further association of PARP1 to Rad51 filament formation.

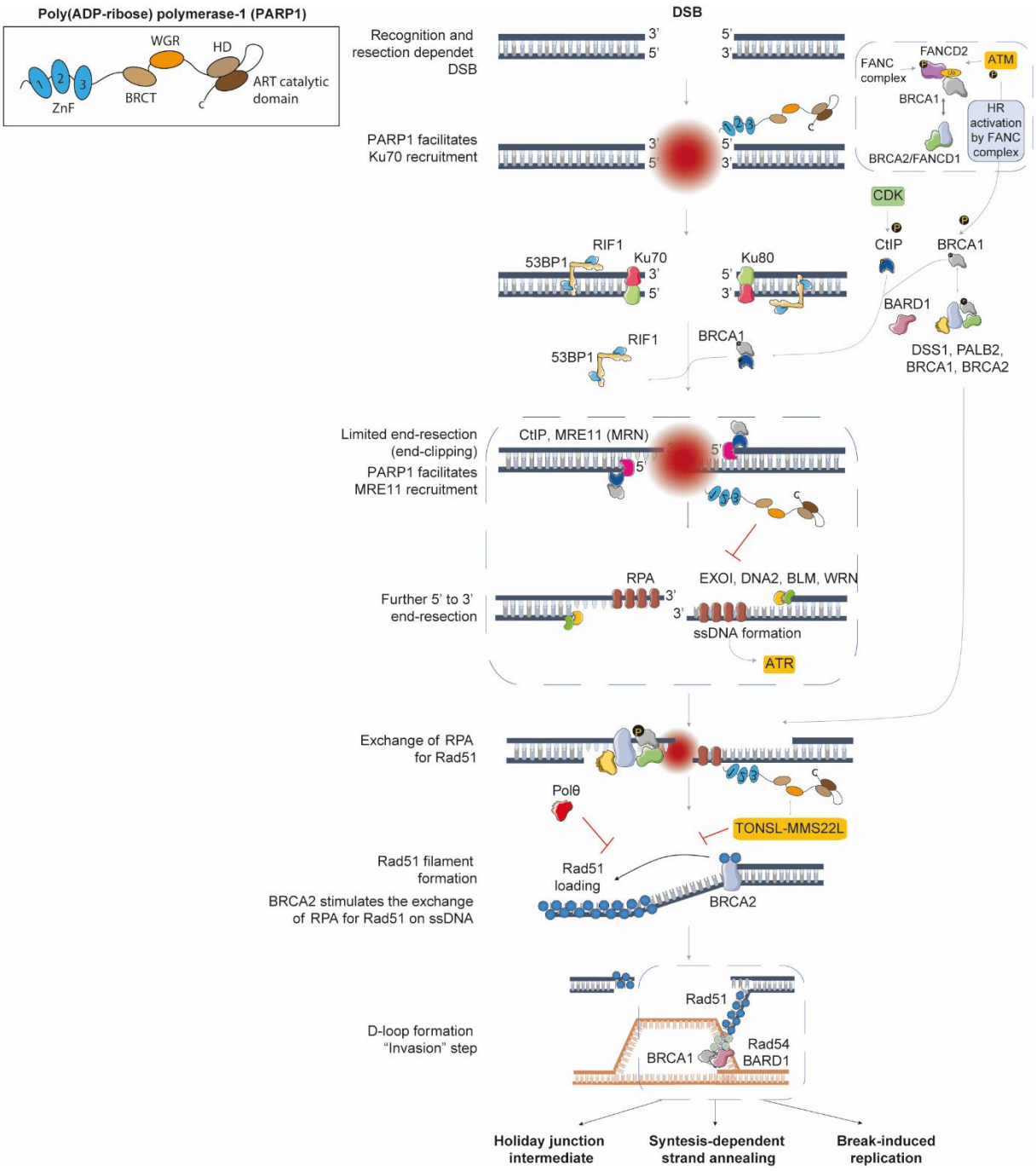

Figure 35: A proposed role of PARP1 in DSB repair choice. PARP is a protein that interacts in multiple steps during the DNA repair process. Recent studies have placed PARP as one of the first responders to a DSB break site, dictating the length of resection by blocking EXO1 and recruiting MRE1. Our data suggest that PARP is also involved in another process relevant to HR, which is the RAD51 filament formation. We hypothesize that PARP is regulating the TONSL-MMS22L complex that also controls the Rad51 loading to the single-stranded DNA.

Discussion

Chapter 9

Discussion

CAT-R reporter assay

The purpose of this Ph.D. thesis is to develop a tool to track and quantify the DNA double-strand break (DSB) repair process. Therefore, we established CAT-R, as an *in vitro* dual fluorescent reporter assay to interrogate the functions of several DSB repair components. CAT-R allows for the simultaneous measurement of end-protection and end-resection based DSB repair upon a single DSB. We show that CAT-R reporter can be utilized as a high-throughput tool that can be coupled to chemical and/or genetic screens in different cell lines.

Over the past decades, several DNA reporter assays have been using I-SceI endonuclease as a tool to induce DSBs. The main drawback of this approach is the relatively low cutting efficiency of I-SceI and the small number of accessible loci for this endonuclease. In addition, the I-SceI endonuclease generates DSB ends with 4 nucleotides (nt) 3' cohesive overhangs, therefore the DNA repair choice is biased to end-resection based mechanisms. We chose to combine CAT-R with CRISPR/Cas9 system and induce a high occurrence of DSB phenotype. CRISPR is currently the most cutting-edge tool to generate DSBs. Among its advantages is the

specificity, adaptability and cutting efficiency that the Cas9 endonuclease exhibits once compared to other genome editing tools. Cas9 endonuclease cleaves the DNA three base pairs upstream of the PAM site, resulting in a blunt-end cleavage of DNA, which mimics a natural occurring DSB. However, due to the continuous cutting efforts of the Cas9 endonuclease, we assume that the repair of a Cas9-mediated DSBs may not be representative of a naturally occurring DSBs. In a recent study (Brinkman et al. 2018) a similar assumption is described, where the cut and repair process of Cas9 endonuclease is investigated. Brinkman *et. al* concluded that when a target site has acquired an InDel, only then Cas9 can no longer recognize the target site.

Furthermore, due to the high efficiency of DSBs that are introduced by the CRISPR/Cas9 system, we can simultaneously assess the frequency of small InDels and large deletions with an unprecedented resolution. We integrated CAT-R in two non-cancerous cell lines with intact DNA repair pathways and observed similar frequencies in the formation of small InDels and large deletions. Some of these occurrences are potentially governed by the cell cycle since end-resection mediated repair primarily occurs in S/G2 phases of the cell cycle, whereas c-NHEJ is active throughout the cell cycle (Ceccaldi et al. 2016; Khanna and Jackson 2001; Mjelle et al. 2015). As far as the formation of larger deletions upon Cas9-mediated breaks the frequency of repair by end-resection may not be uncommon. Our results are consistent with a current study describing that more than 20% of larger deletions ranging from 250 bps to 6 kbs can occur in a haploid cancer cell lines (Kosicki et al. 2018).

DNA repair deficiencies influence CAT-R

While in general the occurrence of the two error-prone populations (small InDels and large deletions) is approximately balanced, this can be altered by channeling the repair of the DSBs to either end-protection or end-resection based mechanisms. This occurs because these two major pathways are competing for the repair of the DSBs. For this reason, blocking end-protection mediated repair by knocking out critical components such as DNA-PK and XRCC4, increased the frequency of large deletions that are presumably products of end-resection. In this case, since the ends of the DSBs cannot be processed by c-NHEJ, they are forced to be resected thus are more prone to give rise to larger deletions (Ceccaldi et al. 2016). On the contrary, when the critical components of resection mechanisms are inhibited such as BRCA1 or FA components, the rate of small InDels increases probably due to an increased availability of end-protection proteins to seal the DNA ends (Barazas et al. 2018; Pilié et al. 2019). Given that such genetic differences can affect the reporter readout so dramatically, we investigated in a pilot RNAi screen how *PRKDC* and *PARP1* KO impacts the DNA repair choice. We showed that in PARP1 deficient background genes that are important in resection are mostly affected and that additional loss of RAD51 can increase the error-free repair. Furthermore, we confirmed that deficiencies in *PRKDC* and *PARP1* genes reduce the frequency of small InDels by alternative types of repair and showcased that PARP1 requires but is not dependent upon microhomologies. In the future, it would be interesting to integrate CAT-R in different cancer cell lines with genetic deficiencies in DDR and measure their differences in generating small InDels versus large deletions.

A platform to screen small pharmacological compounds

We also demonstrated that due to the high efficiency of DSB induction, CAT-R could be used as a platform to screen small-pharmacological compounds to measure their pharmacodynamic properties in cell lines. Inhibiting major components of DDR emerged as a therapeutic strategy since it provides opportunities for exploitation of complementary DDR pathways on which the cancer cells rely on (Curtin 2012; Wright et al. 2017). Understanding a kinase inhibitor's cellular target profile has implications for the correct evaluation of its biological effects in DNA repair choice, as this can assist in dissecting the wiring maps of the targeted signaling networks (Barakat, Gajewski, and Tuszynski 2012; Curtin 2013; Evers, Helleday, and Jonkers 2010; Robert et al. 2015). For instance, inhibitors against classical DDR kinases such as DNA-PK, ATM, and ATR entered phase I/II clinical trials either as inhibitors for monotherapy or in combination with radio- or chemotherapy (Blackford and Jackson 2017; Glorieux, Dok, and Nuyts 2017; Klaeger et al. 2017) due to the increased vulnerabilities of tumors cells to heightened DNA damage or replication stress (Dietlein, Thelen, and Reinhardt 2014; Pearl et al. 2015; Velic et al. 2015).

With CAT-R, we compared the *in vitro* drug efficiencies of 24 compounds and assessed the qualitative and quantitative impact of these compounds on DNA repair in terms of small InDels or large deletion formation. We observed particularly pronounced changes in the CAT-R phenotype upon DNA-PK and ATM inhibition and were able to classify different compounds, consistent with their reported *in vitro* potency.

Cells lacking DNA-PK activity are hypersensitive to ionizing radiation and topoisomerase II inhibitors. A comparison among the DNA-PK_{cs} inhibitors on how they tip the balance of DNA

repair choice reveals why some inhibitors succeed and some others fail in doing so. The NU7026 compound was shown to act *in vitro* as a radiosensitizer and was also found to increase cell sensitivity to topoisomerase II with no intrinsic growth inhibition properties at 10 μM concentration (Dolman et al. 2015; Nutley et al. 2005). We demonstrate that the NU7026 compound has no influence in DNA repair choice at concentrations lower than 500 nM comparing to other potent inhibitors that reach their maximum efficiency in these conditions. Another compound that we evaluated was the NU7441. In a recent publication, it has been reported that 1 μM of NU7441 is enough to increase cell sensitivity to topoisomerase II, doxorubicin as well as IR (Harnor et al. 2017). Even if NU7441 is reported to be selective to DNA-PK_{cs} (Chen et al. 2005), still it is suggested that its pharmacokinetic properties can be improved (Tavecchio et al. 2012; Zhao et al. 2006). Our data showed that NU7441 can influence the DNA repair choice at concentrations around 500 nM but still its efficacy is outrun by other more potent inhibitors. The DNA-PK_{cs} inhibitors that yielded the most robust phenotypes are M3814 and KU-60019. Both compounds show a stable phenotype at concentrations of around 50–500 nM with no intrinsic growth inhibition properties. Of note, M3814 entered phase I clinical development in December 2014 (NCT02316197) for use in patients with solid tumors who had DNA repair deficiencies, and in patients with chronic lymphocytic leukemia. Subsequently, it entered phase I trials in July 2015 (NCT02516813) in combination with DNA damaging modalities such as radio-chemotherapy and radiation. Disclosure of results by Merck in 2016, indicated that M3814 is active in a preclinical setting, exhibiting efficacy in all mouse models of human cancer, in combination with IR (Harnor et al. 2017). In addition, when we compared the enzymatic inhibition and the genetic KO of *PRKDC* we observed the same profile in influencing DDR choice by reducing small InDels.

We also compared a series of ATM inhibitors to screen for their *in-vitro* influence in DNA repair. On average, ATM inhibition influences the DNA repair choice at concentrations around 100 nM, with the frequency of large deletions to be favored and the small InDels population to be strongly reduced. Consequently, a similar profile with the DNA-PK_{cs} inhibition is observed suggesting that ATM inhibition phenocopies DNA-PK_{cs} profile. While we cannot exclude off-target effects of these compounds, activation of DNA-PK_{cs} by ATM phosphorylation may be a key downstream event that is affected. We were also able to highlight the potency of the AZD0156 compound since its influence on DNA repair stands out from the other ATM inhibitors at a concentration as low as 1 nM. Furthermore, by comparing the enzymatic inhibition and the loss of absence of ATM we observed a different profile since in the case of the genetic KO the error-free repair was reduced due to either reduction of HDR or error-free NHEJ. An observation that potentially can be explained by the requirement of the functional ATM protein to phosphorylate BRCA1 protein that regulates the frequency of the error-free repair.

The next class of compounds we compared was the ATR inhibitors, with some of them to be reported to enhance the cytotoxic effects upon radiation (Dillon et al. 2017; Vendetti et al. 2015, 2018). The analysis of ATR inhibitors revealed that DNA repair is driven to end-protection pathways upon ATR inhibition. The M4344 compound exhibits the highest potency by increasing the frequency of small InDels at low concentrations (< 20 nM). It is worth mentioning that all ATR inhibitors showed severe cytotoxic events at concentrations higher than 100 nM.

Another class of inhibitors that we tested was against HDAC. HDAC inhibitors promote the acetylation of histones allowing for DNA repair machinery to have better access to the relaxed

chromatin. However, and in contrast to what was expected, HDAC inhibition with several different pan-spectrum compounds, favors end-protection mechanisms with a substantial increase in the frequency of small InDels. To better understand the causal of this action, we examined the effect of two potent HDAC inhibitors on the cell cycle. Both compounds increased the time cells spent in G1 phase and probably this is enough to explain the increase in the formation of small InDels. Thus, the phenotype of HDACi is mostly attributed to the cell cycle stalling rather than to DDR manipulation.

The last class of inhibitors we compared was PARP inhibitors. Targeting PARP1 has been extensively studied in recent years to exploit the concept of synthetic lethality (Wright et al. 2017). For this reason, understanding the profiles of these inhibitors may have important implications for the correct evaluation of their biological effects in DNA repair choice, and their effects on the cells (Barakat et al. 2012; Curtin 2013; Evers et al. 2010; Robert et al. 2015). We demonstrate that CAT-R can even detect differences in PARP-trapping activity and can be used as a screening platform for a rapid *in vitro* assessment of DDR compound efficiencies. PARP inhibition affects the formation of small InDels, agreeing well with the fact that in the presence of PARP, the DSBs are repaired by the alternative EJ pathway. Our system classifies the compounds based on their efficacy at the same order as the current literature does. Interestingly, when we tested veliparib, iniparib and INO-1001, a group of compounds that are among the first PARP inhibitors that were later shown not to possess any PARP-trapping activity, none of these three compounds exhibited any prominent effect in the repair of Cas9-mediated DSBs. This indicates that our system potentially allows the detection of even minor changes in DSB repair choice.

In the case of PARP1, the genetic KO and the chemical inhibition may be expected to result in different phenotypes. However, the effects that we observed with CAT-R are very similar. The genetic KO may affect only alt-EJ, thus result in a 5–10% reduction in the small InDels, whereas the PARP trapping (inhibition) may affect downstream components of the DSB repair that are responsible for end-resection and result in the same phenotype as the genetic KO of PARP1.

The discovery of additional, more potent and selective compounds is desirable. We demonstrate that CAT-R can be used as a platform to provide further information on DDR kinase or PARP inhibitor drug discovery, serving as a tool to identify more selective inhibitors. We also provided a machine learning-based tool to help classify the unknown compounds in HEK293^{CAT-R} cells, though we note that the model should be reapplied to additional cell lines in order to adapt to the responses in each cell line.

CRISPR/Cas9 arrayed genetic screen

A large number of published studies have utilized CRISPR/Cas9 technology for screening purposes (Agrotis and Ketteler 2015). CRISPR libraries enable reverse genetic screens with a much broader utility in terms of phenotypic readout. With the use of an arrayed genetic library, it is possible to explore complex phenotypes that arise from distinct cell perturbations in parallel. While the experimental conditions vary between screens, there are at least five crucial steps to be considered in an arrayed screen: (1) Preparation of cells; (2) Delivery of the library; (3) Phenotype acquisition; (4) Analysis; (5) Hit validation.

Using the CAT-R, we performed a genetic screen, measuring the effect of knocking out DDR genes on the derived populations. Overall, in our screen, loss of c-NHEJ components decreases

the rate of small InDels formation, whereas loss of FA pathway components increases the number of small InDels and reduces large deletions. Consistently, FA components have been recently shown to be required for Cas9-mediated single-strand template repair (SSTR) but not for c-NHEJ (Richardson et al. 2018). In addition to the known components of end protection and end resection, we revealed components of NER to be necessary for the homology-directed repair. We tested this hypothesis by integrating a ssODN based donor template and measuring the GFP to BFP conversion, thus assessing the rate of SSTR. Though technically more challenging and the frequency of SSTR events are rather low, this conversion allowed us to measure the rate of recombination events, together with error-prone repair. We show that in the absence of crucial NER genes, the rate of SSTR events is increased. While Cas9 cleaves the DNA, the gRNA sequence is bound to the antisense strand as an RNA:DNA hybrid and a 5' to 3' flap is generated at the non-targeted/ sense sequence (Janssen et al. 2019), (Richardson, Ray, Dewitt, et al. 2016). Generally, 5' to 3' flaps can be removed by the NER mechanism. Here, we show that in the absence of these NER genes, most likely the 5' to 3' flap cannot be removed efficiently increasing the chances of a successful KI via SSTA/HDR. These results may have implications for SSTR mediated knock-ins since HDR based genome editing has several potential applications such as correction of disease-causing mutations.

In most cases, since c-NHEJ is more available in the cells, the DSBs are much more commonly repaired in an error-prone fashion; thus, strategies to increase the HR mediated repair are becoming more attractive. So far, inhibition of DNA-PK was shown to increase the rate of HDR by decreasing the accessibility of the c-NHEJ components to the site of repair (Liu et al. 2019). Here we provide an alternative approach to increase the rate of knock-ins. It will be interesting to see if these effects we observe with the NER deficient cells can be uncoupled

from the cell cycle, thus allowing cells that are slow dividing or non-cycling to be edited as well.

Based on the current literature of Cas9-mediated DSB, we propose a mechanism that is derived from our genetic screen data. Once Cas9 is bound to its sequence, it undergoes its conformational changes and cleaves the loci leaving either as blunt or a sticky end, and it seems that the proximal (downstream) to PAM site DNA sequence is left to the end-protection mechanism. The distal (upstream) to PAM site DNA sequence is still bound to Cas9 with an RNA: DNA hybrid link. Either end-protection machinery will act by holding the strands together and favor a quick ligation via c-NHEJ or alt-EJ that will most likely lead to an erroneous repair that signals for the formation of small InDels, or a 5'to 3' flap will be created where end-resection machinery will take over. End-resection will either resect the 5' to 3' flap until a homology is found and this will be repaired with SSA and will lead to large deletions, or the existence of 5' to 3' will favor the SSTA/HDR with a ssODN donor template.

Identifying novel PARP interactions

The impact of the genetic background in DNA repair choice is mostly uninvestigated, with several literature data to suggest that PARP1 antagonizes end-resection based mechanism. Therefore, we used CAT-R to identify novel PARP1 interactions within DDR. We combined the custom arrayed genetic screen with PARP inhibition and were able to identify the 30 most altered genes in terms of DSB choice. This approach helped us to uncover a gene cluster that controls a key step during RAD51 filament formation, suggesting that PARP1 potentially regulates end-resection in more steps, than what was recently being reported. Besides, we show that loss of PARP1, as well as inhibition of PARP, deregulates the DNA repair choice in several

cases mostly in end-resection related genes to favor limited end-resection and channel the repair to alt-EJ or c-NHEJ. Further work needs to be done to understand the precise mechanism of how PARP1 regulates end-resection.

Material and Methods

Chapter 10

Material & Methods

Cell line engineering

Generating Cas9 inducible stable cell lines

The Edit-R inducible lentiviral Cas9 particles (Horizon™ Dharmacon) confer Blasticidin resistance in transduced cells. Both cell lines were Blasticidin resistant, therefore, the CRISPR/Cas9 system was used to disrupt the Blasticidin sequence. Specific gRNAs targeting the Blasticidin sequence were designed and cloned separately into an all-in-one-vector (LentiCRISPR_v2) that expresses both Cas9 endonuclease and the gRNA sequence. After transfection and monoclonal cell line expansion, cells were divided into two 96-well plates and Blasticidin was supplemented into the culture medium of one of the two 96-well plates to determine the number of Blasticidin sensitive clones. Seven days after selection, 90% of the clones were Blasticidin sensitive at concentrations as low as 1 μg/ml.

To generate Cas9 nuclease-expressing cells, the Edit-R™ inducible lentiviral particles (Horizon™ Dharmacon) were used according to the manufacturer's protocol. Cells were seeded in a 24-well plate and incubated overnight. The next day the transduction medium was prepared to have a MOI=0.3 and the cell culture medium was replenished containing the

lentiviral particles. Cells were incubated for 24 h, and then the cell culture medium was replaced with the appropriate amount of blasticidin. The transduced cells were selected in the presence of 1 μg/ml blasticidin for seven days and the expression of Cas9 was controlled by a doxycycline-inducible promoter.

Generating CAT-R stable cell lines

The FLP recombinase methodology was used to integrate the reporter as a single stable copy into the cell lines of interest. The user's protocol, (Flp-In™, Invitrogen™), was followed as described in the manual. Briefly, general molecular biology techniques such as DNA ligation, *E. coli* transformation, restriction enzyme analysis, and DNA sequencing were applied to clone the fluorescent reporter into the constitutively (pcDNA™ 5/FRT) and inducible (pcDNA™ 5/FRT/TO) expression vectors. Specifically, BamH I & Xho I restriction sites were used to ligating the gene of interest to both vectors. The vectors contain the hygromycin resistance gene for selection of the transfectants with the antibiotic hygromycin B. To accommodate a new antibiotic selection gene for future experiments, the pcDNA™ 5/FRT/TO vector was modified. Therefore, the hygromycin resistance gene was replaced by the neomycin resistance gene and the pcDNA™ 5/FRT/TO/Neomycin was generated.

Stable CAT-R expressing cell lines were generated with the Flp-In™ system. The pcDNA5™/FRT or the pcDNA™5/FRT/TO construct along with the pOG44 expression plasmid were co-transfected to the model cell lines. The transfected cells were selected in the presence of 500 μg/μl of hygromycin or neomycin for 4 days. In addition, cells with strong eGFP (488-530/30) and mCherry (561-610/20) signals were sorted using FACSAria I cell sorter (BD Biosciences) to enrich cells harboring the reporter.

Generating cell lines with deficient background

For each gene of interest one gRNA was used to transfect the model cell lines with the use of synthetic gRNA oligonucleotides. Three days post-transfection, monoclonal cell lines were generated by limiting dilution and once fully-grown several clones were selected for validation either with Western blotting or with Immunofluorescence.

Table 3: Summary of the engineered cell lines with their respective genetic background

Nr.	Cell line	Genetic background
1.	HEK293^{CAT-R}	Wild type
2.	HEK293^{CAT-R}	PRKDC$^{-/-}$
3.	HEK293^{CAT-R}	XRCC4$^{-/-}$
4.	HEK293^{CAT-R}	ATM$^{-/-}$
5.	HEK293^{CAT-R}	PARP1$^{-/-}$
6.	HEK293^{CAT-R}	ERCC3$^{-/-}$
7.	HEK293^{CAT-R}	ERCC8$^{-/-}$
8.	HEK293^{CAT-R}	XPC$^{-/-}$
9.	HEK293^{CAT-R}	TP53$^{-/-}$
10.	RPE-1^{CAT-R}	Wild type
11.	RPE-1^{CAT-R}	TP53$^{-/-}$
12.	RPE-1^{CAT-R}	ATM$^{-/-}$

Cell culture

Transformed human embryonic kidney (Flp-In™ HEK293, Life technologies) and hTERT-immortalized retinal pigment epithelial (hTERT T-Rex™ RPE-1, a kind gift from Jonathon Pines) mammalian cell lines were used as model systems. HEK293 cells were cultured in Dulbecco's Modified Eagle Medium, high glucose supplement (DMEM/GlutaMAX™, Life Technologies) containing 10% FBS (Thermo Scientific), 1% Gibco® Antibiotic-Antimycotic.

RPE-1 cells were cultured in Dulbecco's Modified Eagle Medium/Nutrient Mixture F-12 high glucose supplement (DMEM/F12 GlutaMAX™, Life technologies) containing 10% FBS (Thermo Scientific), 1% Gibco® Antibiotic-Antimycotic. All cell lines were cultured at 37ºC and 5% CO_2. For the induction of the reporter and the Cas9 endonuclease, culture media was supplemented with 1 μg/ml Doxycycline for 24 hours.

Liquid phase transfection of siRNA

Cells were seeded (20.000 HEK293, 8.000 RPE-1 cells per 96-well) on 96-well plates (Orange Scientific). 24 h later, cells were 60 - 80% confluent for transfection. The Silencer® GFP (eGFP) siRNA (Invitrogen™) was used as a positive control for lipofection. Lipofectamine™RNAiMAX was used as a transfection reagent, and the general instructions for a 96-well plate transfection were followed. The siRNA was combined with Lipofectamine™RNAiMA in Opti-MEM® Medium to a final concentration of 1 pmol.

Liquid phase transfection of synthetic gRNA oligonucleotides:

Cells were seeded (20.000 HEK293, 8.000 RPE-1 cells per 96-well) on 96-well plates (Orange Scientific), and culture media were supplemented with 1 μg/ml Doxycycline. After 24 hrs, cells were 60 – 80% confluent for transfection. The Alt-R™ CRISPR crRNA and tracrRNA (IDT) were used to form the guide RNA complex (gRNA). Each RNA oligo (Alt-R™ CRISPR-Cas9 crRNA, tracrRNA) was resuspended in nuclease-free IDTE, pH 7.5 (1X TE solution) to a final concentration of 100 μM. The two RNA oligos were mixed at equimolar concentrations to create a final complex concentration of 3 μM. The gRNA complex was heated at 95ºC for 5 min and then allowed to cool to room temperature (15–25ºC). Lipofectamine™ RNAiMAX transfection reagent was used according to the user manual. The

gRNA complex was combined with Lipofectamine™RNAiMAX in a ratio of 2:1 in Opti-MEM® Medium to a final concentration of 30 nM.

Table 4: Selected gRNA designs targeting the eGFP sequence.

Name	Target sequence (5' → 3')	Nucleotide position*	Orientation
gRNA1	GGGCGAGGAGCTGTTCACCG	12 - 31	Sense
gRNA2	GAGCTGGACGGCGACGTAAA	52 - 71	Sense
gRNA3	GGCCACAAGTTCAGCGTGTC	73 - 92	Sense
gRNA4	GGAGCGCACCATCTTCTTCA	285 - 304	Sense
gRNA5	GAAGTTCGAGGGCGACACCC	339 - 358	Sense
gRNA6	GGTGAACCGCATCGAGCTGA	360 - 379	Sense

* *Nucleotide position is determined by the beginning of eGFP sequence*

Solid-phase transfection of synthetic gRNA complexes

For experiments using a solid-phase transfection platform, we used flat bottom white 96 well plates (Costar®Assay plate, 3903) and prepared mixtures that are enough for 9 wells of a 96-well plate. For each reaction to achieve 2.5 pmol RNA complexes in each coated well, 3 µl Opti-MEM/sucrose solution (1.37% w/v) was mixed with 1.75 µl Lipofectamine™2000 (Invitrogen, 11668027). To this mix, 6.75 µl of 3.3 µM crRNA: tracrRNA mixture was added, and the final transfection mix was incubated for 20 mins at room temperature. After incubation, 7 µl of gelatin (0.2% w/v in H_20) was added and mixed. The final mixture was diluted in RNA and DNase free water 1:25 amounting to a total of 450 µl of diluted transfection mixes. From this mix, we plated 50 µl to each well of a 96 well plate. Plates were filled in triplicates and lyophilized using a MiVac vacuum centrifuge, accommodating multi-well plates.

Twenty-four hours before transfection, the culture media was supplemented with 1 μg/ml Doxycycline. Cells on day of seeding need to be 20 – 30% confluent and were seeded on a pre-coated flat bottom, 96-well plate (Costar®Assay plate, Corning) (6.000 HEK293 and 3.000 RPE-1 per 96-well.

Cell compound treatment

Twenty-four small pharmacological inhibitors were selected to target vital DDR proteins. The compounds were stored as 1 mM stocks in DMSO and bought from Selleckchem or were kindly provided (M3814, M3541, M4344 and M6620) by Dr. Frank Zenke at Merck KGaA, Darmstadt, Germany. Cells were seeded (20.000 HEK293, 8.000 RPE-1 cells per 96-well) on the U-bottom 96-well plate (Orange Scientific), and culture media was supplemented with 1 μg/ml Doxycycline. The day after, cells were transfected with gRNA: eGFP and incubated with the inhibitor compounds for three days. Then they were analyzed in a high-throughput FACS LSR Fortessa™ analyzer (BD Biosciences).

Cell viability assay

CellTiter-Glo® (Promega) was used to determine cell viability, according to the manufacturer's protocol. Cells were seeded (6.000 HEK293, 3.000 RPE-1 cells per 96-well) on a 96-well white plate with a clear flat bottom (Costart®Assay plate, Corning) and cultured for three days in the presence of specific inhibitor. The GloMax®-Multi detection system (Promega) was used as a luminometer to quantify the presence of ATP when metabolically active cells exist.

Cell cycle analysis

Click-iT™ EdU Alexa Fluor™ 488 Flow Cytometry Assay Kit (ThermoFisher) was used as an assay for analyzing DNA replication in proliferating cells. The Click-iT® EdU protocol was followed. On the day of analysis, cells were labeled with 10 μM of EdU for 2 h, following several washing steps during fixation and permeabilization. The Click-iT® reaction mixture was prepared according to the manufacturer's protocol, and the reaction mixture was left for incubation for 30 minutes at room temperature protected from light. Cells were stained for DNA content with the FxCycle™ Violet in 1:1000 dilution and left for 30 minutes of incubation. The samples were analyzed by flow cytometry with the use of a FACSAria I cell sorter (BD Biosciences).

CRISPR/Cas9 gRNA library

An arrayed gRNA library is synthesized on 96 well plates targeting a total of 417 genes (IDT). For each gene, 2 individual gRNAs were used. On each plate, we used four positives (POLR2A), and six negatives (Scrambled, non-targeting gRNA) controls to evaluate the solid-phase transfection. On the first day, the culture media was supplemented with 1 μg/ml Doxycycline to induce the Cas9 expression. On day 2, cells were 60-80% confluent and actively dividing. They were seeded in pre-coated plates containing the gRNA library complexes. Three days post-transfection, the gRNA: eGFP was transfected, and three days afterward, the eGFP and mCherry ratios were assessed by high throughput flow cytometry.

Genomic DNA extraction

Cells were collected 24 to 72 h after transfection to a 1.5 ml tube. The genomic DNA was isolated according to the manufacturer's protocol using the DNeasy Blood & Tissue Kit

(Qiagen). In brief, cultured cells were pelleted and resuspended in 200 µl PBS with 20 µl of proteinase K. Afterward, 200 µl of Buffer AL was added to the sample, mixed thoroughly, and left to incubate at 56ºC for 10 min. Then 200 µl of ethanol (96-100%) was used and subsequent washing steps with Buffer AW1 and Buffer AW2 followed. The final elution step was performed with 50 µl of nuclease-free water. The DNA purity and concentration were measured using a NanoDrop™ spectrophotometer. Typically, A260/280 values greater than 1.8 are suitable for analysis.

Cleavage detection assay

The enzyme digest of mispaired dsDNA was performed using the Surveyor® Mutation detection kit (IDT) according to the manufacturer's protocol. The PCR amplification of 100 ng from reference and test samples was completed, using the Q5 Hot Start High-Fidelity 2X Master Mix (#M0494, New England Biolabs). The thermo-cycling conditions of the 25 µl PCR reactions were 98°C for 30 sec, 34 cycles of 98°C for 5 s, 59°C for 10 sec, and 72°C for 20 sec with a final extension at 72°C for 2 min. Next, sample and reference DNA are hybridized to form heteroduplexes using a thermal cycler according to the manufacturer's protocol. Subsequently, 10 µl from the PCR reaction for each sample was used to set up the surveyor nuclease reaction and the mixture was left at 42ºC for 60 min of incubation. Finally, the analysis of DNA fragments was run in a 1.5% TBE agarose gel electrophoresis and imaged with a Gel Doc™ XR+ (Bio-Rad) system.

PCR amplification and Next-Generation Sequencing

For the genome-sequencing assay, DNA was extracted from HEK293 cells using the DNeasy Blood & Tissue Kits (Qiagen, Düsseldorf, Germany) as described in the manufacturer's protocol. After quantification (Qubit High sensitivity assay kit) we employed a two-step PCR protocol. As suggested in the Illumina protocol for 16S Metagenomic Sequencing Library Preparation, the first PCR step is performed to amplify the targeted DNA region. For each sample, 1 μg of DNA was used to prepare the initial 388 bps PCR amplicon. The 50 μl PCR reactions were set up with the NEBNext® Q5® Hot Start Master Mix (New England BioLabs) and the thermo-cycling conditions were 98°C for 3 min, 12 cycles of 98°C for 10 s, 65°C for 30 sec, and 72°C for 20 sec with a final extension at 72°C for 3 min. To verify the success of the PCR, amplification products were electrophoresed on a 2% agarose gel. The second PCR step is performed in order to multiplex individual specimens on the same Illumina MiSeq flowcell and to add necessary Illumina adapters. In this second step, primer pairs used contain the appropriate Illumina adapter allowing amplicons to bind to the flow cell, an 8-nt index sequence (Kozich et al. 2013) and the Illumina sequencing primer sequence.

Next-Generation Sequencing data analysis

The reads quality control was performed with FastQC and MultiQC tools. BBMap (v. 38.34) was used for the alignment because of its accuracy to align reads with long indels. As a reference, the targeted eGFP sequence was used. All the downstream analysis was performed with custom scripts in R (v. 3.4.4). Indels were considered only if they occurred within 1 nucleotide of the Cas9 cleavage site. To guarantee the robustness of the frequency's estimation,

only events (indels with a unique position and length) supported by at least 10 reads were considered.

High-throughput flow cytometry

Cell populations were gated on a forward (FSC)/side scatter (SSC) plot. Cells are further gated on forward-area (FSC-A)/forward-height scatter (FSC-H) plot to determine single cells. Single cells are further gated on side-area scatter (SSC-A)/ (405-450/50A) to determine living cells based on DAPI staining. Live cells are further gated to determine eGFP (488-530/30-A)/ mCherry (561-610/20-A) cell populations and evaluated in a ratiometric way the fluorescent variations in a FACS LSRFortessa™ mounted on a High Throughput Samples (HTS) (BD Biosciences, USA).

Quantify gene expression

Western blotting

Whole-cell lysis extracts of HEK293 and RPE-1 were generated with RIPA buffer (CST – 9806S) or custom made HGNT lysis buffer. An equal amount of protein (25 μg/ml) was loaded to a 7.5% precast polyacrylamide gel (Mini-PROTEAN® TGX™, Bio-Rad). The cell extracts were transferred to a nitrocellulose membrane (Trans-Blot® Turbo™, Bio-Rad) or to a PVDF membrane using a transfer apparatus according to the manufacturer's protocols (Bio-Rad). After incubation with 10% nonfat milk in TBST (10 mM Tris, pH 8.0, 150 mM NaCl, 0.5% Tween 20) for 30 min, the membrane was washed three times with TBST and incubated with antibodies against protein of interest at 4^{o}C for 12 h. Membranes were washed three times and incubated with 1:10000 dilution of IRDye 680RD and IRDye 800CW secondary antibodies for

2 h. Blots were washed with TBST three times and developed with the Odyssey system for 2 min (LI-COR Biosciences).

Table 5: List of protein targets with the respective antibodies used during this study.

Protein target	Dilution	Molecular weight (kDa)	Antibody type	Product number	Company
Cas9	1:1000	160 kDa	Mouse mAb	#14697s	CST
TP53	1:1000	53 kDa	Mouse mAb	#2524S	CST
ATM	1:1000	350 kDa	Rabbit mAb	#2873S	CST
p-CHK2	1:1000	56 kDa	Rabbit mAb	#2197s	CST
XRCC4	1:500	55 kDa	Mouse mAb	sc-271087	Santa Cruz
NHEJ1	1:100	27.8 kDa	Mouse mAb	sc-393844	Santa Cruz
DNA-PK$_{cs}$	1:1000	469 kDa	Rabbit pAb	ab70230	Abcam
eGFP	1:1000	37.2 kDa	Mouse mAb		
GAPDH	1:10000	37 kDa	Rabbit mAb	#5174s	CST
α-Tubulin	1:10000	50 kDa	Mouse mAb	ab67291	Abcam
Vinculin	1:10000	145 kDa	Rabbit mAb	#4650s	CST

CST: Cell Signaling Technology

RNA Extraction, cDNA Synthesis, and RT-qPCR

Total RNA isolation was performed from 10^6 cells using the RNeasy Plus Mini kit (Qiagen, Düsseldorf, Germany). Cells were pelleted and disrupted by adding Buffer RLT that contains β-mercaptoethanol (β-ME) to denature active RNases. After homogenizing the lysates by vortexing for 1 min, 1 volume of 70% ethanol was added to the mixture. Subsequent washing steps, with Buffer RPE, were followed and the elution was performed with 10 µl of nuclease-free water. The RNA samples were diluted to 250 ng/µl final concentration aliquoted and stored in -80^{o}C.

All RNA samples within an experiment were reverse transcribed at the same time with the qScript™ cDNA SuperMix (Quanta Biosciences) using 500 ng of RNA as a template and stored

in aliquots at -80 ºC. Real-time PCR with Fast SYBR® Green (ThermoFisher) detection was performed using a QuantStudio™ 5 Real-Time PCR system (Applied Biosystems™). The relative quantification of each sample was performed using the comparative Ct method. The acidic ribosomal phosphoprotein P0 gene (36B4) is used as a housekeeping gene. To compare the transcript levels between different samples the 2 -ΔΔCt method was used (Livak and Schmittgen, 2001). First, the difference in the cycle threshold (Ct) values between the *18S* gene and a target gene were calculated with or without treatment, $(\Delta Ct_{gene\text{-}18S})_{treated}$, $(\Delta Ct_{gene\text{-}18S})_{non\text{-}treated}$. Then, the difference between these values was calculated as follows: $\Delta Ct_{treated\ -\ non\text{-}treated} = (\Delta Ct_{gene\text{-}18S})_{treated} - (\Delta Ct_{gene\text{-}18S})_{non\text{-}treated}$. Finally, to determine the ratio of expression levels in the treated sample versus non-treated sample, we used the Qr formula ($Qr = 2^{-Ct_{treated-nontreated}}$).

Table 6: RT-PCR primer set

Gene	Orientation	Primer sequence (5' → 3')
ATM	Fwd	ATCTGCTGCCGTCAACTAGAA
	Rev	GATCTCGAATCAGGCGCTTAAA
ATR	Fwd	GGCCAAAGGCAGTTGTATTGA
	Rev	GTGAGTACCCCAAAAATAGCAGG
BRCA1	Fwd	GCTACAGAAACCGTGCCAAA
	Rev	TATCCGCTGCTTTGTCCTCA
BRCA2	Fwd	TGGTATGCTGTTAAGGCCCA
	Rev	CTGGGGCTTCAAGAGGTGTA
ERCC5	Fwd	GACTTAGCGTCCAGTGACTCC
	Rev	GGCAGTTTTGATGGCTTGTCTTT
ERCC8	Fwd	ATGCTGGGGTTTTTGTCCG
	Rev	TCTCCGTGTTGACTCTGCTCT
FANCI	Fwd	CCACCTTTGGTCTATCAGCTTC
	Rev	CAACATCCAATAGCTCGTCACC
FANCM	Fwd	AATCTTGGCTCTAAGTGCCAC
	Rev	TCTGCCCAATTAGCAGGTTAGTA
NHEJ1	Fwd	ATAATCTCCTTCGCCCATTGTTG
	Rev	CCCGTAGAATCAGTGCATCTG
PARP1	Fwd	TGGAAAAGTCCCACACTGGTA
	Rev	AAGCTCAGAGAACCCATCCAC
PARP2	Fwd	GCCTTGCTGTTAAAGGGCAAA
	Rev	TCCTTCACAATACACATGAGCC
PARP3	Fwd	GCCCTGGGTACAGACTGAG
	Rev	CGCTTCTCTGCGGGTATGG
POLQ	Fwd	ACTTTTGCTGACCAAGATTTGCT
	Rev	ACTCATGCCAACGATTTGCAC
PRKDC	Fwd	CTGTGCAACTTCACTAAGTCCA
	Rev	CAATCTGAGGACGAATTGCCT
RAD51B	Fwd	CACCAGACCCAGCTCCTTTA
	Rev	TCTGTTCTGTAAAGGGCGGT
USP1	Fwd	CGTTTCCGGGACCAGAATCC
	Rev	CATCGCCGTCCGTTCTCTTC
XRCC4	Fwd	ATGACTGCTGACCGAGATCC
	Rev	CTGAAGCCAACCCAGAGAGA

Statistical analysis

Compound analysis and statistical testing

Results from the reporter are presented as the mean ±standard deviation of independent experiments. Each independent experiment entails 3 technical replicates. A t-test was used to compare continuous variables between two groups. Box and whiskers plots are used from min to max with median value to be annotated and values to be normalized to gRNA: eGFP control. Scatter plots are also used with a nonlinear regression fit curve and the values to be normalized to gRNA: eGFP control.

Random forest model – a bioinformatics pipeline

Starting from the log10 transformed FACS data, for each sample, the 2D kernel density estimation was computed, and the resulting plot was converted into a 100 x 100 pixels image flatten into a 10000 elements vector. To avoid misleading the modeling process samples that showed a phenotype almost equal to the DSB were removed as follows: assuming that equal phenotypes come from the same distribution, for each sample the statistical distances from the DSB controls within the plate were computed using the Kolmogorov–Smirnov test and an average distance from the DSB controls was calculated. Samples showing an average distance equal to or lower than the upper endpoint of the 95% confidence interval of the average distance among the DSB controls within the plate were filtered out. Specific drugs no longer considered to belong to a specific class were also removed. The data set was split randomly into train and test set using an 80/20 ratio and taking the classes proportion of the data unvaried. Using the train set, we trained a random forest model with a repeated 5-fold cross-validation for the parameter's optimization and an up-sampling strategy for class balancing. In order to

assess the final model, we predicted the classes of the test set. Afterward, we were able to produce the confusion matrix and to calculate the performance of the model. The modeling was performed in R using the *caret* and the *ranger* packages.

CRISPR/Cas9 gRNA library analysis

The data from the two replicates were averaged by the gene name. In statistics, Z-score values are used to describe a value's relationship to the mean of a group of values based on the standard deviations from the mean. Therefore, Z-scores were calculated with the following formula $Z\ score = \frac{(Value - mean)}{SD}$, for all three populations per gene based on non-targeting (scrambled) controls of each 96-well plate. Genes with a low number of counts (< 1500) were removed from the analysis. Among the remaining genes, we formed clusters by the K-Means algorithm, taking into consideration all three populations. K-Means is a popular technique for data cluster analysis that partitions the input data set into k partitions (clusters) starting with the first group of randomly assigned centroids. Once the centroids are stabilized it allocates every data point to the nearest cluster. Next, a pathway enrichment analysis was performed to identify pathways enriched in the given gene list sets derived from the clustering approach. For this purpose, a free online database of biological pathways (Reactome) was used. The website can be used to browse pathways and submit data to a suite of data analysis tools. The pathway over-representation tool was used to present a list of over-represented pathways with a significance level of $p < 0.05$. Next, to identify the most influential genes of a Cas9-mediated DSB, a standard outlier diagnostic tool (Cook's distance) was used. It is commonly used to estimate the influence of a data point when performing a least-squares regression analysis. A model based on the input of the two populations is built in the concept $y = x * \beta + \varepsilon$, with ε to be the error term. If ε is greater than the cut-off (3 times the mean) then it is considered as an outlier.

Bibliography

Abe, Takuya, Ryotaro Kawasumi, Hiroshi Arakawa, Tetsuya Hori, Katsuhiko Shirahige, Ana Losada, Tatsuo Fukagawa, and Dana Branzei. 2016. "Chromatin Determinants of the Inner-Centromere Rely on Replication Factors with Functions That Impart Cohesion." *Oncotarget* 7(42).

Adamo, Adele, Spencer J. Collis, Carrie A. Adelman, Nicola Silva, Zuzana Horejsi, Jordan D. Ward, Enrique Martinez-Perez, Simon J. Boulton, and Adriana La Volpe. 2010. "Preventing Nonhomologous End Joining Suppresses DNA Repair Defects of Fanconi Anemia." *Molecular Cell* 39(1):25–35.

Adamson, Britt, Agata Smogorzewska, Frederic D. Sigoillot, Randall W. King, and Stephen J. Elledge. 2012. "A Genome-Wide Homologous Recombination Screen Identifies the RNA-Binding Protein RBMX as a Component of the DNA-Damage Response." *Nature Cell Biology* 14(3):318–28.

Agrotis, Alexander and Robin Ketteler. 2015. "A New Age in Functional Genomics Using CRISPR/Cas9 in Arrayed Library Screening." *Frontiers in Genetics* 6(SEP):300.

Aida, Tomomi, Keiho Chiyo, Takako Usami, Harumi Ishikubo, Risa Imahashi, Yusaku Wada, Kenji F. Tanaka, Tetsushi Sakuma, Takashi Yamamoto, and Kohichi Tanaka. 2015. "Cloning-Free CRISPR/Cas System Facilitates Functional Cassette Knock-in in Mice." *Genome Biology* 16(1):87.

Allen, Felicity, Luca Crepaldi, Clara Alsinet, Alexander J. Strong, Vitalii Kleshchevnikov, Pietro De Angeli, Petra Páleníková,

Anton Khodak, Vladimir Kiselev, Michael Kosicki, Andrew R. Bassett, Heather Harding, Yaron Galanty, Francisco Muñoz-Martínez, Emmanouil Metzakopian, Stephen P. Jackson, and Leopold Parts. 2019. “Predicting the Mutations Generated by Repair of Cas9-Induced Double-Strand Breaks.” *Nature Biotechnology* 37(1):64–82.

Alphey, Luke. 2016. “Can CRISPR-Cas9 Gene Drives Curb Malaria?” *Nature Biotechnology* 34(2):149–50.

Alt, Frederick W., Eugene M. Oltz, Faith Young, James Gorman, Guillermo Taccioli, and Jianzhu Chen. 1992. “VDJ Recombination.” *Immunology Today* 13(8):306–14.

Aly, Amal and Shridar Ganesan. 2011. “BRCA1, PARP, and 53BP1: Conditional Synthetic Lethality and Synthetic Viability.” *Journal of Molecular Cell Biology* 3(1):66–74.

Anderson, Emily M., Amanda Haupt, John a Schiel, Eldon Chou, Hidevaldo B. Machado, Žaklina Strezoska, Steve Lenger, Shawn McClelland, Amanda Birmingham, Annaleen Vermeulen, and Anja Van Brabant Smith. 2015. “Systematic Analysis of CRISPR-Cas9 Mismatch Tolerance Reveals Low Levels of off-Target Activity.” *Journal of Biotechnology* 211:56–65.

Awasthi, P., M. Foiani, and A. Kumar. 2016. “ATM and ATR Signaling at a Glance.” *Journal of Cell Science* 129(6):1285–1285.

Bachu, Ravichandra, Iñigo Bergareche, and Lawrence a. Chasin. 2015. “CRISPR-Cas Targeted Plasmid Integration into Mammalian Cells via Non-Homologous End Joining.” *Biotechnology and Bioengineering* 112(10):2154–62.

Bakkenist, Christopher J. and Michael B. Kastan. 2004. “Initiating Cellular Stress Responses.” *Cell* 118(1):9–17.

Bakr, A., C. Oing, S. Köcher, K. Borgmann, I. Dornreiter, C. Petersen, E. Dikomey, and W. Y. Mansour. 2015. “Involvement of ATM in Homologous Recombination after End Resection and RAD51 Nucleofilament Formation.” *Nucleic Acids Research* 43(6):3154–66.

Barakat, Khaled, Melissa Gajewski, and Jack a Tuszynski. 2012. “DNA Repair Inhibitors: The next Major Step to Improve Cancer Therapy.” *Current Topics in Medicinal Chemistry* 12(12):1376–90.

Barazas, Marco, Stefano Annunziato, Stephen J. Pettitt, Inge de Krijger, Hind Ghezraoui, Stefan J. Roobol, Catrin Lutz, Jessica Frankum, Fei Fei Song, Rachel Brough, Bastiaan Evers, Ewa Gogola, Jinhyuk Bhin, Marieke van de Ven, Dik C. van Gent, Jacqueline J. L. Jacobs, Ross Chapman, Christopher J. Lord, Jos Jonkers, and Sven Rottenberg. 2018. “The CST Complex Mediates End Protection at Double-Strand Breaks and Promotes PARP Inhibitor Sensitivity in BRCA1-Deficient Cells.” *Cell Reports* 23(7):2107–18.

Barneda-Zahonero, Bruna and Maribel Parra. 2012. “Histone Deacetylases and Cancer.” *Molecular Oncology* 6(6):579–89.

Barrangou, Rodolphe, Anne-Claire Coûté-Monvoisin, Buffy Stahl, Isabelle Chavichvily, Florian Damange, Dennis a Romero, Patrick Boyaval, Christophe Fremaux, and Philippe Horvath. 2013. “Genomic Impact of CRISPR Immunization against Bacteriophages.” *Biochemical Society Transactions* 41(6):1383–91.

Bartek, Jiri. 2011. “DNA Damage Response, Genetic Instability and Cancer: From Mechanistic Insights to Personalized Treatment.” *Molecular Oncology* 5(4):303–7.

Bassett, Andrew R. and Ji-Long Liu. 2014. “CRISPR/Cas9 and Genome Editing in Drosophila.” *Journal of Genetics and Genomics = Yi Chuan Xue Bao* 41(1):7–19.

Batenburg, Nicole L., John R. Walker, Sylvie M. Noordermeer, Nathalie Moatti, Daniel Durocher, and Xu-Dong Zhu. 2017. “ATM and CDK2 Control Chromatin Remodeler CSB to Inhibit RIF1 in DSB Repair Pathway Choice.” *Nature Communications* 8(1):1921.

Batey, M. A., Y. Zhao, S. Kyle, C. Richardson, A. Slade, N. M. B. Martin, A. Lau, D. R. Newell, and N. J. Curtin. 2013. “Preclinical Evaluation of a Novel ATM Inhibitor, KU59403, In Vitro and In Vivo in P53 Functional and Dysfunctional Models of Human Cancer.” *Molecular Cancer Therapeutics* 12(6):959–67.

Belhaj, Khaoula, Angela Chaparro-Garcia, Sophien Kamoun, and Vladimir Nekrasov. 2013. “Plant Genome Editing Made Easy: Targeted Mutagenesis in Model and Crop Plants Using the CRISPR/Cas System.” *Plant Methods* 9(1):39.

Bennardo, Nicole, Anita Cheng, Nick Huang, and Jeremy M. Stark. 2008. “Alternative-NHEJ Is a Mechanistically Distinct Pathway of Mammalian Chromosome Break Repair.” *PLoS Genetics* 4(6):e1000110.

Bennardo, Nicole, Amanda Gunn, Anita Cheng, Paul Hasty, and Jeremy M. Stark. 2009. “Limiting the Persistence of a Chromosome Break Diminishes Its Mutagenic Potential.” *PLoS Genetics* 5(10).

Bervoets, Indra and Daniel Charlier. 2018. “A Novel and Versatile Dual Fluorescent Reporter Tool for the Study of Gene Expression and Regulation in Multi- and Single Copy Number.” *Gene* 642(2):474–82.

Bétermier, Mireille, Pascale Bertrand, and Bernard S. Lopez. 2014. “Is Non-Homologous End-Joining Really an Inherently Error-Prone Process?” *PLoS Genetics* 10(1).

Bhargava, Ragini, David O. Onyango, and Jeremy M. Stark. 2016. “Regulation of Single-Strand Annealing and Its Role in Genome Maintenance.” *Trends in Genetics* 32(9):566–75.

Bharti, Sanjay Kumar, Irfan Khan, Taraswi Banerjee, Joshua A. Sommers, Yuliang Wu, and Robert M. Brosh. 2014.

"Molecular Functions and Cellular Roles of the ChlR1 (DDX11) Helicase Defective in the Rare Cohesinopathy Warsaw Breakage Syndrome." *Cellular and Molecular Life Sciences* 71(14):2625–39.

Biagioni, A., A. Chillà, E. Andreucci, A. Laurenzana, F. Margheri, S. Peppicelli, M. Del Rosso, and G. Fibbi. 2017. "Type II CRISPR/Cas9 Approach in the Oncological Therapy." *Journal of Experimental and Clinical Cancer Research* 36(1):1–8.

Bibikova, M., Beumer, K., Trautman, J.K., Carroll, D. 2003. "Enhancing Gene Targeting with Designed Zinc Finger Nucleases." *Science* 300(5620):764–764.

Blackburn, Patrick R., Jarryd M. Campbell, Karl J. Clark, and Stephen C. Ekker. 2013. "The CRISPR System--Keeping Zebrafish Gene Targeting Fresh." *Zebrafish* 10(1):116–18.

Blackford, Andrew N. and Stephen P. Jackson. 2017. "ATM, ATR, and DNA-PK: The Trinity at the Heart of the DNA Damage Response." *Molecular Cell*.

Boch, Jens, Heidi Scholze, Sebastian Schornack, Angelika Landgraf, Simone Hahn, Sabine Kay, Thomas Lahaye, Anja Nickstadt, and Ulla Bonas. 2009. "Breaking the Code of DNA Binding Specificity of TAL-Type III Effectors." *Science* 326(5959):1509–12.

Bothmer, Anne, Tanushree Phadke, Luis A. Barrera, Carrie M. Margulies, Christina S. Lee, Frank Buquicchio, Sean Moss, Hayat S. Abdulkerim, William Selleck, Hariharan Jayaram, Vic E. Myer, and Cecilia Cotta-Ramusino. 2017. "Characterization of the Interplay between DNA Repair and CRISPR/Cas9-Induced DNA Lesions at an Endogenous Locus." *Nature Communications* 8(May 2016):13905.

Boulton, S. J. and S. P. Jackson. 1996a. "Identification of a Saccharomyces Cerevisiae Ku80 Homologue: Roles in DNA Double Strand Break Rejoining and in Telomeric Maintenance." *Nucleic Acids Research* 24(23):4639–48.

Boulton, S. J. and S. P. Jackson. 1996b. "Saccharomyces Cerevisiae Ku70 Potentiates Illegitimate DNA Double-Strand Break Repair and Serves as a Barrier to Error-Prone DNA Repair Pathways." *The EMBO Journal* 15(18):5093–5103.

Bourton, Emma C., Pia-Amata Ahorner, Piers N. Plowman, Sheba Adam Zahir, Hussein Al-Ali, and Christopher N. Parris. 2017. "The PARP-1 Inhibitor Olaparib Suppresses BRCA1 Protein Levels, Increases Apoptosis and Causes Radiation Hypersensitivity in BRCA1+/-Lymphoblastoid Cells." *Journal of Cancer* 8(19):4048–56.

Brenner, J. Chad, Bushra Ateeq, Yong Li, Anastasia K. Yocum, Qi Cao, Irfan A. Asangani, Sonam Patel, Xiaoju Wang, Hallie Liang, Jindan Yu, Nallasivam Palanisamy, Javed Siddiqui, Wei Yan, Xuhong Cao, Rohit Mehra, Aaron Sabolch,

Venkatesha Basrur, Robert J. Lonigro, Jun Yang, Scott A. Tomlins, Christopher A. Maher, Kojo S. J. Elenitoba-Johnson, Maha Hussain, Nora M. Navone, Kenneth J. Pienta, Sooryanarayana Varambally, Felix Y. Feng, and Arul M. Chinnaiyan. 2011. "Mechanistic Rationale for Inhibition of Poly(ADP-Ribose) Polymerase in ETS Gene Fusion-Positive Prostate Cancer." *Cancer Cell* 19(5):664–78.

Brinkman, Eva K., Tao Chen, Marcel de Haas, Hanna A. Holland, Waseem Akhtar, and Bas van Steensel. 2018. "Kinetics and Fidelity of the Repair of Cas9-Induced Double-Strand DNA Breaks." *Molecular Cell* 70(5):801-813.e6.

Brown, Eric J. and David Baltimore. 2000. "ATR Disruption Leads to Chromosomal Fragmentation and Early Embryonic Lethality." *Genes and Development* 14(4):397–402.

Brown, Jessica S. and Stephen P. Jackson. 2015. "Ubiquitylation, Neddylation and the DNA Damage Response." *Open Biology* 5(4).

Brown, Jessica S., Brent O'Carrigan, Stephen P. Jackson, and Timothy A. Yap. 2017. "Targeting DNA Repair in Cancer: Beyond PARP Inhibitors." *Cancer Discovery* 7(1):20–37.

Bryant, Helen E. and Thomas Helleday. 2006. "Inhibition of Poly (ADP-Ribose) Polymerase Activates ATM Which Is Required for Subsequent Homologous Recombination Repair." *Nucleic Acids Research* 34(6):1685–91.

Buck, Dietke, Laurent Malivert, Régina De Chasseval, Anne Barraud, Marie Claude Fondanèche, Ozden Sanal, Alessandro Plebani, Jean Louis Stéphan, Markus Hufnagel, Françoise Le Deist, Alain Fischer, Anne Durandy, Jean Pierre De Villartay, and Patrick Revy. 2006. "Cernunnos, a Novel Nonhomologous End-Joining Factor, Is Mutated in Human Immunodeficiency with Microcephaly." *Cell* 124(2):287–99.

Bunting, Samuel F., Elsa Callén, Marina L. Kozak, Jung Min Kim, Nancy Wong, Andrés J. López-Contreras, Thomas Ludwig, Richard Baer, Robert B. Faryabi, Amy Malhowski, Hua-Tang Chen, Oscar Fernandez-Capetillo, Alan D'Andrea, and André Nussenzweig. 2012. "BRCA1 Functions Independently of Homologous Recombination in DNA Interstrand Crosslink Repair." *Molecular Cell* 46(2):125–35.

Bunting, Samuel F. and Andre Nussenzweig. 2013. "End-Joining, Translocations and Cancer." *Nature Reviews. Cancer* 13(7):443–54.

Callesen, Morten M., Martin F. Berthelsen, Sira Lund, Annette C. Füchtbauer, Ernst Martin Füchtbauer, and Jannik E. Jakobsen. 2016. "Recombinase-Mediated Cassette Exchange (RMCE)-in Reporter Cell Lines as an Alternative to the FLP-in System." *PLoS ONE* 11(8):1–14.

Carney, Brandon, Susanne Kossatz, Benjamin H. Lok, Valentina Schneeberger, Kishore K. Gangangari, Naga Vara Kishore Pillarsetty, Wolfgang A. Weber, Charles M. Rudin, John T. Poirier, and Thomas Reiner. 2018. "Target Engagement Imaging of PARP Inhibitors in Small-Cell Lung Cancer." *Nature Communications* 9(1).

Caron, Marie-Christine, Ajit K. Sharma, Julia O'Sullivan, Logan R. Myler, Maria Tedim Ferreira, Amélie Rodrigue, Yan Coulombe, Chantal Ethier, Jean-Philippe Gagné, Marie-France Langelier, John M. Pascal, Ilya J. Finkelstein, Michael J. Hendzel, Guy G. Poirier, and Jean-Yves Masson. 2019. "Poly(ADP-Ribose) Polymerase-1 Antagonizes DNA Resection at Double-Strand Breaks." *Nature Communications* 10(1):2954.

Ceccaldi, Raphael, Beatrice Rondinelli, and Alan D. D'Andrea. 2016. "Repair Pathway Choices and Consequences at the Double-Strand Break." *Trends in Cell Biology* 26(1):52–64.

Certo, Michael T., Kamila S. Gwiazda, Ryan Kuhar, Blythe Sather, Gabrielle Curinga, Tyler Mandt, Michelle Brault, Abigail R. Lambert, Sarah K. Baxter, Kyle Jacoby, Byoung Y. Ryu, Hans Peter Kiem, Agnes Gouble, Frederic Paques, David J. Rawlings, and Andrew M. Scharenberg. 2012. "Coupling Endonucleases with DNA End-Processing Enzymes to Drive Gene Disruption." *Nature Methods* 9(10):973–75.

Certo, Michael T., Byoung Y. Ryu, James E. Annis, Mikhail Garibov, Jordan Jarjour, David J. Rawlings, and Andrew M. Scharenberg. 2011. "Tracking Genome Engineering Outcome at Individual DNA Breakpoints." *Nature Methods* 8(8):671–76.

Chakrabarti, Anob M, Tristan Henser-Brownhill, Josep Monserrat, Anna R. Poetsch, Nicholas M. Luscombe, and Paola Scaffidi. 2019. "Target-Specific Precision of CRISPR-Mediated Genome Editing." *Molecular Cell* 73(4):699-713.e6.

Chakrabarti, Anob M., Tristan Henser-Brownhill, Josep Monserrat, Anna R. Poetsch, Nicholas M. Luscombe, and Paola Scaffidi. 2019. "Target-Specific Precision of CRISPR-Mediated Genome Editing." *Molecular Cell* 73(4):699-713.e6.

Chakraborty, Ujani, Carolyn M. George, Amy M. Lyndaker, and Eric Alani. 2016. "A Delicate Balance between Repair and Replication Factors Regulates Recombination between Divergent DNA Sequences in Saccharomyces Cerevisiae." *Genetics* 202(2):525–40.

Chang, Howard H.Y., Nicholas R. Pannunzio, Noritaka Adachi, and Michael R. Lieber. 2017. "Non-Homologous DNA End Joining and Alternative Pathways to Double-Strand Break Repair." *Nature Reviews Molecular Cell Biology* 18(8):495–506.

Chang, Howard H. Y., Nicholas R. Pannunzio, Noritaka Adachi, and Michael R. Lieber. 2017. "Non-Homologous DNA End Joining and Alternative Pathways to Double-Strand Break Repair." *Nature Reviews Molecular Cell Biology*.

Chen, Benjamin P. C., Doug W. Chan, Junya Kobayashi, Sandeep Burma, Aroumougame Asaithamby, Keiko Morotomi-Yano, Elliot Botvinick, Jun Qin, and David J. Chen. 2005. "Cell Cycle Dependence of DNA-Dependent Protein Kinase Phosphorylation in Response to DNA Double Strand Breaks." *Journal of Biological Chemistry* 280(15):14709–15.

Chen, Chin-Chuan, Ju-Sui Huang, Tong-Hong Wang, Chen-Hsin Kuo, Chia-Jen Wang, Shu-Huei Wang, and Yann-Lii Leu. 2017. "Dihydrocoumarin, an HDAC Inhibitor, Increases DNA Damage Sensitivity by Inhibiting Rad52." *International Journal of Molecular Sciences* 18(12):2655.

Chen, Min-bin, Zhen-tao Zhou, Lan Yang, Mu-xin Wei, and Min Tang. 2016. "KU-0060648 Inhibits Hepatocellular Carcinoma Cells through DNA-PKcs-Dependent And." *Oncotarget* 7(13):17047–59.

Chen, Yu, Haiping Zhang, Zhu Xu, Huanyin Tang, Anke Geng, Bailian Cai, Tao Su, Jiejun Shi, Cizhong Jiang, Xiao Tian, Andrei Seluanov, Jun Huang, Xiaoping Wan, Ying Jiang, Vera Gorbunova, and Zhiyong Mao. 2019. "A PARP1-BRG1-SIRT1 Axis Promotes HR Repair by Reducing Nucleosome Density at DNA Damage Sites." *Nucleic Acids Research* 1–18.

Chevalier, Brett S., Tanja Kortemme, Meggen S. Chadsey, David Baker, Raymond J. Monnat, and Barry L. Stoddard. 2002. "Design, Activity, and Structure of a Highly Specific Artificial Endonuclease." *Molecular Cell* 10(4):895–905.

Chirgadze, Dimitri Y., David B. Ascher, Tom L. Blundell, and Bancinyane L. Sibanda. 2017. *DNA-PKcs, Allostery, and DNA Double-Strand Break Repair: Defining the Structure and Setting the Stage*. Vol. 592. 1st ed. Elsevier Inc.

Chiruvella, Kishore K., Zhuobin Liang, and Thomas E. Wilson. 2013. "Repair of Double-Strand Breaks by End Joining." *Cold Spring Harbor Perspectives in Biology* 5(5):a012757.

Cho, J., M. E. Parks, and P. B. Dervan. 1995. "Cyclic Polyamides for Recognition in the Minor Groove of DNA." *Proceedings of the National Academy of Sciences of the United States of America* 92(22):10389–92.

Cho, Seung Woo and Howard Y. Chang. 2015. "Genomics: CRISPR Engineering Turns on Genes." *Nature* 517(7536):560–62.

Cho, Seung Woo, Sojung Kim, Yongsub Kim, Jiyeon Kweon, Heon Seok Kim, Sangsu Bae, and Jin-soo Kim. 2014. "Analysis of Off-Target Effects of CRISPR/Cas-Derived RNA-Guided Endonucleases and Nickases." *Genome Research* 24(1):132–41.

Choe, Juno, Haiwei H. Guo, and Ger van den Engh. 2005. "A Dual-Fluorescence Reporter System for High-Throughput Clone Characterization and Selection by Cell Sorting." *Nucleic Acids Research* 33(5):1–7.

Chun, Pusoon. 2015. “Histone Deacetylase Inhibitors in Hematological Malignancies and Solid Tumors.” *Archives of Pharmacal Research* 38(6):933–49.

Ciccia, Alberto and Stephen J. Elledge. 2010. “The DNA Damage Response: Making It Safe to Play with Knives.” *Molecular Cell* 40(2):179–204.

Cong, Le, F. Ann Ran, David Cox, Shuailiang Lin, Robert Barretto, Naomi Habib, Patrick D. Hsu, Xuebing Wu, Wenyan Jiang, Luciano a Marraffini, and Feng Zhang. 2013. “Multiplex Genome Engineering Using CRISPR/Cas Systems.” *Science (New York, N.Y.)* 339(6121):819–23.

Costantini, Silvia, Lisa Woodbine, Lucia Andreoli, Penny A. Jeggo, and Alessandro Vindigni. 2007. “Interaction of the Ku Heterodimer with the DNA Ligase IV/Xrcc4 Complex and Its Regulation by DNA-PK.” *DNA Repair* 6(6):712–22.

Costanzo, Vincenzo, Jayanta Chaudhuri, Jennifer C. Fung, and John V Moran. 2009. “Dealing with Dangerous Accidents: DNA Double-Strand Breaks Take Centre Stage. Symposium on Genome Instability and DNA Repair.” *EMBO Reports* 10(8):837–42.

Cox, David Benjamin Turitz, Randall Jeffrey Platt, and Feng Zhang. 2015. “Therapeutic Genome Editing: Prospects and Challenges.” *Nature Medicine* 21(2):121–31.

Cullot, Grégoire, Julian Boutin, Jérôme Toutain, Florence Prat, Perrine Pennamen, Caroline Rooryck, Martin Teichmann, Emilie Rousseau, Isabelle Lamrissi-Garcia, Véronique Guyonnet-Duperat, Alice Bibeyran, Magalie Lalanne, Valérie Prouzet-Mauléon, Béatrice Turcq, Cécile Ged, Jean Marc Blouin, Emmanuel Richard, Sandrine Dabernat, François Moreau-Gaudry, and Aurélie Bedel. 2019. “CRISPR-Cas9 Genome Editing Induces Megabase-Scale Chromosomal Truncations.” *Nature Communications* 10(1):1–14.

Curtin, N. J. 2013. “Inhibiting the DNA Damage Response as a Therapeutic Manoeuvre in Cancer.” *British Journal of Pharmacology* 169(8):1745–65.

Curtin, Nicola J. 2012. “DNA Repair Dysregulation from Cancer Driver to Therapeutic Target.” *Nature Reviews. Cancer* 12(12):801–17.

Daley, James M., William A. Gaines, Young Ho Kwon, and Patrick Sung. 2014. “Regulation of DNA Pairing in Homologous Recombination.” *Cold Spring Harbor Perspectives in Biology* 6(11):a017954.

Daley, James M. and Thomas E. Wilson. 2005. “Rejoining of DNA Double-Strand Breaks as a Function of Overhang Length.” *Molecular and Cellular Biology* 25(3):896–906.

Davis, Anthony J. and David J. Chen. 2013. “DNA Double Strand Break Repair via Non-Homologous End-Joining.” *Translational Cancer Research* 2(3):130–43.

Deriano, Ludovic and David B. Roth. 2013. “Modernizing the Nonhomologous End-Joining Repertoire: Alternative and Classical NHEJ Share the Stage.” *Annual Review of Genetics* 47(1):433–55.

Dietlein, Felix, Lisa Thelen, and H. Christian Reinhardt. 2014. “Cancer-Specific Defects in DNA Repair Pathways as Targets for Personalized Therapeutic Approaches.” *Trends in Genetics : TIG* 30(8):326–39.

Difilippantonio, M. J., J. Zhu, H. T. Chen, E. Meffre, M. C. Nussenzweig, E. E. Max, T. Ried, and A. Nussenzweig. 2000. “DNA Repair Protein Ku80 Suppresses Chromosomal Aberrations and Malignant Transformation.” *Nature* 404(6777):510–14.

Dillon, Magnus T., Holly E. Barker, Malin Pedersen, Hind Hafsi, Shreerang A. Bhide, Kate L. Newbold, Christopher M. Nutting, Martin McLaughlin, and Kevin J. Harrington. 2017. “Radiosensitization by the ATR Inhibitor AZD6738 through Generation of Acentric Micronuclei.” *Molecular Cancer Therapeutics* 16(1):25–34.

Dimitrova, N. and T. de Lange. 2009. “Cell Cycle-Dependent Role of MRN at Dysfunctional Telomeres: ATM Signaling-Dependent Induction of Nonhomologous End Joining (NHEJ) in G1 and Resection-Mediated Inhibition of NHEJ in G2.” *Molecular and Cellular Biology* 29(20):5552–63.

Dip, Ramiro and Hanspeter Naegeli. 2005. “More than Just Strand Breaks: The Recognition of Structural DNA Discontinuities by DNA-Dependent Protein Kinase Catalytic Subunit.” *The FASEB Journal* 19(7):704–15.

Dolman, M. Emmy M., Ida Van Der Ploeg, Jan Koster, Laurel Tabe Bate-Eya, Rogier Versteeg, Huib N. Caron, and Jan J. Molenaar. 2015. “DNA-Dependent Protein Kinase as Molecular Target for Radiosensitization of Neuroblastoma Cells.” *PLoS ONE* 10(12):1–18.

Doudna, Jennifer A. and Emmanuelle Charpentier. 2014. “Genome Editing. The New Frontier of Genome Engineering with CRISPR-Cas9.” *Science (New York, N.Y.)* 346(6213):1258096.

Dueva, Rositsa and George Iliakis. 2013. “Alternative Pathways of Non-Homologous End Joining (NHEJ) in Genomic Instability and Cancer.” *Translational Cancer Research* 2(3):163–77.

Dungl, Daniela A., Elaina N. Maginn, and Euan A. Stronach. 2015. “Preventing Damage Limitation: Targeting DNA-PKcs and DNA Double-Strand Break Repair Pathways for Ovarian Cancer Therapy.” *Frontiers in Oncology* 5(October):1–9.

Durkacz, Barbara W., Olusesan Omidiji, Douglas A. Gray, and Sydney Shall. 1980. "(ADP-Ribose)n Participates in DNA Excision Repair [23]." *Nature* 283(5747):593–96.

Duro, Eris, Cecilia Lundin, Katrine Ask, Luis Sanchez-Pulido, Thomas J. MacArtney, Rachel Toth, Chris P. Ponting, Anja Groth, Thomas Helleday, and John Rouse. 2010. "Identification of the MMS22L-TONSL Complex That Promotes Homologous Recombination." *Molecular Cell* 40(4):632–44.

Eichmiller, Robin, Melisa Medina-Rivera, Rachel DeSanto, Eugen Minca, Christopher Kim, Cory Holland, Ja Hwan Seol, Megan Schmit, Diane Oramus, Jessica Smith, Ignacio F. Gallardo, Ilya J. Finkelstein, Sang Eun Lee, and Jennifer A. Surtees. 2018. "Coordination of Rad1-Rad10 Interactions with Msh2-Msh3, Saw1 and RPA Is Essential for Functional 3′ Non-Homologous Tail Removal." *Nucleic Acids Research* 46(10):5075–96.

Escribano-Díaz, Cristina, Alexandre Orthwein, Amélie Fradet-Turcotte, Mengtan Xing, Jordan T. F. Young, Ján Tkáč, Michael A. Cook, Adam P. Rosebrock, Meagan Munro, Marella D. Canny, Dongyi Xu, and Daniel Durocher. 2013. "A Cell Cycle-Dependent Regulatory Circuit Composed of 53BP1-RIF1 and BRCA1-CtIP Controls DNA Repair Pathway Choice." *Molecular Cell*.

Evers, Bastiaan, Thomas Helleday, and Jos Jonkers. 2010. "Targeting Homologous Recombination Repair Defects in Cancer." *Trends in Pharmacological Sciences* 31(8):372–80.

Faruqi, A. F., M. Egholm, and P. M. Glazer. 1998. "Peptide Nucleic Acid-Targeted Mutagenesis of a Chromosomal Gene in Mouse Cells." *Proceedings of the National Academy of Sciences* 95(4):1398–1403.

Feehan, R. P. and L. M. Shantz. 2016. "Molecular Signaling Cascades Involved in Nonmelanoma Skin Carcinogenesis." *Biochemical Journal* 473(19):2973–94.

Ferguson, D. O., J. M. Sekiguchi, S. Chang, K. M. Frank, Y. Gao, R. A. DePinho, and F. W. Alt. 2000. "The Nonhomologous End-Joining Pathway of DNA Repair Is Required for Genomic Stability and the Suppression of Translocations." *Proceedings of the National Academy of Sciences of the United States of America* 97(12):6630–33.

Flavahan, William A., Elizabeth Gaskell, and Bradley E. Bernstein. 2017. "Epigenetic Plasticity and the Hallmarks of Cancer." *Science* 357(6348).

Fokas, E., R. Prevo, J. R. Pollard, P. M. Reaper, P. A. Charlton, B. Cornelissen, K. A. Vallis, E. M. Hammond, M. M. Olcina, W. Gillies McKenna, R. J. Musche, and T. B. Brunner. 2012. "Targeting ATR in Vivo Using the Novel Inhibitor VE-822 Results in Selective Sensitization of Pancreatic Tumors to Radiation." *Cell Death and Disease* 3(12):e441-10.

Forst, Alexandra H., Tobias Karlberg, Nicolas Herzog, Ann-Gerd Thorsell, Annika Gross, Karla L. H. Feijs, Patricia Verheugd, Petri Kursula, Bianca Nijmeijer, Elisabeth Kremmer, Henning Kleine, Andreas G. Ladurner, Herwig Schüler, and Bernhard Lüscher. 2013. "Recognition of Mono-ADP-Ribosylated ARTD10 Substrates by ARTD8 Macrodomains." *Structure (London, England : 1993)* 21(3):462–75.

Frank, Stefan, Boris V Skryabin, and Boris Greber. 2013. "A Modified TALEN-Based System for Robust Generation of Knock-out Human Pluripotent Stem Cell Lines and Disease Models." *BMC Genomics* 14(1):773.

Friedland, A. E., Y. B. Tzur, K. M. Esvelt, M. P. Colaiacovo, G. M. Church, and J. A. Calarco. 2013. "Heritable Genome Editing in C. Elegans via a CRISPR-Cas9 System." *Nat Methods* 10(8):741–43.

Frit, Philippe, Nadia Barboule, Ying Yuan, Dennis Gomez, and Patrick Calsou. 2014. "Alternative End-Joining Pathway(s): Bricolage at DNA Breaks." *DNA Repair* 17:81–97.

Fujinaka, Yoshihiko, Kazuaki Matsuoka, Makoto Iimori, Munkhbold Tuul, Ryo Sakasai, Keiji Yoshinaga, Hiroshi Saeki, Masaru Morita, Yoshihiro Kakeji, David A. Gillespie, Ken-Ichi Yamamoto, Minoru Takata, Hiroyuki Kitao, and Yoshihiko Maehara. 2012. "ATR-Chk1 Signaling Pathway and Homologous Recombinational Repair Protect Cells from 5-Fluorouracil Cytotoxicity." *DNA Repair* 11(3):247–58.

Garcia, Tamara B., Jonathan C. Snedeker, Dmitry Baturin, Lori Gardner, Susan P. Fosmire, Chengjing Zhou, Craig T. Jordan, Sujatha Venkataraman, Rajeev Vibhakar, and Christopher C. Porter. 2017. "A Small-Molecule Inhibitor of WEE1, AZD1775, Synergizes with Olaparib by Impairing Homologous Recombination and Enhancing DNA Damage and Apoptosis in Acute Leukemia." *Molecular Cancer Therapeutics* 16(10):2058–68.

Gasperini, Molly, Gregory M. Findlay, Aaron McKenna, Jennifer H. Milbank, Choli Lee, Melissa D. Zhang, Darren A. Cusanovich, and Jay Shendure. 2017. "CRISPR/Cas9-Mediated Scanning for Regulatory Elements Required for HPRT1 Expression via Thousands of Large, Programmed Genomic Deletions." *American Journal of Human Genetics* 101(2):192–205.

Gell, David and Stephen P. Jackson. 1999. "Mapping of Protein-Protein Interactions within the DNA-Dependent Protein Kinase Complex." *Nucleic Acids Research* 27(17):3494–3502.

van Gent, Dik C., J. H. Hoeijmakers, and Roland Kanaar. 2001. "Chromosomal Stability and the DNA Double-Stranded Break Connection." *Nature Reviews. Genetics* 2(3):196–206.

George, Carolyn M. and Eric Alani. 2012. "Multiple Cellular Mechanisms Prevent Chromosomal Rearrangements Involving Repetitive DNA." *Critical Reviews in Biochemistry and Molecular Biology* 47(3):297–313.

Geuting, Verena, Christian Reul, and Markus Löbrich. 2013. “ATM Release at Resected Double-Strand Breaks Provides Heterochromatin Reconstitution to Facilitate Homologous Recombination.” *PLoS Genetics* 9(8):e1003667.

Ghelli Luserna di Rora’, A., I. Iacobucci, and G. Martinelli. 2017. “The Cell Cycle Checkpoint Inhibitors in the Treatment of Leukemias.” *Journal of Hematology & Oncology* 10(1):77.

Glaser, Astrid, Bradley McColl, and Jim Vadolas. 2016. “GFP to BFP Conversion: A Versatile Assay for the Quantification of CRISPR/Cas9-Mediated Genome Editing.” *Molecular Therapy. Nucleic Acids* 5(7):e334.

Glorieux, Mary, Rüveyda Dok, and Sandra Nuyts. 2017. “Novel DNA Targeted Therapies for Head and Neck Cancers: Clinical Potential and Biomarkers.” *Oncotarget* 8(46):81662–78.

Goglia, A. G., R. Delsite, A. N. Luz, D. Shahbazian, A. F. Salem, R. K. Sundaram, J. Chiaravalli, P. J. Hendrikx, J. A. Wilshire, M. Jasin, H. M. Kluger, J. F. Glickman, S. N. Powell, and R. S. Bindra. 2015. “Identification of Novel Radiosensitizers in a High-Throughput, Cell-Based Screen for DSB Repair Inhibitors.” *Molecular Cancer Therapeutics* 14(2):326–42.

Gomez-Cabello, Daniel, Sonia Jimeno, María Jesús Fernández-Ávila, and Pablo Huertas. 2013. “New Tools to Study DNA Double-Strand Break Repair Pathway Choice.” *PLoS ONE* 8(10):1–9.

Gong, Fade, Li Ya Chiu, Ben Cox, François Aymard, Thomas Clouaire, Justin W. Leung, Michael Cammarata, Mercedes Perez, Poonam Agarwal, Jennifer S. Brodbelt, Gaëlle Legube, and Kyle M. Miller. 2015. “Screen Identifies Bromodomain Protein ZMYND8 in Chromatin Recognition of Transcription-Associated DNA Damage That Promotes Homologous Recombination.” *Genes and Development* 29(2):197–211.

Gottesfeld, J. M., L. Neely, J. W. Trauger, E. E. Baird, and P. B. Dervan. 1997. “Regulation of Gene Expression by Small Molecules.” *Nature* 387(6629):202–5.

Grabarz, Anastazja, Josée Guirouilh-Barbat, Aurélia Barascu, Gaëlle Pennarun, Diane Genet, Emilie Rass, Susanne M. Germann, Pascale Bertrand, Ian D. Hickson, and Bernard S. Lopez. 2013. “A Role for BLM in Double-Strand Break Repair Pathway Choice: Prevention of CtIP/Mre11-Mediated Alternative Nonhomologous End-Joining.” *Cell Reports* 5(1):21–28.

Grawunder, Ulf, Matthias Wilm, Xiantuo Wu, Peter Kulesza, Thomas E. Wilson, Matthias Mann, and Michael R. Lieber. 1997. “Activity of DNA Ligase IV Stimulated by Complex Formation with XRCC4 Protein in Mammalian Cells.” *Nature* 388(6641):492–95.

Gu, Wei Wei, Jie Lin, and Xing Yu Hong. 2017. “Cyclin A2 Regulates Homologous Recombination DNA Repair and

Sensitivity to DNA Damaging Agents and Poly(ADP-Ribose) Polymerase (PARP) Inhibitors in Human Breast Cancer Cells." *Oncotarget* 8(53):90842–51.

Gudmundsdottir, K. and A. Ashworth. 2006. "The Roles of BRCA1 and BRCA2 and Associated Proteins in the Maintenance of Genomic Stability." *Oncogene* 25(43):5864–74.

Gunn, Amanda and Jeremy M. Stark. 2012. "I-SceI-Based Assays to Examine Distinct Repair Outcomes of Mammalian Chromosomal Double Strand Breaks." *Methods in Molecular Biology (Clifton, N.J.)* 920(9):379–91.

Guo, Kexiao, Anang A. Shelat, R. Kiplin Guy, and Michael B. Kastan. 2014. "Development of a Cell-Based, High-Throughput Screening Assay for ATM Kinase Inhibitors." *Journal of Biomolecular Screening* 19(4):538–46.

Haber, James E. and J. Kent Moore. 1996. "Cell Cycle and Genetic Requirements of Two Pathways of Nonhomologous End-Joining Repair of Double-Strand Breaks in Saccharomyces Cerevisiae." *Molecular and Cellular Biology* 16(5):2164–73.

Hanahan, D. and R. A. Weinberg. 2000. "The Hallmarks of Cancer." *Cell* 100(1):57–70.

Hanahan, Douglas and Robert A. Weinberg. 2011. "Hallmarks of Cancer: The next Generation." *Cell* 144(5):646–74.

Harnor, Suzannah J., Alfie Brennan, and Céline Cano. 2017. "Targeting DNA-Dependent Protein Kinase for Cancer Therapy." *ChemMedChem* 12(12):895–900.

He, Xiangjun, Chunlai Tan, Feng Wang, Yaofeng Wang, Rui Zhou, Dexuan Cui, Wenxing You, Hui Zhao, Jianwei Ren, and Bo Feng. 2016. "Knock-in of Large Reporter Genes in Human Cells via CRISPR/Cas9-Induced Homology-Dependent and Independent DNA Repair." *Nucleic Acids Research* 44(9).

Hegan, D. C., Y. Lu, G. C. Stachelek, M. E. Crosby, R. S. Bindra, and P. M. Glazer. 2010. "Inhibition of Poly(ADP-Ribose) Polymerase down-Regulates BRCA1 and RAD51 in a Pathway Mediated by E2F4 and P130." *Proceedings of the National Academy of Sciences* 107(5):2201–6.

Hengel, Sarah R., M. Ashley Spies, and Maria Spies. 2017. "Small-Molecule Inhibitors Targeting DNA Repair and DNA Repair Deficiency in Research and Cancer Therapy." *Cell Chemical Biology* 24(9):1101–19.

Hirai, H., Y. Iwasawa, M. Okada, T. Arai, T. Nishibata, M. Kobayashi, T. Kimura, N. Kaneko, J. Ohtani, K. Yamanaka, H. Itadani, I. Takahashi-Suzuki, K. Fukasawa, H. Oki, T. Nambu, J. Jiang, T. Sakai, H. Arakawa, T. Sakamoto, T. Sagara, T. Yoshizumi, S. Mizuarai, and H. Kotani. 2009. "Small-Molecule Inhibition of Wee1 Kinase by MK-1775 Selectively Sensitizes P53-Deficient Tumor Cells to DNA-Damaging Agents." *Molecular Cancer Therapeutics* 8(11):2992–3000.

Hopkins, T. A., Y. Shi, L. E. Rodriguez, L. R. Solomon, C. K. Donawho, E. L. DiGiammarino, S. C. Panchal, J. L. Wilsbacher, W. Gao, A. M. Olson, D. F. Stolarik, D. J. Osterling, E. F. Johnson, and D. Maag. 2015. "Mechanistic Dissection of PARP1 Trapping and the Impact on In Vivo Tolerability and Efficacy of PARP Inhibitors." *Molecular Cancer Research* 13(11):1465–77.

House, Nealia C. M., Melissa R. Koch, and Catherine H. Freudenreich. 2014. "Chromatin Modifications and DNA Repair: Beyond Double-Strand Breaks." *Frontiers in Genetics* 5(SEP):1–18.

Hsu, P., E. Lander, and F. Zhang. 2014. "Development and Applications of CRIPR-Cas9 for Genome Engineering." *Cell* 157(6):1262–78.

Hsu, Patrick D., David A. Scott, Joshua A. Weinstein, F. Ann Ran, Silvana Konermann, Vineeta Agarwala, Yinqing Li, Eli J. Fine, Xuebing Wu, Ophir Shalem, Thomas J. Cradick, Luciano A. Marraffini, Gang Bao, and Feng Zhang. 2013. "DNA Targeting Specificity of RNA-Guided Cas9 Nucleases." *Nature Biotechnology* 31(9):827–32.

Huertas, Pablo. 2010. "DNA Resection in Eukaryotes: Deciding How to Fix the Break." *Nature Structural & Molecular Biology* 17(1):11–16.

Hurov, Kristen E., Cecilia Cotta-Ramusino, and Stephen J. Elledge. 2010. "A Genetic Screen Identifies the Triple T Complex Required for DNA Damage Signaling and ATM and ATR Stability." *Genes and Development* 24(17):1939–50.

Hustedt, Nicole and Daniel Durocher. 2017. "The Control of DNA Repair by the Cell Cycle." *Nature Cell Biology*.

Iliakis, George, Bustanur Rosidi, Minli Wang, and Huichen Wang. 2008. "Plasmid-Based Assays for DNA End-Joining In Vitro." *DNA Repair Protocols* 123–31.

Jackson, Stephen P. and Jiri Bartek. 2009. "The DNA-Damage Response in Human Biology and Disease." *Nature* 461(7267):1071–78.

Jacquier, Alain and Bernard Dujon. 1985. "An Intron-Encoded Protein Is Active in a Gene Conversion Process That Spreads an Intron into a Mitochondrial Gene." *Cell* 41(2):383–94.

Janssen, Josephine M., Xiaoyu Chen, Jin Liu, and Manuel A. F. V. Gonçalves. 2019. "The Chromatin Structure of CRISPR-Cas9 Target DNA Controls the Balance between Mutagenic and Homology-Directed Gene-Editing Events." *Molecular Therapy - Nucleic Acids* 16(June):141–54.

Jette, Nicholas and Susan P. Lees-Miller. 2015. "The DNA-Dependent Protein Kinase: A Multifunctional Protein Kinase with Roles in DNA Double Strand Break Repair and Mitosis." *Progress in Biophysics and Molecular Biology* 117(2–3):194–

205.

Ji, Xiaofei, Ying Wang, Jiaojiao Li, Qianyu Rong, Xingxing Chen, Ying Zhang, Xiaoning Liu, Boqing Li, and Huilin Zhao. 2017. “Application of FLP-FRT System to Construct Unmarked Deletion in Helicobacter Pylori and Functional Study of Gene Hp0788 in Pathogenesis.” *Frontiers in Microbiology* 8(NOV):1–12.

Jiang, Wenxia, Jennifer L. Crowe, Xiangyu Liu, Satoshi Nakajima, Yunyue Wang, Chen Li, Brian J. Lee, Richard L. Dubois, Chao Liu, Xiaochun Yu, Li Lan, and Shan Zha. 2015. “Differential Phosphorylation of DNA-PKcs Regulates the Interplay between End-Processing and End-Ligation during Nonhomologous End-Joining.” *Molecular Cell* 58(1):172–85.

Jin, Juan, Hehui Fang, Fang Yang, Wenfei Ji, Nan Guan, Zijia Sun, Yaqin Shi, Guohua Zhou, and Xiaoxiang Guan. 2018. “Combined Inhibition of ATR and WEE1 as a Novel Therapeutic Strategy in Triple-Negative Breast Cancer.” *Neoplasia (New York, N.Y.)* 20(5):478–88.

Jinek, Martin, Krzysztof Chylinski, Ines Fonfara, Michael Hauer, Jennifer a. Doudna, and Emmanuelle Charpentier. 2012. “A Programmable Dual-RNA-Guided DNA Endonuclease in Adaptive Bacterial Immunity.” *Science (New York, N.Y.)* 337(6096):816–21.

Jinek, Martin, Alexandra East, Aaron Cheng, Steven Lin, Enbo Ma, and Jennifer Doudna. 2013. “RNA-Programmed Genome Editing in Human Cells.” *ELife* 2(3):e00471.

Johnson, R. D. and M. Jasin. 2000. “Sister Chromatid Gene Conversion Is a Prominent Double-Strand Break Repair Pathway in Mammalian Cells.” *The EMBO Journal* 19(13):3398–3407.

Johnson, Roger D., Nan Liu, and Maria Jasin. 1999. “Mammalian XRCC2 Promotes the Repair of DNA Double-Strand Breaks by Homologous Recombination.” *Nature* 401(6751):397–99.

Johnson, Sam A., Zhongsheng You, and Tony Hunter. 2007. “Monitoring ATM Kinase Activity in Living Cells.” *DNA Repair* 6(9):1277–84.

Kandoth, Cyriac, Michael D. McLellan, Fabio Vandin, Kai Ye, Beifang Niu, Charles Lu, Mingchao Xie, Qunyuan Zhang, Joshua F. McMichael, Matthew A. Wyczalkowski, Mark D. M. Leiserson, Christopher A. Miller, John S. Welch, Matthew J. Walter, Michael C. Wendl, Timothy J. Ley, Richard K. Wilson, Benjamin J. Raphael, and Li Ding. 2013. “Mutational Landscape and Significance across 12 Major Cancer Types.” *Nature* 502(7471):333–39.

Khanna, K. K. and S. P. Jackson. 2001. “DNA Double-Strand Breaks: Signaling, Repair and the Cancer Connection.” *Nature*

Genetics 27(3):247–54.

Kim, Hye-young, Yunhee Cho, Hyeokgu Kang, Ye-seal Yim, Jaewhan Song, and Kyung-hee Chun. 2016. "Targeting the WEE1 Kinase as a Molecular Targeted Therapy for Gastric Cancer." *Oncotarget* 7(31):49902–16.

Kim, Hyongbum and Jin-Soo Kim. 2014. "A Guide to Genome Engineering with Programmable Nucleases." *Nature Reviews. Genetics* 15(5):321–34.

Kim, Jun-Seob, Da-Hyeong Cho, Myeongseo Park, Woo-Jae Chung, Dongwoo Shin, Kwan Soo Ko, and Dae-Hyuk Kweon. 2016. "CRISPR/Cas9-Mediated Re-Sensitization of Antibiotic-Resistant Escherichia Coli Harboring Extended-Spectrum β-Lactamases." *Journal of Microbiology and Biotechnology* 26(2):394–401.

Klaeger, Susan, Stephanie Heinzlmeir, Mathias Wilhelm, Harald Polzer, Binje Vick, Paul-Albert Albert Koenig, Maria Reinecke, Benjamin Ruprecht, Svenja Petzoldt, Chen Meng, Jana Zecha, Katrin Reiter, Huichao Qiao, Dominic Helm, Heiner Koch, Melanie Schoof, Giulia Canevari, Elena Casale, Stefania Re Depaolini, Annette Feuchtinger, Zhixiang Wu, Tobias Schmidt, Lars Rueckert, Wilhelm Becker, Jan Huenges, Anne-Kathrin Kathrin Garz, Bjoern-Oliver Oliver Gohlke, Daniel Paul Zolg, Gian Kayser, Tonu Vooder, Robert Preissner, Hannes Hahne, Neeme Tõnisson, Karl Kramer, Katharina Götze, Florian Bassermann, Judith Schlegl, Hans-Christian Christian Ehrlich, Stephan Aiche, Axel Walch, Philipp A. Greif, Sabine Schneider, Eduard Rudolf Felder, Juergen Ruland, Guillaume Médard, Irmela Jeremias, Karsten Spiekermann, Bernhard Kuster, Stefania Re Depaolini, Annette Feuchtinger, Zhixiang Wu, Tobias Schmidt, Lars Rueckert, Wilhelm Becker, Jan Huenges, Anne-Kathrin Kathrin Garz, Bjoern-Oliver Oliver Gohlke, Daniel Paul Zolg, Gian Kayser, Tonu Vooder, Robert Preissner, Hannes Hahne, Neeme Tõnisson, Karl Kramer, Katharina Götze, Florian Bassermann, Judith Schlegl, Hans-Christian Christian Ehrlich, Stephan Aiche, Axel Walch, Philipp A. Greif, Sabine Schneider, Eduard Rudolf Felder, Juergen Ruland, Guillaume Médard, Irmela Jeremias, Karsten Spiekermann, and Bernhard Kuster. 2017. "The Target Landscape of Clinical Kinase Drugs." *Science (New York, N.Y.)* 358(6367).

Klein, Carmen, Ivana Dokic, Andrea Mairani, Stewart Mein, Stephan Brons, Peter Häring, Thomas Haberer, Oliver Jäkel, Astrid Zimmermann, Frank Zenke, Andree Blaukat, Jürgen Debus, and Amir Abdollahi. 2017. "Overcoming Hypoxia-Induced Tumor Radioresistance in Non-Small Cell Lung Cancer by Targeting DNA-Dependent Protein Kinase in Combination with Carbon Ion Irradiation." *Radiation Oncology* 12(1):1–8.

Klein, Hannah L., Giedrė Bačinskaja, Jun Che, Anais Cheblal, Rajula Elango, Anastasiya Epshtein, Devon M. Fitzgerald, Belén Gómez-González, Sharik R. Khan, Sandeep Kumar, Bryan A. Leland, Léa Marie, Qian Mei, Judith Miné-Hattab, Alicja Piotrowska, Erica J. Polleys, Christopher D. Putnam, Elina A. Radchenko, Anissia Ait Saada, Cynthia J. Sakofsky, Eun Yong Shim, Mathew Stracy, Jun Xia, Zhenxin Yan, Yi Yin, Andrés Aguilera, Juan Lucas Argueso,

Catherine H. Freudenreich, Susan M. Gasser, Dmitry A. Gordenin, James E. Haber, Grzegorz Ira, Sue Jinks-Robertson, Megan C. King, Richard D. Kolodner, Andrei Kuzminov, Sarah AE Lambert, Sang Eun Lee, Kyle M. Miller, Sergei M. Mirkin, Thomas D. Petes, Susan M. Rosenberg, Rodney Rothstein, Lorraine S. Symington, Pawel Zawadzki, Nayun Kim, Michael Lisby, and Anna Malkova. 2019. "Guidelines for DNA Recombination and Repair Studies: Cellular Assays of DNA Repair Pathways." *Microbial Cell* 6(1):1–64.

Kleinstiver, Benjamin P., Vikram Pattanayak, Michelle S. Prew, Shengdar Q. Tsai, Nhu T. Nguyen, Zongli Zheng, and J. Keith Joung. 2016. "High-Fidelity CRISPR-Cas9 Nucleases with No Detectable Genome-Wide off-Target Effects." *Nature* 529(7587):490–95.

Knight, S., L. Xie, W. Deng, B. Guglielmi, L. B. Witkowsky, L. Bosanac, E. T. Zhang, M. El Beheiry, J. B. Masson, M. Dahan, Z. Liu, J. a. Doudna, and R. Tjian. 2015. "Dynamics of CRISPR-Cas9 Genome Interrogation in Living Cells." *Science* 350(6262):823–26.

Knobel, Philip and Thomas Marti. 2011. "Translesion DNA Synthesis in the Context of Cancer Research." *Cancer Cell International* 11(1):39.

Kojima, Shin-Ichiro and Gary G. Borisy. 2014. "An Image-Based, Dual Fluorescence Reporter Assay to Evaluate the Efficacy of ShRNA for Gene Silencing at the Single-Cell Level." *F1000Research* 3(0):1–26.

Konstantinopoulos, Panagiotis A., Raphael Ceccaldi, Geoffrey I. Shapiro, and Alan D. D'Andrea. 2015. "Homologous Recombination Deficiency: Exploiting the Fundamental Vulnerability of Ovarian Cancer." *Cancer Discovery* 5(11):1137–54.

Kosicki, Michael, Kärt Tomberg, and Allan Bradley. 2018. "Repair of Double-Strand Breaks Induced by CRISPR–Cas9 Leads to Large Deletions and Complex Rearrangements." *Nature Biotechnology* 36(8).

Kozich, James J., Sarah L. Westcott, Nielson T. Baxter, Sarah K. Highlander, and Patrick D. Schloss. 2013. "Development of a Dual-Index Sequencing Strategy and Curation Pipeline for Analyzing Amplicon Sequence Data on the Miseq Illumina Sequencing Platform." *Applied and Environmental Microbiology* 79(17):5112–20.

Kuhar, Ryan, Kamila S. Gwiazda, Olivier Humbert, Tyler Mandt, Joey Pangallo, Michelle Brault, Iram Khan, Nancy Maizels, David J. Rawlings, Andrew M. Scharenberg, and Michael T. Certo. 2016. "Novel Fluorescent Genome Editing Reporters for Monitoring DNA Repair Pathway Utilization at Endonuclease-Induced Breaks." *Nucleic Acids Research* 42(1):e4.

Langhans, Mark T. and Michael J. Palladino. 2009. "Cleavage of Mispaired Heteroduplex DNA Substrates by Numerous

Restriction Enzymes." *Current Issues in Molecular Biology* 11(1):1–12.

Li, Xuan and Wolf-Dietrich Heyer. 2008. "Homologous Recombination in DNA Repair and DNA Damage Tolerance." *Cell Research* 18(1):99–113.

Li, Yixuan and Edward Seto. 2016. "HDACs and HDAC Inhibitors in Cancer Development and Therapy." *Cold Spring Harbor Perspectives in Medicine* 6(10):1–10.

Li, Zhiming and Wei Guo Zhu. 2014. "Targeting Histone Deacetylases for Cancer Therapy: From Molecular Mechanisms to Clinical Implications." *International Journal of Biological Sciences* 10(7):757–70.

Lieber, Michael R. 2011. "The Mechanism of Double-Strand DNA Break Repair by the Nonhomologous DNA End Joining Pathway." *Annual Review of Biochemistry* 19(3):181–211.

Liu, Mingjie, Saad Rehman, Xidian Tang, Kui Gu, Qinlei Fan, Dekun Chen, and Wentao Ma. 2019. "Methodologies for Improving HDR Efficiency." *Frontiers in Genetics* 10(JAN):1–9.

Liu, Rui, Ling Chen, Yanping Jiang, Zhihua Zhou, and Gen Zou. 2015. "Efficient Genome Editing in Filamentous Fungus Trichoderma Reesei Using the CRISPR/Cas9 System." *Cell Discovery* 1:15007.

Liu, Ting and Jun Huang. 2016. "DNA End Resection: Facts and Mechanisms." *Genomics, Proteomics & Bioinformatics* 14(3):126–30.

López-Saavedra, Ana, Daniel Gómez-Cabello, María Salud Domínguez-Sánchez, Fernando Mejías-Navarro, María Jesús Fernández-Ávila, Christoffel Dinant, María Isabel Martínez-Macías, Jiri Bartek, and Pablo Huertas. 2016. "A Genome-Wide Screening Uncovers the Role of CCAR2 as an Antagonist of DNA End Resection." *Nature Communications* 7.

Lord, Christopher J. and Alan Ashworth. 2012. "The DNA Damage Response and Cancer Therapy." *Nature* 481(7381):287–94.

Lord, Christopher J. and Alan Ashworth. 2017. "PARP Inhibitors: Synthetic Lethality in the Clinic." *Science* 355(6330):1152–58.

Malaby, Andrew W., Sara K. Martin, Richard D. Wood, and Sylvie Doublié. 2017. "Expression and Structural Analyses of Human DNA Polymerase θ (POLQ)." *Methods in Enzymology* 592:103–21.

Mansour, Wael Y., Sabine Schumacher, Raphael Rosskopf, Tim Rhein, Filip Schmidt-Petersen, Fruszina Gatzemeier, Friedrich Haag, Kerstin Borgmann, Henning Willers, and Jochen Dahm-Daphi. 2008. "Hierarchy of Nonhomologous End-Joining, Single-Strand Annealing and Gene Conversion at Site-Directed DNA Double-Strand Breaks." *Nucleic*

Acids Research 36(12):4088–98.

Marnef, Aline and Gaëlle Legube. 2017. “Organizing DNA Repair in the Nucleus: DSBs Hit the Road.” *Current Opinion in Cell Biology* 46:1–8.

McVey, Mitch and Sang Eun Lee. 2008. “MMEJ Repair of Double-Strand Breaks (Director’s Cut): Deleted Sequences and Alternative Endings.” *Trends in Genetics : TIG* 24(11):529–38.

Miller, Kyle M., Jorrit V. Tjeertes, Julia Coates, Gaëlle Legube, Sophie E. Polo, Sébastien Britton, and Stephen P. Jackson. 2010. “Human HDAC1 and HDAC2 Function in the DNA-Damage Response to Promote DNA Nonhomologous End-Joining.” *Nature Structural and Molecular Biology* 17(9):1144–51.

Minchom, Anna, Caterina Aversa, and Juanita Lopez. 2018. “Dancing with the DNA Damage Response: Next-Generation Anti-Cancer Therapeutic Strategies.” *Therapeutic Advances in Medical Oncology* 10(4):1758835918786658.

Mjelle, Robin, Siv Anita Hegre, Per Arne Aas, Geir Slupphaug, Finn Drabløs, Pål Sætrom, and Hans E. Krokan. 2015. “Cell Cycle Regulation of Human DNA Repair and Chromatin Remodeling Genes.” *DNA Repair* 30:53–67.

Mojumdar, Aditya, Kyle Sorenson, Marcel Hohl, Susan Lees-Miller, Karine Dubrana, John Petrini, and Jennifer A. Cobb. 2019. “Nej1 Interacts with Mre11 to Regulate-Tethering and Dna2 Binding at DNA Double-Strand Breaks.” *SSRN Electronic Journal* 28(6):1564-1573.e3.

Mondesert, Odile, Céline Frongia, Olivia Clayton, Marie Laure Boizeau, Valérie Lobjois, and Bernard Ducommun. 2015. “Monitoring the Activation of the DNA Damage Response Pathway in a 3D Spheroid Model.” *PLoS ONE* 10(7):1–12.

Moscou, Matthew J. and Adam J. Bogdanove. 2009. “Recognition by TAL Effectors.” *Science (New York, N.Y.)* 326(December):1501.

Moshous, Despina, Régina De Chasseval, Barbara Corneo, Marina Cavazzana-Calvo, Françoise Le Deist, Alain Fischer, Jean-Pierre De Villartay, Isabelle Callebaut, Ilhan Tezcan, Ozden Sanal, Yves Bertrand, and Noel Philippe. 2001. “Artemis, a Novel DNA Double-Strand Break Repair/V(D)J Recombination Protein, Is Mutated in Human Severe Combined Immune Deficiency.” *Cell* 105(2):177–86.

Mukherjee-Clavin, Bipasha, Mark Tomishima, and Gabsang Lee. 2013. “Current Approaches for Efficient Genetic Editing in Human Pluripotent Stem Cells.” *Frontiers in Biology* 8(5):461–67.

Murai, Junko, Kailin Yang, Donniphat Dejsuphong, Kouji Hirota, Shunichi Takeda, and Alan D. D’Andrea. 2011. “The USP1/UAF1 Complex Promotes Double-Strand Break Repair through Homologous Recombination.” *Molecular and*

Cellular Biology 31(12):2462–69.

Muraki, Keiko, Limei Han, Douglas Miller, and John P. Murnane. 2013. "The Role of ATM in the Deficiency in Nonhomologous End-Joining near Telomeres in a Human Cancer Cell Line." *PLoS Genetics* 9(3):e1003386.

Muthurajan, U. M., M. R. D. Hepler, A. R. Hieb, N. J. Clark, M. Kramer, T. Yao, and K. Luger. 2014. "Automodification Switches PARP-1 Function from Chromatin Architectural Protein to Histone Chaperone." *Proceedings of the National Academy of Sciences* 111(35):12752–57.

Nishimasu, Hiroshi, F. Ann Ran, Patrick D. Hsu, Silvana Konermann, Soraya I. Shehata, Naoshi Dohmae, Ryuichiro Ishitani, Feng Zhang, and Osamu Nureki. 2014. "Crystal Structure of Cas9 in Complex with Guide RNA and Target DNA." *Cell* 156(5):935–49.

Nutley, B. P., N. F. Smith, A. Hayes, L. R. Kelland, L. Brunton, B. T. Golding, G. C. M. Smith, N. M. B. Martin, P. Workman, and F. I. Raynaud. 2005. "Preclinical Pharmacokinetics and Metabolism of a Novel Prototype DNA-PK Inhibitor NU7026." *British Journal of Cancer* 93(9):1011–18.

O'Driscoll, Mark and Penny A. Jeggo. 2006. "The Role of Double-Strand Break Repair - Insights from Human Genetics." *Nature Reviews Genetics* 7(1):45–54.

Ochi, Takashi, Bancinyane Lynn Sibanda, Qian Wu, Dimitri Y. Chirgadze, Victor M. Bolanos-Garcia, and Tom L. Blundell. 2010. "Structural Biology of DNA Repair: Spatial Organisation of the Multicomponent Complexes of Nonhomologous End Joining." *Journal of Nucleic Acids* 2010.

van Oorschot, Bregje, Giovanna Granata, Simone Di Franco, Rosemarie ten Cate, Hans M. Rodermond, Matilde Todaro, Jan Paul Medema, and Nicolaas A. P. Franken. 2016. "Targeting DNA Double Strand Break Repair with Hyperthermia and DNA-PKcs Inhibition to Enhance the Effect of Radiation Treatment." *Oncotarget* 7(40):65504–13.

van Overbeek, Megan, Daniel Capurso, Matthew M. Carter, Matthew S. Thompson, Elizabeth Frias, Carsten Russ, John S. Reece-Hoyes, Christopher Nye, Scott Gradia, Bastien Vidal, Jiashun Zheng, Gregory R. Hoffman, Christopher K. Fuller, and Andrew P. May. 2016. "DNA Repair Profiling Reveals Nonrandom Outcomes at Cas9-Mediated Breaks." *Molecular Cell* 63(4):633–46.

Pace, Paul, Georgina Mosedale, Michael R. Hodskinson, Ivan V Rosado, Meera Sivasubramaniam, and Ketan J. Patel. 2010. "Ku70 Corrupts DNA Repair in the Absence of the Fanconi Anemia Pathway." *Science (New York, N.Y.)* 329(5988):219–23.

Pascale, Rosa M., Christy Joseph, Gavinella Latte, Matthias Evert, Francesco Feo, and Diego F. Calvisi. 2016. "DNA-PKcs: A Promising Therapeutic Target in Human Hepatocellular Carcinoma?" *DNA Repair* 47:12–20.

Pavletich, N. P. and C. O. Pabo. 1991. "Zinc Finger-DNA Recognition: Crystal Structure of a Zif268-DNA Complex at 2.1 A." *Science (New York, N.Y.)* 252(5007):809–17.

Pearl, Laurence H., Amanda C. Schierz, Simon E. Ward, Bissan Al-Lazikani, and Frances M. G. Pearl. 2015. "Therapeutic Opportunities within the DNA Damage Response." *Nature Reviews. Cancer* 15(3):166–80.

Perez-Pinera, Pablo, David G. Ousterout, and Charles A. Gersbach. 2012. "Advances in Targeted Genome Editing." *Current Opinion in Chemical Biology* 16(3–4):268–77.

Pierce, Andrew J., Roger D. Johnson, Larry H. Thompson, and Maria Jasin. 1999. "XRCC3 Promotes Homology-Directed Repair of DNA Damage in Mammalian Cells." *Genes and Development* 13(20):2633–38.

Pilié, Patrick G., Chad Tang, Gordon B. Mills, and Timothy A. Yap. 2019. "State-of-the-Art Strategies for Targeting the DNA Damage Response in Cancer." *Nature Reviews Clinical Oncology* 16(2):81–104.

Piwko, Wojciech, Lucie J. Mlejnkova, Karun Mutreja, Lepakshi Ranjha, Diana Stafa, Alexander Smirnov, Mia ML Brodersen, Ralph Zellweger, Andreas Sturzenegger, Pavel Janscak, Massimo Lopes, Matthias Peter, and Petr Cejka. 2016. "The MMS22L–TONSL Heterodimer Directly Promotes RAD51-dependent Recombination upon Replication Stress." *The EMBO Journal* 35(23):2584–2601.

Pommier, Yves, Mark J. O'Connor, and Johann De Bono. 2016. "Laying a Trap to Kill Cancer Cells: PARP Inhibitors and Their Mechanisms of Action." *Science Translational Medicine* 8(362):1–8.

Purnell, M. R. and W. J. Whish. 1980. "Novel Inhibitors of Poly(ADP-Ribose) Synthetase." *Biochemical Journal* 185(3):775–77.

Rakauskait, Rasa, Pei Yu Liao, Michael H. J. Rhodin, Kelvin Lee, and Jonathan D. Dinman. 2011. "A Rapid, Inexpensive Yeast-Based Dual-Fluorescence Assay of Programmed-1 Ribosomal Frameshifting for High-Throughput Screening." *Nucleic Acids Research* 39(14):1–7.

Ramirez, Cherie L., Michael T. Certo, Claudio Mussolino, Mathew J. Goodwin, Thomas J. Cradick, Anton P. McCaffrey, Toni Cathomen, Andrew M. Scharenberg, and J. Keith Joung. 2012. "Engineered Zinc Finger Nickases Induce Homology-Directed Repair with Reduced Mutagenic Effects." *Nucleic Acids Research* 40(12):5560–68.

Ran, Fa Ann, Patrick D. Pd Patrick D. Hsu, Jason Wright, Vineeta Agarwala, David a Scott, and Feng Zhang. 2013. "Genome

Engineering Using the CRISPR-Cas9 System." *Nature Protocols* 8(11):2281–2308.

Raphael, Ceccaldi, Rondinelli Beatrice, and Alan D. D'Andrea. 2016. "Repair Pathway Choices and Consequences at the Double- Strand Break." *Trends Cell Biol.* 16(3):338–48.

Ray Chaudhuri, Arnab and André Nussenzweig. 2017. "The Multifaceted Roles of PARP1 in DNA Repair and Chromatin Remodelling." *Nature Reviews. Molecular Cell Biology* 18(10):610–21.

Ren, Chonghua, Kun Xu, Zhongtian Liu, Juncen Shen, Furong Han, Zhilong Chen, and Zhiying Zhang. 2015. "Dual-Reporter Surrogate Systems for Efficient Enrichment of Genetically Modified Cells." *Cellular and Molecular Life Sciences* 72(14):2763–72.

Ren, Qingpeng, Chan Li, Pengfei Yuan, Changzu Cai, Linqi Zhang, Guangxiang George Luo, and Wensheng Wei. 2015. "A Dual-Reporter System for Real-Time Monitoring and High-Throughput CRISPR/Cas9 Library Screening of the Hepatitis C Virus." *Scientific Reports* 5:2–8.

Rezza, Amélie, Christelle Jacquet, Amélie Le Pillouer, Florian Lafarguette, Charlotte Ruptier, Marion Billandon, Patricia Isnard Petit, Séverine Trouttet, Kader Thiam, Alexandre Fraichard, and Yacine Chérifi. 2019. "Unexpected Genomic Rearrangements at Targeted Loci Associated with CRISPR/Cas9-Mediated Knock-In." *Scientific Reports* 9(1):1–8.

Ricci, Clarisse G., Janice S. Chen, Yinglong Miao, Martin Jinek, Jennifer A. Doudna, J. Andrew McCammon, and Giulia Palermo. 2019. "Deciphering Off-Target Effects in CRISPR-Cas9 through Accelerated Molecular Dynamics." *ACS Central Science* 5(4):651–62.

RICH, A. 1958. "Formation of Two- and Three-Stranded Helical Molecules by Polyinosinic Acid and Polyadenylic Acid." *Nature* 181(4608):521–25.

Rich, T., R. L. Allen, and a H. Wyllie. 2000. "Defying Death after DNA Damage." *Nature* 407(6805):777–83.

Richardson, Chris D., Katelynn R. Kazane, Sharon J. Feng, Elena Zelin, Nicholas L. Bray, Axel J. Schäfer, Stephen N. Floor, and Jacob E. Corn. 2018. "CRISPR–Cas9 Genome Editing in Human Cells Occurs via the Fanconi Anemia Pathway." *Nature Genetics* 50(8):1132–39.

Richardson, Christopher D., Graham J. Ray, Mark A. Dewitt, Gemma L. Curie, and Jacob E. Corn. 2016. "Enhancing Homology-Directed Genome Editing by Catalytically Active and Inactive CRISPR-Cas9 Using Asymmetric Donor DNA." *Nature Publishing Group* (September 2015):1–7.

Richardson, Christopher D., Graham J. Ray, Mark A. DeWitt, Gemma L. Curie, and Jacob E. Corn. 2016. "Enhancing

Homology-Directed Genome Editing by Catalytically Active and Inactive CRISPR-Cas9 Using Asymmetric Donor DNA." *Nature Biotechnology* 34(3):339–44.

Robert, Francis, Mathilde Barbeau, Sylvain Éthier, Josée Dostie, and Jerry Pelletier. 2015. "Pharmacological Inhibition of DNA-PK Stimulates Cas9-Mediated Genome Editing." *Genome Medicine* 7(1):93.

Ronco, Cyril, Anthony R. Martin, Luc Demange, and Rachid Benhida. 2017. "ATM, ATR, CHK1, CHK2 and WEE1 Inhibitors in Cancer and Cancer Stem Cells." *MedChemComm* 8(2):295–319.

Ronson, George E., Ann Liza Piberger, Martin R. Higgs, Anna L. Olsen, Grant S. Stewart, Peter J. McHugh, Eva Petermann, and Nicholas D. Lakin. 2018. "PARP1 and PARP2 Stabilise Replication Forks at Base Excision Repair Intermediates through Fbh1-Dependent Rad51 Regulation." *Nature Communications* 9(1).

Rose, John C., Jason J. Stephany, William J. Valente, Bridget M. Trevillian, Ha V. Dang, Jason H. Bielas, Dustin J. Maly, and Douglas M. Fowler. 2017. "Rapidly Inducible Cas9 and DSB-DdPCR to Probe Editing Kinetics." *Nature Methods* 14(9):891–96.

Roth, D. B., T. N. Porter, and J. H. Wilson. 1985. "Mechanisms of Nonhomologous Recombination in Mammalian Cells." *Molecular and Cellular Biology* 5(10):2599–2607.

Roth, D. B. and J. H. Wilson. 1986. "Nonhomologous Recombination in Mammalian Cells: Role for Short Sequence Homologies in the Joining Reaction." *Molecular and Cellular Biology* 6(12):4295–4304.

Rundle, Stuart, Alice Bradbury, Yvette Drew, and Nicola J. Curtin. 2017. "Targeting the ATR-CHK1 Axis in Cancer Therapy." *Cancers* 9(5):41.

Ruscetti, Tracy, Bruce E. Lehnert, James Halbrook, Hai Le Trong, Merl F. Hoekstra, David J. Chen, and Scott R. Peterson. 1998. "Stimulation of the DNA-Dependent Protein Kinase by Poly(ADP-Ribose) Polymerase." *Journal of Biological Chemistry* 273(23):14461–67.

Rybanska-Spaeder, Ivana, Taylor L. Reynolds, Jeremy Chou, Mansi Prakash, Tameca Jefferson, David L. Huso, Stephen Desiderio, and Sonia Franco. 2013. "53BP1 Is Limiting for NHEJ Repair in ATM-Deficient Model Systems That Are Subjected to Oncogenic Stress or Radiation." *Molecular Cancer Research : MCR* 11(10):1223–34.

Sabath, Daniel E. and Mi Hyun Shim. 2000. "Use of Green Fluorescent Protein/Flp Recombinase Fusion Protein and Flow Cytometric Sorting to Enrich for Cells Undergoing Flp-Mediated Recombination." *BioTechniques* 28(5):966–74.

Sander, Jeffry D. and J. Keith Joung. 2014. "CRISPR-Cas Systems for Editing, Regulating and Targeting Genomes." *Nature*

Biotechnology 32(4):347–55.

Sandor, Zoltan and Anders Bredberg. 1995. “Deficient DNA Repair of Triple Helix-Directed Double Psoralen Damage in Human Cells.” *FEBS Letters* 374(2):287–91.

Sarkaria, Jann N., Ericka C. Busby, Randal S. Tibbetts, Pia Roos, Yoichi Taya, Larry M. Karnitz, and Robert T. Abraham. 1999. “Inhibition of ATM and ATR Kinase Activities by the Radiosensitizing Agent, Caffeine.” *Cancer Research* 59(17):4375–82.

Sarkaria, Jann N., Randal S. Tibbetts, Ericka C. Busby, Amy P. Kennedy, David E. Hill, and Robert T. Abraham. 1998. “Inhibition of Phosphoinositide 3-Kinase Related Kinases by the Radiosensitizing Agent Wortmannin.” *Cancer Research* 58(19):4375–82.

Sartori, Alessandro A., Claudia Lukas, Julia Coates, Martin Mistrik, Shuang Fu, Jiri Bartek, Richard Baer, Jiri Lukas, and Stephen P. Jackson. 2007. “Human CtIP Promotes DNA End Resection.” *Nature* 450(7169):509–14.

Schultz, Niklas, Elena Lopez, Nasrollah Saleh-Gohari, and Thomas Helleday. 2003. “Poly(ADP-Ribose) Polymerase (PARP-1) Has a Controlling Role in Homologous Recombination.” *Nucleic Acids Research* 31(17):4959–64.

Senderowicz, A. M. 2000. “Small Molecule Modulators of Cyclin-Dependent Kinases for Cancer Therapy.” *Oncogene* 19(56):6600–6606.

Shen, Max W., Mandana Arbab, Jonathan Y. Hsu, Daniel Worstell, Sannie J. Culbertson, Olga Krabbe, Christopher A. Cassa, David R. Liu, David K. Gifford, and Richard I. Sherwood. 2018. “Predictable and Precise Template-Free CRISPR Editing of Pathogenic Variants.” *Nature* 563(7733):646–51.

Shibata, Atsushi, Davide Moiani, Andrew S. Arvai, Jefferson Perry, Shane M. Harding, Marie Michelle Genois, Ranjan Maity, Sari van Rossum-Fikkert, Aryandi Kertokalio, Filippo Romoli, Amani Ismail, Ermal Ismalaj, Elena Petricci, Matthew J. Neale, Robert G. Bristow, Jean Yves Masson, Claire Wyman, Penny A. Jeggo, and John A. Tainer. 2014a. “DNA Double-Strand Break Repair Pathway Choice Is Directed by Distinct MRE11 Nuclease Activities.” *Molecular Cell* 53(1):7–18.

Shibata, Atsushi, Davide Moiani, Andrew S. Arvai, Jefferson Perry, Shane M. Harding, Marie Michelle Genois, Ranjan Maity, Sari van Rossum-Fikkert, Aryandi Kertokalio, Filippo Romoli, Amani Ismail, Ermal Ismalaj, Elena Petricci, Matthew J. Neale, Robert G. Bristow, Jean Yves Masson, Claire Wyman, Penny A. Jeggo, and John A. Tainer. 2014b. “DNA Double-Strand Break Repair Pathway Choice Is Directed by Distinct MRE11 Nuclease Activities.” *Molecular Cell* 53(1):7–18.

Shibata, Atsushi, Monika Steinlage, Olivia Barton, Szilvia Juh??sz, Julia K??nzel, Julian Spies, Atsushi Shibata, Penny A. Jeggo, and Markus L??brich. 2017. “DNA Double-Strand Break Resection Occurs during Non-Homologous End Joining in G1 but Is Distinct from Resection during Homologous Recombination.” *Molecular Cell* 65(4):671-684.e5.

Shibata, Mikihiro, Hiroshi Nishimasu, Noriyuki Kodera, Seiichi Hirano, Toshio Ando, Takayuki Uchihashi, and Osamu Nureki. 2017. “Real-Space and Real-Time Dynamics of CRISPR-Cas9 Visualized by High-Speed Atomic Force Microscopy.” *Nature Communications* 8(1):1–9.

So, Clare C. and Alberto Martin. 2019. “DSB Structure Impacts DNA Recombination Leading to Class Switching and Chromosomal Translocations in Human B Cells.” *PLoS Genetics* 15(4):e1008101.

Sontheimer, Erik J. and Rodolphe Barrangou. 2015. “The Bacterial Origins of the CRISPR Genome-Editing Revolution.” *Human Gene Therapy* 26(7):413–24.

Stark, J. M. and M. Jasin. 2003. “Extensive Loss of Heterozygosity Is Suppressed during Homologous Repair of Chromosomal Breaks.” *Molecular and Cellular Biology* 23(2):733–43.

Stengel, Kristy R. and Scott W. Hiebert. 2015. “Class I HDACs Affect DNA Replication, Repair, and Chromatin Structure: Implications for Cancer Therapy.” *Antioxidants & Redox Signaling* 23(1):51–65.

Sternberg, Samuel H. and Jennifer A. Doudna. 2015. “Expanding the Biologist’s Toolkit with CRISPR-Cas9.” *Molecular Cell* 58(4):568–74.

Sternberg, Samuel H., Benjamin LaFrance, Matias Kaplan, and Jennifer a. Doudna. 2015. “Conformational Control of DNA Target Cleavage by CRISPR–Cas9.” *Nature* 527(7576):110–13.

Sternberg, Samuel H., Sy Redding, Martin Jinek, Eric C. Greene, and Jennifer A. Doudna. 2014. “DNA Interrogation by the CRISPR RNA-Guided Endonuclease Cas9.” *Nature* 507(7490):62–67.

Stracker, Travis H. and John H. J. Petrini. 2011. “The MRE11 Complex: Starting from the Ends.” *Nature Reviews Molecular Cell Biology* 12(2):90–103.

Stracker, Travis H., Takehiko Usui, and John H. J. Petrini. 2009. “Taking the Time to Make Important Decisions: The Checkpoint Effector Kinases Chk1 and Chk2 and the DNA Damage Response.” *DNA Repair* 8(9):1047–54.

Strobel, Scott A. and Peter B. Dervan. 1990. “Site-Specific Cleavage of a Yeast Chromosome by Oligonucleotide-Directed Triple-Helix Formation.” *Science* 249(4964):73–75.

Strobel, Scott A., Lynn A. Doucette-Stamm, Laura Riba, David E. Housman, and Peter B. Dervan. 1991. “Site-Specific

Cleavage of Human Chromosome 4 Mediated by Triple-Helix Formation." *Science* 254(5038):1639–42.

Sugawara, Etsuko and Hiroshi Nikaido. 2014. "Properties of AdeABC and AdeIJK Efflux Systems of Acinetobacter Baumannii Compared with Those of the AcrAB-TolC System of Escherichia Coli." *Antimicrobial Agents and Chemotherapy* 58(12):7250–57.

Sugawara, N., T. Goldfarb, B. Studamire, E. Alani, and J. E. Haber. 2004. "Heteroduplex Rejection during Single-Strand Annealing Requires Sgs1 Helicase and Mismatch Repair Proteins Msh2 and Msh6 but Not Pms1." *Proceedings of the National Academy of Sciences* 101(25):9315–20.

Sugawara, N., F. Paques, M. Colaiacovo, and J. E. Haber. 2002. "Role of Saccharomyces Cerevisiae Msh2 and Msh3 Repair Proteins in Double-Strand Break-Induced Recombination." *Proceedings of the National Academy of Sciences* 94(17):9214–19.

Sullenger, B. A. and T. R. Cech. 1994. "Ribozyme-Mediated Repair of Defective MRNA by Targeted, Trans-Splicing." *Nature* 371(6498):619–22.

Takai, Hiroyuki, Kaoru Tominaga, Noboru Motoyama, Yohji A. Minamishima, Hiroyasu Nagahama, Tadasuke Tsukiyama, Kyoji Ikeda, Keiko Nakayama, Makoto Nakanishi, and Kei Ichi Nakayama. 2000. "Aberrant Cell Cycle Checkpoint Function and Early Embryonic Death in Chk1(-/-) Mice." *Genes and Development* 14(12):1439–47.

Tan, E. Pien, Yilong Li, Martin Del Castillo Velasco-Herrera, Kosuke Yusa, and Allan Bradley. 2015. "Off-Target Assessment of CRISPR-Cas9 Guiding RNAs in Human IPS and Mouse ES Cells." *Genesis (New York, N.Y. : 2000)* 53(2):225–36.

Tavecchio, Michele, Joanne M. Munck, Celine Cano, David R. Newell, and Nicola J. Curtin. 2012. "Further Characterisation of the Cellular Activity of the DNA-PK Inhibitor, NU7441, Reveals Potential Cross-Talk with Homologous Recombination." *Cancer Chemotherapy and Pharmacology* 69(1):155–64.

Terada, M., H. Fujiki, P. A. Marks, and T. Sugimura. 1979. "Induction of Erythroid Differentiation of Murine Erythroleukemia Cells by Nicotinamide and Related Compounds." *Proceedings of the National Academy of Sciences* 76(12):6411–14.

Theodosiou, Nicole A. and Tian Xu. 1998. "Use of FLP/FRT System to Study." *Methods in Enzymology* 365:355–65.

Thurn, K. T., S. Thomas, P. Raha, I. Qureshi, and P. N. Munster. 2013. "Histone Deacetylase Regulation of ATM-Mediated DNA Damage Signaling." *Molecular Cancer Therapeutics* 12(10):2078–87.

Tibbetts, Randal S., David Cortez, Kathryn M. Brumbaugh, Ralph Scully, David Livingston, Stephen J. Elledge, and Robert T. Abraham. 2000. "Functional Interactions between BRCA1 and the Checkpoint Kinase ATR during Genotoxic

Stress.” *Genes and Development* 14(23):2989–3002.

Toledo, Luis I., Matilde Murga, Rafal Zur, Rebeca Soria, Antonio Rodriguez, Sonia Martinez, Julen Oyarzabal, Joaquin Pastor, James R. Bischoff, and Oscar Fernandez-Capetillo. 2011. “A Cell-Based Screen Identifies ATR Inhibitors with Synthetic Lethal Properties for Cancer-Associated Mutations.” *Nature Structural and Molecular Biology* 18(6):721–27.

Torgovnick, Alessandro and Björn Schumacher. 2015. “DNA Repair Mechanisms in Cancer Development and Therapy.” *Frontiers in Genetics* 6(April):157.

Tsai, Albert G., Haihui Lu, Sathees C. Raghavan, Markus Muschen, Chih-Lin Hsieh, and Michael R. Lieber. 2008. “Human Chromosomal Translocations at CpG Sites and a Theoretical Basis for Their Lineage and Stage Specificity.” *Cell* 135(6):1130–42.

Tsai, Shengdar Q. and J. Keith Joung. 2016. “Defining and Improving the Genome-Wide Specificities of CRISPR-Cas9 Nucleases.” *Nature Reviews. Genetics* 17(5):300–312.

Tse, Archie N., Richard Carvajal, and Gary K. Schwartz. 2007. “Targeting Checkpoint Kinase 1 in Cancer Therapeutics.” *Clinical Cancer Research* 13(7):1955–60.

Tubbs, Anthony and André Nussenzweig. 2017. “Endogenous DNA Damage as a Source of Genomic Instability in Cancer.” *Cell* 168(4):644–56.

Um, Jee Hyun, Chi Dug Kang, Byung Wook Hwang, Mee Young Ha, Joong Gu Hur, Dong Wan Kim, Byung Seon Chung, and Sun Hee Kim. 2003. “Involvement of DNA-Dependent Protein Kinase in Regulation of the Mitochondrial Heat Shock Proteins.” *Leukemia Research* 27(6):509–16.

Varshavsky, Alexander. 2006. “Discovering the RNA Double Helix and Hybridization.” *Cell* 127(7):1295–97.

Velic, Denis, Anthony M. Couturier, Maria Tedim Ferreira, Amélie Rodrigue, Guy G. Poirier, Fabrice Fleury, and Jean Yves Masson. 2015. “DNA Damage Signalling and Repair Inhibitors: The Long-Sought-after Achilles’ Heel of Cancer.” *Biomolecules* 5(4):3204–59.

Vendetti, Frank P., Pooja Karukonda, David A. Clump, Troy Teo, Ronald Lalonde, Katriana Nugent, Matthew Ballew, Brian F. Kiesel, Jan H. Beumer, Saumendra N. Sarkar, Thomas P. Conrads, Mark J. O’Connor, Robert L. Ferris, Phuoc T. Tran, Greg M. Delgoffe, and Christopher J. Bakkenist. 2018. “ATR Kinase Inhibitor AZD6738 Potentiates CD8+ T Cell-Dependent Antitumor Activity Following Radiation.” *Journal of Clinical Investigation* 128(9):3926–40.

Vendetti, Frank P., Alan Lau, Sandra Schamus, Thomas P. Conrads, Mark J. O'Connor, and Christopher J. Bakkenist. 2015. "The Orally Active and Bioavailable ATR Kinase Inhibitor AZD6738 Potentiates the Anti-Tumor Effects of Cisplatin to Resolve ATM-Deficient Non-Small Cell Lung Cancer in Vivo." *Oncotarget* 6(42):44289–305.

Veres, Adrian, Bridget S. Gosis, Qiurong Ding, Ryan Collins, Ashok Ragavendran, Harrison Brand, Serkan Erdin, Chad A. Cowan, Michael E. Talkowski, and Kiran Musunuru. 2014. "Low Incidence of Off-Target Mutations in Individual CRISPR-Cas9 and TALEN Targeted Human Stem Cell Clones Detected by Whole-Genome Sequencing." *Cell Stem Cell* 15(1):27–30.

Walker, John R., Richard A. Corpina, and Jonathan Goldberg. 2001. "Structure of the Ku Heterodimer Bound to Dna and Its Implications for Double-Strand Break Repair." *Nature* 412(6847):607–14.

Walsh, Ryan M. and Konrad Hochedlinger. 2013. "A Variant CRISPR-Cas9 System Adds Versatility to Genome Engineering." *Proceedings of the National Academy of Sciences of the United States of America* 110(39):15514–15.

Wang, Anderson T., Taeho Kim, John E. Wagner, Brooke A. Conti, Francis P. Lach, Athena L. Huang, Henrik Molina, Erica M. Sanborn, Heather Zierhut, Belinda K. Cornes, Avinash Abhyankar, Carrie Sougnez, Stacey B. Gabriel, Arleen D. Auerbach, Stephen C. Kowalczykowski, and Agata Smogorzewska. 2015. "A Dominant Mutation in Human RAD51 Reveals Its Function in DNA Interstrand Crosslink Repair Independent of Homologous Recombination." *Molecular Cell* 59(3):478–90.

Wang, Huichen, Ange Ronel Perrault, Yoshihiko Takeda, Wei Qin, Hongyan Wang, and George Iliakis. 2003. "Biochemical Evidence for Ku-Independent Backup Pathways of NHEJ." *Nucleic Acids Research* 31(18):5377–88.

Wei, Huiting and Xiaochun Yu. 2016. "Functions of PARylation in DNA Damage Repair Pathways." *Genomics, Proteomics and Bioinformatics*.

Wen, Yahong, Grace Liao, Thomas Pritchard, Ting Ting Zhao, Jon P. Connelly, Shondra M. Pruett-Miller, Valerie Blanc, Nicholas O. Davidson, and Blair B. Madison. 2017. "A Stable but Reversible Integrated Surrogate Reporter for Assaying CRISPR/Cas9-Stimulated Homology-Directed Repair." *Journal of Biological Chemistry* 292(15):6148–62.

Wood, Richard D. and Sylvie Doublié. 2016. "DNA Polymerase θ (POLQ), Double-Strand Break Repair, and Cancer." *DNA Repair* 44(512):22–32.

Wray, Justin, Elizabeth A. Williamson, Sudha B. Singh, Yuehan Wu, Christopher R. Cogle, David M. Weinstock, Yu Zhang, Suk Hee Lee, Daohong Zhou, Lijian Shao, Martin Hauer-Jensen, Rupak Pathak, Virginia Klimek, Jac A. Nickoloff, and Robert Hromas. 2013. "PARP1 Is Required for Chromosomal Translocations." *Blood* 121(21):4359–65.

Wright, Gabriela, Volha Golubeva, Lily L. Remsing Rix, Norbert Berndt, Yunting Luo, Grace A. Ward, Jhanelle E. Gray, Ernst Schonbrunn, Harshani R. Lawrence, Alvaro N. A. Monteiro, and Uwe Rix. 2017. "Dual Targeting of WEE1 and PLK1 by AZD1775 Elicits Single Agent Cellular Anticancer Activity." *ACS Chemical Biology* 12(7):1883–92.

Y., Kan, Ruis B., Takasugi T., and Hendrickson E.A. 2017. "Mechanisms of Precise Genome Editing Using Oligonucleotide Donors." *Genome Research* 27(7):1099–1111.

Yang, Chuanjie, Quanxu Wang, Xiaodan Liu, Xiulian Cheng, Xiaoyu Jiang, Yuan Zhang, Zhijie Feng, and Pingkun Zhou. 2016. "NU7441 Enhances the Radiosensitivity of Liver Cancer Cells." *Cellular Physiology and Biochemistry* 38(5):1897–1905.

Yang, Jian, Steven Zimmerly, Philip S. Perlman, and Alan M. Lambowitz. 1996. "Efficient Integration of an Intron RNA into Double-Stranded DNA by Reverse Splicing." *Nature* 381(6580):332–35.

Yang, Luhan, Dennis Grishin, Gang Wang, John Aach, Cheng-Zhong Zhang, Raj Chari, Jason Homsy, Xuyu Cai, Yue Zhao, Jian-Bing Fan, Christine Seidman, Jonathan Seidman, William Pu, and George Church. 2014. "Targeted and Genome-Wide Sequencing Reveal Single Nucleotide Variations Impacting Specificity of Cas9 in Human Stem Cells." *Nature Communications* 5:5507.

Yang, X. J. and E. Seto. 2007. "HATs and HDACs: From Structure, Function and Regulation to Novel Strategies for Therapy and Prevention." *Oncogene* 26(37):5310–18.

Yin, Hao, Chun-Qing Song, Joseph R. Dorkin, Lihua J. Zhu, Yingxiang Li, Qiongqiong Wu, Angela Park, Junghoon Yang, Sneha Suresh, Aizhan Bizhanova, Ankit Gupta, Mehmet F. Bolukbasi, Stephen Walsh, Roman L. Bogorad, Guangping Gao, Zhiping Weng, Yizhou Dong, Victor Koteliansky, Scot A. Wolfe, Robert Langer, Wen Xue, and Daniel G. Anderson. 2016. "Therapeutic Genome Editing by Combined Viral and Non-Viral Delivery of CRISPR System Components in Vivo." *Nature Biotechnology* 34(3):328–33.

Zhang, Mingjie, Feng Wang, Shifei Li, Yan Wang, Yun Bai, and Xueqing Xu. 2014. "TALE: A Tale of Genome Editing." *Progress in Biophysics and Molecular Biology* 114(1):25–32.

Zhang, Xiao Hui, Louis Y. Tee, Xiao Gang Wang, Qun Shan Huang, and Shi Hua Yang. 2015. "Off-Target Effects in CRISPR/Cas9-Mediated Genome Engineering." *Molecular Therapy - Nucleic Acids* 4(11):e264.

Zhang, Yu and Maria Jasin. 2011. "An Essential Role for CtIP in Chromosomal Translocation Formation through an Alternative End-Joining Pathway." *Nature Structural & Molecular Biology* 18(1):80–84.

Zhao, Juan, Xindi Dang, Peixin Zhang, Lam Nhat Nguyen, Dechao Cao, Lin Wang, Xiaoyuan Wu, Zheng D. Morrison, Ying Zhang, Zhansheng Jia, Qian Xie, Ling Wang, Shunbin Ning, Mohamed El Gazzar, Jonathan P. Moorman, and Zhi Q. Yao. 2018. "Insufficiency of DNA Repair Enzyme ATM Promotes Naive CD4 T-Cell Loss in Chronic Hepatitis C Virus Infection." *Cell Discovery* 4(1).

Zhao, Yan, Huw D. Thomas, Michael A. Batey, Ian G. Cowell, Caroline J. Richardson, Roger J. Griffin, A. Hilary Calvert, David R. Newell, Graeme C. M. Smith, and Nicola J. Curtin. 2006. "Preclinical Evaluation of a Potent Novel DNA-Dependent Protein Kinase Inhibitor NU7441." *Cancer Research* 66(10):5354–62.

Zhou, Bin-bing S. and Stephen J. Elledge. 2000. "Checkpoints in Perspective." *Nature* 408(November):433–39.

Zhu, Xing, Ryan Clarke, Anupama K. Puppala, Sagar Chittori, Alan Merk, Bradley J. Merrill, Miljan Simonović, and Sriram Subramaniam. 2019. "Cryo-EM Structures Reveal Coordinated Domain Motions That Govern DNA Cleavage by Cas9." *Nature Structural & Molecular Biology*.

Zimmerly, Steven, Huatao Guo, Robert Eskest, Jian Yang, Philip S. Perlman, and Alan M. Lambowitz. 1995. "A Group II Intron RNA Is a Catalytic Component of a DNA Endonuclease Involved in Intron Mobility." *Cell* 83(4):529–38.